CHARGE CARRIER AND PHONON TRANSPORT IN NANOSTRUCTURED THERMOELECTRICS

By

PAYAM NOROUZZADEH

Bachelor of Science in Applied Physics
Sharif University of Technology
Tehran, Iran
1996

Master of Science in Applied Physics
Iran University of Science and Technology
Tehran, Iran
1999

Submitted to the Faculty of the
Electrical and Computer Engineering
Graduate College of the
Oklahoma State University
in partial fulfillment of
the requirements for
the Degree of
DOCTOR OF PHILOSOPHY
December, 2012

CHARGE CARRIER AND PHONON TRANSPORT IN NANOSTRUCTURED THERMOELECTRICS

Dissertation Approved:

Dr. DaryooshVashaee

Dissertation Adviser

Dr. Jerzy S. Krasinski

Dr. John M. Acken

Dr. Kenneth F. Ede

ACKNOWLEDGEMENTS

I would like to begin by acknowledging my advisor and mentor, Professor DaryooshVashaee, for giving me this opportunity to learn from him. He is a wonderful educator and I have benefited from his brightness of thought and passion for hard working. I would also like to acknowledge Professors Jerzy S. Krasinski, John M. Acken, and Kenneth F. Ede for serving on my dissertation committee and for their valuable helps during my defense. Every teacher I have studied under has made some impact in my education and I would also like to convey my heartfelt and sincere appreciation to all of them.

I would specially like to express my deepest gratitude to my wife: Bahareh for all her love and support.

This dissertation is dedicated to my parents, the heroes of my life,for their love, endless support and encouragement.

Acknowledgements reflect the views of the author and are not endorsed by committee members or Oklahoma State University.

Name: PAYAM NOROUZZADEH

Date of Degree: DECEMBER, 2012

Title of Study: CHARGE CARRIER AND PHONON TRANSPORT IN NANOSTRUCTURED THERMOELECTRICS

Major Field: ELECTRICAL ENGINEERING

Abstract: There is currently no quantum mechanical transport model for charge (or phonon) transport in multiphase nano-crystalline structures. Due to absence of periodicity, one cannot apply any of the elegant theorems, such as Bloch's theorem, which are implicit in the basic theory of crystalline solids. Atomistic models such as Kubo and NEGF may assume an accurate knowledge of the interatomic potentials; however, calculations for real 3D random multi-phase systems require so large computational times that makes them practically impossible.

In a multi-phase nano-crystalline material, grains and interfacial microstructures may have three distinct types as depicted in figure. In such a material, the physical processes in each individual grain no longer follow the well described classical continuum linear transport theory. Therefore, a proper model for coupled transport of charge carriers and phonons that takes into account the effect of their non-equilibrium energy distribution is highly desirable.

Two new theories and associated codes based on Coherent Potential Approximation (CPA) one for electron transport and one for phonon transport are developed. The codes calculate the charge and phonon transport parameters in nanocomposite structures. These can be nano-crystalline (symmetric case) or the material with embedded nano-particles (dispersion case). CPA specifically considers multi-scattering effect that cannot be explained with other semi-classical methods such as Partial Wave or Fermi's golden rule. To our knowledge this is the first CPA code developed to study both charge and phonon transport in nanocomposite structures.

The codes can be extend to different types of nano-crystalline materials taking into account the average grain size, as well as the grain size distribution, and volume fraction of the different constituents in the materials. This is a strong tool that can describe more complex systems such as nano-crystals with *randomly oriented grains* with predictive power for the properties of electrical and thermal properties of disordered nano-crystalline electronic materials.

TABLE OF CONTENTS

Chapter Page

LIST OF TABLES

LIST OF FIGURES

Chapter I

Chapter II

Chapter III

Chapter V

CHAPTER I

INTRODUCTION

1.1 Outline

The efforts in thermoelectrics research have been focused on enhancing thermoelectric figure of merit ZT. The best thermoelectric materials are recognized as "phonon-glass electron-crystal" (or PGEC in short), which means that the materials should have a low lattice thermal conductivity like a glass, and a high electrical conductivity and charge carrier mobility like crystals [1]. Unlike insulators which have poor electrical conductivity and metals which have low Seebeck coefficient, the heavily doped semiconductors seem to be the best candidates for thermoelectric materials. In semiconductors, the thermal conductivity has contributions from both charge carriers (k_e) and phonons ($k_{p(l)}$), with the majority usually coming from quantized lattice vibrations or phonons. The reduction in phonon thermal conductivity without causing too much reduction in the electrical conductivity is possible. A well-known approach to reduce the phonon thermal conductivity is through alloying [2]. The scattering due to mass difference in an alloy reduces the phonon thermal conductivity significantly without considerable deterioration to the electrical conductivity.

Most of the existing theoretical studies heavily rely on information about the force constants of the pure materials [3, 1]. A direct first principles calculation of the electronic band structure and phonon dispersion for such systems is very demanding computationally even with the highly efficient linear response techniques presently available. Therefore,devising a method to treat disordered alloys and nanocomposites with an affordable amount of computer resources retaining an accuracy similar to that of direct first principles calculationsis desirable.

In this dissertation the methods based on coherent potential approximation as introduced by Sheng [4] are developed and presented within effective mass approach for calculating relaxation times of grain boundaries for both charge carriers and phonons in nanocomposite thermoelectrics. The method takes into account the average grain size as well as the grain size distribution and volume fraction of the different constituent in the nanocomposite material. Furthermore, an approach to describe more complex systems such as nanocomposite thermoelectrics with randomly oriented grains is developed. In the remainder of this chapter, some background on the theory and the motivations for investigating the electronic and phononic properties of composite mixtures are discussed. Remarkably, in nanocomposites the granularity is largely high and the physical processes in each individual grain are well described by classical continuum linear transport theory. D. J. Bergman [5] showed that in a composite material thermoelectric power factor, the product of the square of the Seebeck coefficient and electrical conductivity, can be

enhanced over that of the individual constituents, but the figure-of-merit cannot. This predication is expected to fail in nanocomposites due to the size effects which are ignored in this theory.

In the following sections, firstlythe importance of new concept of nanostructuring in the context of thermoelectrics is mentioned.In Chapter II,a detailed theoretical description of modeling charge carriertransport for semiconductors by Boltzmann transport equation (BTE)is given. Chapter III contains a review of phonon transport for semiconductors by BTE and also Callaway method [50]. The necessary details of general coherent potential approximation (CPA)are presented in Chapter IV. Chapter V presents the boundary value mathematical formalism of the CPA and its relation to Green's function based formalism. The numerical results, analysis, verification of code, future studies and conclusion are given in Chapter VI .

The predictive power of these methods in the case of disordered materials such as nanocomposites where some established experimental results existis demonstrated. These developed methods have been applied to charge carrier and phonon transport in nanocompositesBi_2Te_3-Sb_2Te_3Si-Ge to calculatethe grain boundary scattering time. The dependency of charge carrier and phonon scattering ratesas a function of the grain size is shown in this dissertation.

1.2 The Theory of Electronic Structure of Alloys

The charge carrier transport models of substitutionally disordered alloys cannot be applied exactly for arbitrary alloy compositions. Even for very simple model compositions, one can obtain exact spectra only by numerical calculations on a system of several thousand atoms. The primary difficulty in developing a theory to treat such a system stems directly from the absence of any real simplifying features in the system geometry. In fact, there is no periodicity in the system. The atom configurations are locally ordered and periodic within each individual grain but grains are randomly oriented and there is no long range periodicity or order. Thus one cannot apply any of the elegant theorems, such as Bloch's theorem, which are implicit in the basic theory of crystalline solids. Furthermore, disordered systems in general and alloy compositions in particular are systems for which the perturbative approach is most likely to be unsuccessful. This situation is mainly caused by lack of a definite small parameter which describes the system. Nevertheless, many approximate approaches, of varying degrees of efficiency and simplicity have been developed to deal with such systems over the past years [4]. For disordered alloys or composite systems, a common method for developing a theory of the electronic properties is to treat the electronic structure in a tight binding picture with both the diagonal and off-diagonal matrix elements of the tight binding Hamiltonian being taken as random variables which take on different values depending on the probability of a given site being occupied by a given type of atomic constituent. Many approximate approaches have been proposed to calculate the electronic properties of disordered alloys in such a model, with most theories focusing on determining the electronic band structure and density of states. These approximate methods includes the Virtual Crystal Approximation (VCA)[6], the Average T-Matrix Approximation (ATA) [7], the Coherent Potential Approximation (CPA)[8], the Embedded Cluster Method [9], various cluster generalizations of the CPA [9]. Several sources such as books by Sheng [4] and Economou [10] give detailed discussions of some of these methods. The Coherent Potential Approximation

(CPA) as an approach to the theory of disordered alloys has proven successful in application to a large number of electronic properties under the above mentioned tight binding model. The CPA has been shown to be one of the most effective out of a class of theories known as "single-cell" theories. The CPA can predict successfully the major trends in the band structures of alloys as a function of their composition. Nevertheless, the calculations remain relatively simple for applications to real systems. Historically, this approximation was based on the multiple scattering approach of Lax [11]. The multiple scattering approach was originally developed by Taylor [12] (for vibrational properties) and by Soven [13] (for electronic properties) for binary alloys. The CPA is a mean-field theory approach which replaces the random alloy by an effective medium. The effective medium is self-consistently determined, so that the average scattering of waves or quasi-particles from each unit cell vanishes. Another way to express this approximation is that the self-consistently determined effective medium leads to a zero average electronic scattering from a single unit cell embedded in the effective medium. In this way one obtains the average eigenvalues for the random alloy. The CPA will be discussed in detail in chapters IV and V. After the pioneering papers of Taylor and Soven, various extensions of the CPA have been made by many researchers. Some of these extensions and generalizations may be found in papers by Sen and Hartman [14] and in the Refs. [15,16].

1.3 Nanostructured Thermoelectric Materials

Superlattices, quantum wires, quantum wells and quantum dots as nanostructured or low-dimensional materials, offer new ways to manipulate the charge carrier and phonon transport properties of a given material [17]. When the quantum effects are dominant, the energy spectra of charge carriers and phonons can be controlled through varying the size of the structures. So, the quantum effects offer a possible way for enhancement of the ZT. In this regime, the nanostructured materialsshow new physical properties despite the fact that they are made of the same atomic components as their parent materials. Thus looking for high ZT systems in nanostructured materials can be considered as analogous to synthesizing many different bulk materials and measuring their thermoelectric properties. When quantum size effects are not dominant, improving classical size effects to adjust the transport processes is still possible. The exploitation of interfaces and boundaries to scatter phonons more effectively than charge carriers is a possibility. Investigations over the past decade on nanostructured materials have utilized both quantum and classical size effects for charge carriers and phonons. As another possibility, Dresselhaus proposed the use of quantum wells to increase the power factor via quantum size effects of electrons in 1993 [18]. The implementation of these quantum-well structures calls for superlattices or multiple quantum well structures. Meanwhile, there were also suggestions and experimental evidence that superlattices could be made into superior thermal insulators, promising another method to enhance the figure-of-merit [19]. Later experimental efforts have demonstrated significantreduction of the thermal conductivity in superlattices [20].

To explain the reduction in thermal conductivity of nanostructures, many different approaches have been developed. These approaches can be categorized in two different groups. In the first group the phonons are considered as incoherent particles, and interface scattering is treated as a classical size effect [21,22]. These approaches assume that interface scattering is partially specular and partially diffusive, with the fraction of specular interface scattering as a fitting parameter. In the second group of approaches the phonons are considered totally coherent. Three

major effects on the phonon spectra in superlattice nanostructures can be attributed to the periodicity:

(1) phonon branches are folded in the growth direction due to the new periodicity,
(2) small band-gaps appear, and
(3) thespectrum of acoustic phonons with higher frequency becomes flat or confined because of the spectrum mismatch.

As a result, the phonon group velocity in the cross-plane direction is reduced which in turn lowers the thermal conductivity [23]. Nevertheless, compared to experimental data, the reduction in the phonon group velocity alone is not enough to explain the magnitude of the thermal conductivity reduction perpendicular to the film plane. Additionally, the reduction in the phonon group velocity fails to explain the thermal conductivity reduction across the film plane [24]. A possible explanation is that the lattice dynamics model does not include the possibility of diffusive interface scattering, which destroys the phase coherence.

To overcome this difficulty a partially coherent phonon transport model was introduced that can describe the thermal conductivity behavior in superlattices over the full range of period thicknesses for both the in-plane and the cross-plane directions [24]. These theoretical and experimental efforts show difficulty of involving wave effects in phonon transport mechanisms due to the small phonon wavelength compared to the characteristic roughness and geometric variations of typical nanostructures. As an example a typical dominant phonon room temperature wavelength for most of materials is ~10-20 nm [25]. The wavelength must be much smaller than the interface roughness to consider it as a smooth interface. Therefore, interface imperfections resulted from mixing of atoms or formation of steps can easily destroy the phonon coherence. For thermoelectric applications, this destruction of phonon coherence is favored.

1.4 Transport Theory for Nanostructures

The conductance formula $G = \frac{\sigma A}{L}$where $\sigma$is theconductivity, A is the area of cross-section of the conductor,and L is its length, breaks down at sub-micrometer length scales and electrical conductivity reaches a limiting value G_c. Quantum mechanics explains that we should put aside the charged particle picture of electrons and consider them as wave-particles. This wavecharacter of theelectrons is responsible for many phenomena like Anderson localization,propagation of light through arandom medium, and mesoscopic conduction through adisordered sample. A mesoscopiclength scaleis defined as lengthscale at which the wave character of electrons has definiteeffect on the measurable physical properties. The conductance no longer monotonicallychanges but it shows jumps in units of$G_c = 2e^2/h$.

The charge carrier transport needs quantum mechanics to be utilized when the following three parameters become ofthe order of the sample size:

(1) the de-Broglie wavelength associated with the charge carriers,
(2) the mean free path,which is the distance traveled by the charge carriers before theirinitial momentum are destroyed, and
(3) the phase relaxationlength, which is the distance traveled by thecharge carriers before their initial phase are destroyed,

In this regime, all of our intuition about charge carrier transportcollapses. Newinteresting effects, such as conductance quantization, conductance fluctuations, Coulomb blockade in quantum dots, Kondo effect, non-equilibrium Kondo effect, etc. appear in this regime.
Primitive quantum theories of charge carrier transport in bulkmaterials were semi-classical in nature, and includedtwo steps:

(1) The charge carriers were accelerated by external forces across Bloch states, and then scattered between Bloch states by impurities or phonons.
(2) Balancing processes were handled using simple occupation probability distributions, which do not consider any coherent processes and all the phase information was neglected in scattering.

This semi-classicalapproach completely fails forcharge carrier transportin nanostructuredmaterials, where the phase relaxationlength of charge carriers becomes of the order of the size ofthe sample. A new approach wasneeded to explain coherent transport in nanostructured materials. The first steps were takenby Landauer [26] and Buttiker [27]. In brief, the recent transport theory through a nanostructuredsample can be categorized into three regimes:

1. Ballistic regime.If the sample size is very small thenthe elastic scattering of charge carriers by the impurities will be negligibledue to few impurities in the path of charge carriers, and a new regime which is called ballistic transport regime is appeared. Considering conductance as an average transmission of the sample is very helpful, conceptually and computationally. The transmission properties of the sample depend effectively on the shape and size of the sample. The transport in this regime can be very well understood by using the Landauer formalism. Buttiker generalized the twoterminalsLandauer formalism to a multi-terminal formalism [27].

2. Diffusive regime. The 2D (two dimensionalelectron) gas at the interface of a hetero-junction like GaAs/GaAlAs has some special features. The 2D electron gas has very low electron density (~ 10^{12}/cm^2) which is controllable by gate electrodes. The electron density implies large electron mean free path (~10μm) at low temperatures and the quantum interference effects extend over the length of the sample. There is no phonon generation and inelastic scattering.The electrical conductivity of a disordered sample is mainly influenced by the distribution of impurities in the sample. Electrical conductivity differs from sample to sample and grain to grain. In this regime the sample is muchlarger than the average electron mean free path. Another important length scale is the localization length. In strongly disorder materials, charge carriers form localized states due to back scattering and quantum interference effects. The length scale over whichthe wave packet is localized is named the localization length [4].
In this dissertation a diffusive regime is assumedunless stated.

3. Adiabatic regime. Adiabatic regimeoccurs in 2D systems in the presence of a strong perpendicular magnetic field. In this case, a shell of charge carriers around the Fermi levelis divided into levels called Landau levels. In this situation, the new length scale is the magnetic length of the electron ($\sqrt{\hbar/eB}$ ~10 nm). If the magnetic length is of the order of the sample size, then inter-Landau level scattering of the charge carriers is annihilated and there will be no scattering. This regime is called the adiabatic transport regime. In most of the quantum transport

cases we have a non-equilibrium situation. Therefore, a different theory called non-equilibrium Green's function formalism (NEGF) is required to describe the interacting non-equilibrium nanostructuredmaterials. Moreover, the semi-classical kinetic transport theory of Boltzmann can be derived from the NEGF formalism.

1.5 Motivation for Studying

Despite theindustrial and experimental importance of nanostructured thermoelectrics very few systematic theoretical treatments of their transport properties have been carried out. An understanding of the electronic and phononic properties of these materials, particularly of their electronic band structures, densities of states, and phonon dispersion could be of importance for increasing the understanding of charge carrier and heat transport phenomena in these systems, and thus could contribute to the improvement of the devices manufactured from these materials. To the best of our knowledge, the theory of these properties is not yet sufficiently developed to enable the accurate prediction of either band structures and the density of states spectra or phonon dispersion.

The work presented in this dissertation was motivated by a desire to understand and to be able to predict transport properties of these technologically important nanostructured thermoelectrics. The main purpose of the work presented here is thus to lay the foundation for a theory of the electronic properties and thermal properties of nanostructured thermoelectric materials.

The Coherent Potential Approximation (CPA) introduced by Soven [13] has been used widely to calculate electronic properties of disordered alloys and composites. CPA has shown excellent agreement with experiments for scattering related quantities. In the CPA as a mean field and single site theoryone assumption is that a localized region of a material like a single site can specify the behavior of the entire material. The CPA introduces an effective medium with a complex propagation constant (wave number) which represents the electronic features of materials. This effective medium is characterized by requiring that the total cross section resulting from the difference between scattering of the host and embedded nanoparticle vanish on the average. In fact, the scattering medium is embedded in a host material in such a way that each single scatterer sees all other scatterers as composing the host. When the composite inclusion is embedded in the host, the net scattering when$r \rightarrow \infty$ should be zero if the scattering amplitudes of the single scatterers satisfy the CPA condition. The host material has adjustable properties (like elastic constants). The requirement of no net scattering gives rise to same effective properties for both composite and the host material. The properties of the effective medium are affected by its microstructure. The volume fractions of the components, the shapes and geometric arrangement of the inhomogeneties specify the microstructure of an effective medium. The microstructure represents the statistical correlation in a disordered alloy or composite. Therefore, to determine an effective medium both the material properties of the components and their microstructure should be specified. Therefore, the CPA is based on three main concepts:

(1) Introduction of a periodic effective medium with a complex propagation constant by a self-consistency requirement. The CPA condition sets the average value of scattering amplitude equal to zero and eliminates its local fluctuations.
(2) Calculating the average of a desired property of a disordered material.
(3) Choosing a structural unit to represent the microstructural information of a disordered medium.

Several particular features of the CPA were especially interesting for the purpose of this work. Firstly, its mathematical formalism based on multiple scattering is simple and easy to understand. Secondly, the CPA is not computationally demanding. Thirdly, the CPA works well for samples even with high volume fraction of nanoparticles. For low concentrations of nanoparticles (<0.01), one may apply partial wave method, but as the concentration increases, the partial wave method fails. Finally, besides electron wave, the extension of the CPA to classical waves in disordered alloys enables us to treat the acoustic wave propagation in random media with a similar theoretical framework.

The discussion on the thermal conductivity reduction mechanism mentioned above suggests that the periodicity of superlattices is not a necessary condition for thermal conductivity reduction. The reduced thermal conductivity in superlattices comes from the sequential interface scattering of phonons rather than the coherent superposition of phonon waves. This conclusion leads naturally to the idea of using nanocomposites as a possibleinexpensive alternative to superlattices in the quest for high ZT materials [28]. Such nanocomposites can be in the form of nano-particles and nanowires embedded in a host matrix material, or mixtures of two different kinds of nanoparticles [29]. To reduce the thermal conductivity without deteriorating the charge carrier transport properties, one should work with constituent materials that have significant differences in lattice properties, but negligible differences in electronic properties. Recent experimental results on Bi_2Te_3/Sb_2Te_3 superlattices and PbTe/PbSeTe quantum dots superlattices [30,31] show no significant reduction in the electrical conductivity were observed for current flow perpendicular to the interface of Bi_2Te_3/Sb_2Te_3 superlattices and no reduction of electrical conductivity along the interface of PbTe/PbSeTe quantum-dot superlattices. Therefore, by properly choosing the mismatch in electronic properties, the electron transport properties can be maintained at a level comparable to bulk materials or even enhanced using interfaces as energy filters or energy quantization barriers.

Although the nanocomposite approach seems promising, currently there are few theoretical or modeling papers regarding thermoelectric properties of nanocomposites that one can rely on to achieve good design of nanocomposites. There exists a variety of challenges for simulation of both charge carrier and phonon thermoelectric transport in nanocomposites. First of all, question often rises whether one needs to look into the wave effect in transport processes in nanostructures [25]. Another challenge to study the thermoelectric properties of nanocomposites is to simulate the charge carrier and phonon transport in the whole composite structure with nanoparticles or nanowires embedded in a host material. The distribution of the size and location of nanoparticles can vary considerably. To accurately model the transport, the simulation box should be as large as possible, or even the same size as the sample made. The memory and computational time requirements for such a multiscale problem are very demanding.

Both the deterministic solution of phonon BTE and Monte Carlo simulation have been used to predict the thermal conductivity of nanocomposites with Si nanowires and nanoparticles embedded in Ge matrix [29]. The study shows that the prevailing approach to model thermal conductivity of nanocomposites, which includes the interface thermal resistance, or Kapitza resistance [32], with the Fourier heat conduction theory [33], underpredicts the effect of interface for thermal conductivity reduction. This is understandable since the Fourier heat conduction theory is based on the diffusion picture and is not applicable when the phonon mean free path is longer than the characteristic length of the nanocomposites such as the particle diameter and/or inter-particle separation distance.

To conclude, thermal conductivity of nanocomposites can be effectively reduced which, renders nanocomposite approach as potentially inexpensive alternative to superlattices for high ZT material development. The challenge is to properly choose the mismatch in electronic properties between the constituent materials so that the electron transport properties can be maintained or even enhanced. There are few modeling tools for electron transport in nanocomposites [5] but the methodology developed for studying thermal conductivity of nanocomposites can be extended to study the electron performance of nanocomposites and thus facilitate the material optimization.

In summary, there is currently no transport model for coupled charge and phonon transport in nanocomposites. The physical processes in each individual grains no longer follow the well described classical continuum linear transport theory. Therefore, a proper model for coupled transport of charge carriers and phonons that takes into account the effect of their non-equilibrium energy distribution is highly desirable [34].

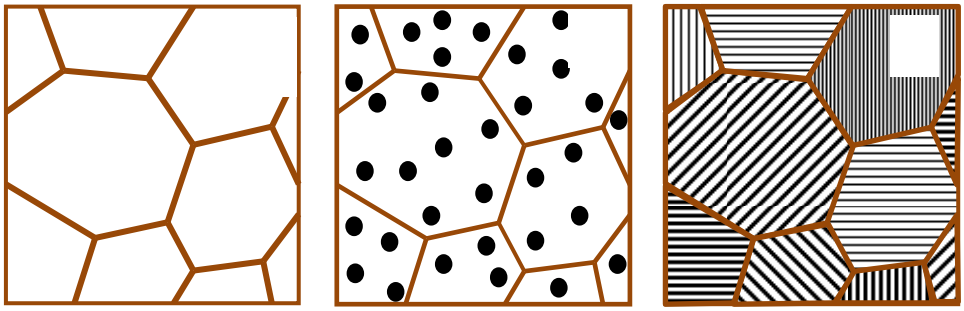

Figure 1.1: Schematics of three kinds of nanocomposites: (a) coated grains, (b) embedded nano-particles, and (c) multi-component grains.

In a nanocomposite material, grains and interfacial microstructures may have three distinct structures as depicted in Figure 1.1. In Type 1 (Figure 1.1-a), a thin layer of a secondary phase at the grain boundaries is introduced. Type 2 (Figure 1.1-b) consists of embedded nano-particles inside the grains. Figure 1.1-c is a mixture of two or more of different materials or phases. Phonon scattering at grain boundaries (GBs) reduces bipolar thermal diffusion of electron-hole pairs. Eelectron transitions through the same and different valleys at GBs, and thermionic emission at GBs are some of the main mechanisms that can significantly affect the TE properties of nanocomposites.

CHAPTER II

SEMICLASSICAL THEORY OF CHARGE CARRIER TRANSPORT

To achieve a high value of ZT a properly designed composition that can reduce the thermal conductivity without significantly deteriorating the power factor is needed. In a good design the interface boundaries for such a random structure must be carefully modeled. Space charge effects, additional scatterings due to the rotation of crystal orientation at the boundaries, and electron-phonon non-equilibrium transport are some of the main factors that must be studied. With proper engineering of the impurity atoms, designing a structure that can maintain or even increase the effective power factor of the active media for an optimum ZT might be possible. Increasing the power factor can be achieved with an increased Seebeck coefficient due to the electron filtering at the barriers, a reduction in thermal conductivity, and increased carrier density for a high electrical conductivity. Transport theory deals with flow of charge carriers and/or flow of heat by phonons through a solid material under external fields, such as an electric field and/or a temperature gradiant. The motions of charge carriers or phonons are driven by the external fields but resisted by internal scattering processes between them and other particles or quasi-particles. There are energy and momentum exchanges within the interactions resulting in finite electric or thermal conductivity. On the other hand, the interactions have the consequence that the conducted carriers are not in their equilibrium states. There are two approaches to deal with a non-equilibrium transport, the Green- Kubo theory [35] and the semi-classical Boltzmann transport theory [36]. The former relates transport coefficients to the autocorrelation function of the current or heat flux. The latter treats effects of various scattering mechanisms on transport properties in terms of relaxation times. The Boltzmann transport theory has proven its validity in numerous applications where calculated transport coefficients can be readily compared with experimental results. First,a general discussion of the Boltzmann transport equation, which is needed for power factor modeling is provided. The effects of boundary scattering on electrical conductivity and the Seebeck coefficient are then presented.

2.1 The Boltzmann Transport Equation

Transport phenomena such as the flow of electric current in solids; involve two characteristic mechanisms with opposite effects:

(1) The driving force of the external fields and

(2) The dissipative effect of the scattering of the carriers by phonons and defects.

The interplay between the two mechanisms is described by the Boltzman transport equation. One may investigate how the distribution function of charge carriers in thermal equilibrium is changed in the presence of external forces with the help of this equation and as a result of charge carrier scattering processes. In thermal equilibrium and with no external fields, this distribution function is simply the Fermi-Dirac distribution as defined by:

$$f_0(T,E) = \frac{1}{e^{[E-E_F]/k_BT} + 1} \qquad \textbf{(2-1)}$$

whereE_f and k_B are the Fermi energy and Boltzmann constant respectively. A typical system may consist of charge carriers in a material that is acted upon by stationary external electric and magnetic fields. When the steady state current is flowing, the system is in a dynamical equilibrium. The distribution function for such a system of charge carriers is given by:

$f(x, y, z, u_x, u_y, u_z,)$

where$x, y, z,$ are the coordinates of an electron and u_x, u_y, u_z are velocity components. To derive the equation consider a region of space about the point (x, y, z, u_x, u_y, u_z). The number of particles having position coordinates in the range from $x$to $x + dx$, y to $y + dy$, z to $z + dz$ and velocity coordinates in the range u, to u_x+$du_y u_y$+$du_y u_z$ to $u_z + du_z$ can be represented by the following function:

$f(x, y, z, , u_x, u_y, u_z)$ dx dydz $du_x du_y du_z$.

The time variation of function is due to two independent phenomena:

1-Drift. The function may vary with time because the particles are moving from one region of space to another and are accelerated by external fields during motion. Consider the group of particles at an instant t + dt, that are drifted to a cell of phase space corresponding to the coordinates (x, y, z,u_x, u_y, u_z). The number of particles is the same as were in a cell located at $x - u_x dt, y - u_y dt, z - u_z dt, u_x - \alpha_x dt, u_x - \alpha_y dt, u_z - \alpha_z dt$ at a time t. Here α_x, α_y and α_z are the components of acceleration. The relationship holds for a small time interval dt for which the collisions have no significant effect on the distribution. Thus the change due to drift in number of particles having coordinates x, y, z and velocity u_x, $u_y$and u_z in time dt is given by:

$$(\Delta f)d =$$
$$f(x-u_x dt, y-u_y dt, z-u_z dt, u_x-\alpha_x dt, u_y dt, u_z-\alpha_z dt, t)-f(x, y, z, u_x, u_y, u_z, t) \quad \textbf{(2-2)}$$

Using Taylor's expansion and keeping only first order terms in the limit dt→ 0 the above equation can be expressed as

$$=\left(-u_x\frac{\partial f}{dx}-u_y\frac{\partial f}{dy}-u_z\frac{\partial f}{\partial z}-\alpha_x\frac{\partial f}{\partial u_x}-\alpha_y\frac{\partial f}{\partial u_y}-\alpha_z\frac{\partial f}{\partial u_z}\right)dt$$

Consequently the rate of change of f caused by drift is

$$\left(\frac{df}{dt}\right)_d=-u_x\frac{\partial f}{dx}-u_y\frac{\partial f}{dy}-u_z\frac{\partial f}{\partial z}-\alpha_x\frac{\partial f}{\partial u_x}-\alpha_y\frac{\partial f}{\partial u_y}-\alpha_z\frac{\partial f}{\partial u_z} \quad \textbf{(2-3)}$$

in which subscript d indicates the contribution of drift variation.

2-Scattering mechanisms. Scattering mechanism is due to relatively discontinuous changes in velocity that accompany collisions. If $P(u_{x,}u_y,u_z;u'_x,u'_y,u'_z)du'_x\,du'_y\,du'_z$ represents the probability per unit time that a particle will change its velocity from u_x, u_y, $u_z$to a value having components in the range extending from u'_x *to* $u'_x+du'_z$ etc. the total number the velocity of which alters fromu_x, u_y, u_z to some other value is

$$\text{a} = f(\text{x, y, z, } u_x, u_y, u_z)\int P(u_{x,}u_y,,u_z;u'_x,u'_y,u'_z)du'_x\,du'_y\,du'_z \quad \textbf{(2-4)}$$

similarly, the number the velocity of which changes to u_x, u_y, $u_z$from another values is

$$b=\int f(u''_x,u''_y,u''_z)\theta(u''_x,u''_y,u''_z\,u_x,u_y,u_z)du''_x\,du''_y\,du''_z \quad \textbf{(2-5)}$$

while the $\theta(u''_x,u''_y,u''_z\,u_x,u_y,u_z)du''_x,du''_y,du''$ is the probability per unit time that a particle change its velocity from u''_x,u''_y,u''_z tou_x, u_y, u_z. Thus the rate of change of f caused by collisions is $\left(\frac{df}{dt}\right)_{coll}=b-a.$

The total rate of time variation is sum of the drift variation and the scattering interactions. Hence for equilibrium the sum should vanish *i.e.,* $\left(\frac{df}{dt}\right)_d + \left(\frac{df}{dt}\right)_{coll.} = 0$

Substituting the values from above equations, the following relation is given

$$u_x \frac{\partial f}{\partial x} - u_y \frac{\partial f}{\partial y} - u_z \frac{\partial f}{\partial z} - \alpha_x \frac{\partial f}{\partial u_x} - \alpha_y \frac{\partial f}{\partial u_y} - \alpha_z \frac{\partial f}{\partial u_z} + (b-a) = 0$$
$$-u_x \frac{\partial f}{dx} - u_y \frac{\partial f}{dy} - u_z \frac{\partial f}{dz} - \alpha_x \frac{\partial f}{\partial u_x} - \alpha_y \frac{\partial f}{\partial u_y} + \alpha_z \frac{\partial f}{\partial u_z} = (b-a) \quad \textbf{(2-6)}$$

whichis called Bolltzmann transport equation. Now two cases can be studied:

(1) when the material is homogeneous *i.e.,* at the constant temperature in a field free space, then

$\frac{\partial f}{\partial x}, \frac{\partial f}{\partial y}, \frac{\partial f}{\partial z} = 0$, and $\quad \alpha_x, \alpha_y, \alpha_z = 0$

$\therefore \left(\frac{df}{dt}\right)_{coll.} = 0$

or

$$a = b \quad \textbf{(2-7)}$$

which shows that the number of particles that leave and enter a given volume of momentum space are equal as a result of collisions.

(2) for a heterogeneous medium if there is temperature gradient

$$\frac{\partial f}{\partial x}, \frac{\partial f}{\partial y}, \frac{\partial f}{\partial z} \neq 0 \left(\frac{df}{dt}\right)_{coll.} \neq 0 \quad \textbf{(2-8)}$$

2.2 General Formulation of Charge Transport

The current and heat flux carried by charge in a solid can be written

$$J_e = L_{11}\left(-\frac{d\Phi}{dx}\right) + L_{12}\left(-\frac{d\mathrm{T}}{dx}\right) \quad \textbf{(2-9)}$$

$$J_q = L_{21}\left(-\frac{d\Phi}{dx}\right) + L_{22}\left(-\frac{dT}{dx}\right) \quad \textbf{(2-10)}$$

whereΦ is the electrochemical potential and T is the temperature. From the electron Boltzmann equation under relaxation time approximation, the coefficients can be written as

$$L_{11} = -\frac{e^2}{3}\int \mathrm{v}^{\,2}\,\tau\frac{\partial \mathrm{f_o}}{\partial \mathrm{E}}\mathrm{D}\left(\mathrm{E}\right)\mathrm{dE} = \sigma \quad \textbf{(2-11)}$$

$$L_{12} = \frac{e}{3T}\int \mathrm{v}^2\tau\left(E - E_f\right)\frac{\partial f_o}{\partial E}D\left(E\right)dE \quad \textbf{(2-12)}$$

$$\mathrm{L}_{21} = \frac{\mathrm{e}}{3}\int\left(\mathrm{E} - \mathrm{E}_f\right)\mathrm{v}^2\tau\frac{\partial \mathrm{f_o}}{\partial \mathrm{E}}\mathrm{D}\left(\mathrm{E}\right)\mathrm{dE} = \mathrm{T}\times\mathrm{L}_{12} \quad \textbf{(2-13)}$$

$$\mathrm{L}_{22} = -\frac{1}{3\mathrm{T}}\int\left(\mathrm{E} - \mathrm{E}_f\right)^2\mathrm{v}^2\tau\frac{\partial \mathrm{f_o}}{\partial \mathrm{E}}\mathrm{D}\left(\mathrm{E}\right)\mathrm{dE} \quad \textbf{(2-14)}$$

Here D(E) is the density of states, E is the electron energy, E_f is the chemical potential, f_o is the Fermi-Dirac distribution, e is the absolute charge of an electron, v is the electron group velocity and τ is the relaxation time. Equation (2-11) gives the electrical conductivity. The Seebeck coefficient and electronic contributions to the thermal conductivity are obtained from

$$S = \frac{-d\Phi/dx}{dT/dx} = \frac{L_{12}}{L_{11}} = -\frac{1}{eT}\frac{\int \mathrm{v}^2\tau\left(E - E_f\right)\frac{\partial f_o}{\partial E}D\left(E\right)dE}{\int \mathrm{v}^{\,2}\,\tau\frac{\partial \mathrm{f_o}}{\partial \mathrm{E}}\mathrm{D}\left(\mathrm{E}\right)\mathrm{dE}} \quad \textbf{(2-15)}$$

$$k_e = L_{22} - \frac{L_{12}L_{21}}{L_{11}} \quad \textbf{(2-16)}$$

Band Structures. The density of states and group velocity depend on the band structure. Often, the parabolic band approximation is used. However, for thermoelectric materialsnon-parabolicity should be considered because the dopant concentration is high. The model which is used is a Kane-type dispersion relation:

$$E\left(1+\alpha E\right) = \frac{\hbar^2 k^2}{2m^*} \quad \textbf{(2-17)}$$

where α is the non-parabolicity, k the wave vector and m^* the effective mass.

2.2 Explanation of Calculations

Here the details of the calculations procedure to model bulk and nanostructured materials are explained. In the following discussion, E is the energy, α is the non-parabolicity, $x = E/k_BT$ is the reduced energy, and $\beta = \alpha k_B T$ is the reduced non-parabolicity. The Fermi-Dirac distribution function is denoted f_0 and is given by Equation (2-1). Its derivative, which appears in many of the calculations, is given by:

$$\left(-\frac{\partial f_0}{\partial E}\right) = \frac{1/k_BT}{e^{(E-E_F)/k_BT} + 2 + e^{-(E-E_F)/kT}} = \frac{1/k_BT}{4\cosh^2\left((E-E_F)/2k_BT\right)} \quad \textbf{(2-18)}$$

Determine Fermi level E_f. The Fermi level determines the carrier concentration, which is determined by the dopant concentration. If the number of impurities is N_d and the energy of donor is E_d then the number of impurities that are ionized, and thus the number of donor electrons, is given by:

$$N_i = \frac{N_d}{1 + \frac{1}{2}e^{(E_f - E_d)/T\,k_B}} \quad \textbf{(2-19)}$$

Using Boltzmann statistics the total number of electrons in all the bands using the standard expressions can also be determined:

$$n_d = \sum_i \frac{\sqrt{2}\left(k_BTm_i^*\right)^{3/2}}{\pi^2\hbar^3} F_{1/2}\left(\left(\frac{E_f - E_{(cv),i}}{kT}\right), \beta\right) \quad \textbf{(2-20)}$$

$$F_n(x) = \int_0^\infty \frac{x(1+\beta x)^n(1+2\beta x)}{1+e^x}dx$$

where $E_{(cv),i}$ is the bottom of the conduction band for the i^{th} band, and $\beta=(\alpha/k_BT)$ is normalized non-parobalicity parameter. By enforcing $N_i=n_d$, it can be solved for E_f using an appropriate root-finding method.

Electron/Hole concentration. The electron concentration can be determined from

$$n_e = \frac{\left(2m_{DOS}^3 kT\right)^{3/2}}{3\pi^2\hbar^3}\int_{x_f}^\infty \left(-\frac{\partial f_0}{\partial x}\right)\frac{\left(x+\beta x^2\right)^{3/2}}{1+2\beta x}dx \quad \textbf{(2-21)}$$

Note that this is the number of electrons available for transport and is, in general, not equal to the total number of electrons given by the previous equations.

Screening length. The screening length determines the extent of the electric field generated by an ionized impurity.

$$R^{-2} = \frac{2^{5/2} e^2 (kT)^{1/2}}{\pi \hbar^3 \varepsilon} \sum_i m^*_{DOS,i} \int_{x_f}^{\infty} \left(-\frac{\partial f_0}{\partial x} \right) (x + \beta x^2)^{1/2} (1 + 2\beta x)\, dx \tag{2-22}$$

Conductivity mass. The conductivity mass is used in the calculation of the subsequent transport properties:

$$m^*_{nx} = \frac{3K_n m_{nt}}{2K_n + 1} \frac{\int_{x_f}^{\infty} \left(-\frac{\partial f_0}{\partial x} \right) \left(x + \beta x^2 \right)^{3/2} dx}{\int_{x_f}^{\infty} \left(-\frac{\partial f_0}{\partial x} \right) \frac{\left(x + \beta x^2 \right)^{3/2}}{1 + 2\beta x} dx} \tag{2-23}$$

$$K_n = m_{nl} / m_{nt}$$

The transport properties can now be calculated. These standard expressions are derived from the Boltzmann equation under the relaxation time approximation. The equations are slightly more complex than their standard forms due to the inclusion of non-parabolicity. To account for multiple bands, firstthe transport property for each band is calculated, and then the results are combined in the appropriate linear combination to get the overall transport property.

Mobility. For each valley and scattering mechanism, the mobility can be calculated from

$$\mu = \frac{e}{m_{nx}} \frac{\int_{x_f}^{\infty} \frac{\left(-\frac{\partial f_0}{\partial x} \right) \tau(x) \left(x + \beta x^2 \right)^{3/2}}{1 + 2\beta x} dx}{\int_{x_f}^{\infty} \left(-\frac{\partial f_0}{\partial x} \right) \tau(x) \left(x + \beta x^2 \right)^{3/2} dx} \tag{2-24}$$

To determine the mobility for all scattering mechanisms the total relaxation time, which is determined from Matthiessen's rule is used:

$$\tau^{-1} = \sum_i \tau_i^{-1} \tag{2-25}$$

TheMatthiessen's rule is not applicable for mobilities since the relaxation times do not have the same energy dependence.The overall mobility for all the bands is given by the sum of the mobilities weighted by the normalized electron concentration of each band:

$$\mu_{TOT} = \frac{\sum_i \mu_i n_i}{\sum_i n_i} \tag{2-26}$$

Electrical conductivity. For each band, the electrical conductivity is given by:

$$\sigma = \frac{e^2 \left(2m^*_{DOS} kT\right)^{3/2}}{m_{nx}\pi^2\hbar^3} \int_{x_f}^{\infty} \left(-\frac{\partial f_0}{\partial x}\right) \tau(x) \frac{\left(x+\beta x^2\right)^{3/2}}{1+2\beta x} dx \tag{2-27}$$

The total electrical conductivity is simply the sum of the electron and hole conductivities:

$$\sigma_{TOT} = \sum_i \sigma_{e,i} + \sum_j \sigma_{h,j} \tag{2-28}$$

Seebeck coefficient. The Seebeck coefficient is given by

$$S = -\frac{k_B}{e}\left(\frac{\int_{x_f}^{\infty} \frac{\left(-\frac{\partial f_0}{\partial x}\right)\tau(x)\, x\left(x+\beta x^2\right)^{3/2}}{1+2\beta x} dx}{\int_{x_f}^{\infty} \frac{\left(-\frac{\partial f_0}{\partial x}\right)\tau(x)\left(x+\beta x^2\right)^{3/2}}{1+2\beta x} dx} - x_{Fermi}\right) \tag{2-29}$$

The overall Seebeck coefficient is obtained by weighting each band's contribution by its normalized electrical conductivity:

$$S_{TOT} = \sum_i \frac{S_{e,i}\sigma_{e,i}}{\sigma_{TOT}} + \sum_i \frac{S_{h,i}\sigma_{h,i}}{\sigma_{TOT}} \tag{2-30}$$

Lorentz number. The Lorentz number is given by:

$$L_i = \frac{\sigma_i}{o_{TOT}}\left(\frac{\int_{x_f}^{\infty} \frac{\left(-\frac{\partial f_0}{\partial x}\right)\tau(x)\, x^2\left(x+\beta x^2\right)^{3/2} dx}{1+2\beta x}}{\int_{x_f}^{\infty} \frac{\left(-\frac{\partial f_0}{\partial x}\right)\tau(x)\left(x+\beta x^2\right)^{3/2} dx}{1+2\beta x}} - \frac{\int_{x_f}^{\infty} \frac{\left(-\frac{\partial f_0}{\partial x}\right)\tau(x)\, x\left(x+\beta x^2\right)^{3/2} dx}{1+2\beta x}}{\int_{x_f}^{\infty} \frac{\left(-\frac{\partial f_0}{\partial x}\right)\tau(x)\left(x+\beta x^2\right)^{3/2} dx}{1+2\beta x}}\right)^2 \tag{2-31}$$

The electronic thermal conductivity can be obtained from the Lorentz number using the formula given below. First, however, the bipolar thermal conductivity contribution to the electronic thermal conductivitymust be considered. This type of conduction occurs when carriers moving

between different bands carry heat due to the Peltier effect, and can still transport heat even if the net electric current is zero. The Lorentz number for bipolar conduction is given by:

$$L_b = \left(\frac{e}{k_B}\right)^2 \frac{\sigma_1\sigma_2\left(S_1 - S_2\right)^2}{\left(\sigma_1 + \sigma_2\right)^2} \tag{2-32}$$

Thus we see that bipolar thermal conduction is particularly strong between electrons and holes since the Seebeck coefficients are of the opposite sign. Once the Lorentz numbers are calculated the electrical thermal conductivity can be determined:

$$k_e = \left(\frac{k_B}{e}\right)^2 \left(\sum_i L_{e,i} + \sum_i L_{h,i} + \sum_i L_{b,i}\right)\sigma_{TOT}T \tag{2-33}$$

2.3 Relaxation Times

All the expressions needed to calculate the transport properties of the thermoelectric materials now are available. Next, the relaxation timefor each scattering mechanism must be determined. Assuming the scattering mechanisms are independent the total relaxation time can be determined from Matthiessen's rule, i.e., Equation (2-25). For bulk materials, there are standard expressions for most of the scattering mechanisms, which are enumerated below. The grain-boundary scattering relaxation time, which is used to model nanostructured materials,has been developed. It should be noted that the relaxation time expressions used are typically for non-degenerate semiconductors, and their validity for heavily doped thermoelectric materials are not fully validated, although it was found that we can use them to fit experimental data.

Acoustic phonon scattering. This scattering mechanism is caused by longitudinal phonons compressing and expanding the lattice as they travel through the material. The relaxation time is given by:

$$\frac{1}{\tau} = \frac{kTE_{ac}^2}{N_v v_s^2 \rho} \frac{\sqrt{2}\left(m_{DOS}^*\right)^{3/2}}{\pi\hbar^4} \sqrt{E + \alpha E^2}\left(1 + 2\alpha E\right) \tag{2-34}$$

where E_{ac} is the deformation potential, v_s is the sound speed, and ρ is the mass density. The correction for anisotropic bands can be conducted as:

$$K_a = E_{av} / E_{ac}$$
$$A = \frac{\beta x\left(1-K_a\right)}{1+2\beta x}$$
$$B = \frac{8\beta x\left(1+\beta x\right)K_a}{3\left(1+2\beta x\right)^2} \qquad \textbf{(2-35)}$$
$$\tau' = \frac{\tau}{\left(\left(1-A\right)^2 - B\right)}$$

Optical phonon scattering. Optical phonon scattering is similar to acoustic deformation potential scattering except that the deformation potential E_{ac}becomes $E_{ac}= \hbar\omega_0$, and it is assumed that K_a is the same as in the acoustic case.

$$\tau_0 = \frac{2\hbar^2 a^2 \rho\left(\hbar\omega\right)^2}{\pi\left(2m^*_{DOS}kT\right)^{3/2}E^2_{OC}}$$
$$A = \frac{\beta x\left(1-K_{op}\right)}{1+2\beta x}$$
$$B = \frac{8\beta x\left(1+\beta x\right)K_{op}}{3\left(1+2\beta x\right)^2} \qquad \textbf{(2-36)}$$
$$\tau = \frac{\tau_0}{\sqrt{x+\beta x^2}\left(1+2\beta x\right)\left(\left(1-A\right)^2 - B\right)}$$

Ionized impurity scattering. Thermoelectric materials are usually highly doped. When the dopants become ionized they generate a net electric field which scatters electrons as they pass through the lattice. This scattering mechanism is called ionized impurity scattering, and it is one of the most important scattering mechanisms at low temperature. The somewhat complicated expression for the ionized impurity relaxation time is given below [37]:

$$\frac{1}{\tau} = 8\pi\left(\frac{1}{64\hbar k^4}\left(\frac{4\pi Ze^2}{\varepsilon}\right)^2\right) g \cdot F \cdot N_I$$

$$g = \frac{\sqrt{2}m_{DOS}^{3/2}}{\pi^2\hbar^3}\sqrt{E\left(1+\alpha E\right)}\left(1+2\alpha E\right)$$

$$F = \begin{cases} \dfrac{z^2}{2}+\dfrac{2}{3}z^3 & z<10^{-5} \\ \ln\left(\dfrac{1+z}{e^{z-z^2/2}}\right)+z-z^2/2-\dfrac{z}{1+z} & z<1 \\ \ln\left(1+z\right)-\dfrac{z}{1+z} & o/w \end{cases} \qquad \textbf{(2-37)}$$

$$z = \left(2kR\right)^2$$

$$k = \left(\frac{2m_{DOS}^{*}E\left(1+\alpha E\right)}{\hbar^2}\right)^{1/2}$$

Polar longitudinal optical phonon scattering. In materials where there are two or more constituent atoms, such as GaAs, it is possible for the bond to become ionic, with each atom becoming slightly oppositely charged. When a phonon travels through the solid and deforms the lattice, a perturbing potential is generated which can scatter electrons. This scattering is called polar longitudinal optical scattering when the phonon is in the optical branch and piezoelectric scattering when the phonon is acoustic. Piezoelectric scattering is negligible compared to polar optical scattering at the temperature ranges of interest and is not included in the calculations.
Polar optical scattering is one of the most important scattering mechanisms at high temperature for polar materials. Strictly speaking, defining a relaxation time for this scattering mechanism is impossible since the collision is not elastic. However, when the thermal energy k_BT is much smaller than the collision energy the collision can be taken as nearly elastic and a relaxation time can be defined. The relaxation time is taken from Gelmont and Shur, who show that their relaxation time also extrapolates well to high temperature [38]

$$\frac{1}{\tau} = \frac{4\pi\varepsilon_0\hbar}{3e^2N_0}\left(\frac{1}{1/\varepsilon_\infty - 1/\varepsilon_0}\right)\sqrt{\frac{2\hbar}{m_{DOS}^{*}\omega_{op}\left(1+\hbar\omega_{op}\alpha\right)}}\frac{x+\beta x^2}{1+2\beta x} \qquad \textbf{(2-38)}$$

Alloy scattering. In randomly distributed alloys the lattice will not be uniform due to the distribution of different types of atoms throughout the material. These non-uniformities in the lattice can act as scattering sites for electrons. This scattering mechanism is known as alloy scattering, and, though it is not a primary scattering mechanism, can alter the calculated transport properties by up to ten percent. The standard expression for alloy scattering is given as:

$$\frac{1}{\tau}=\frac{3\sqrt{2}}{32}\frac{\pi a^3 U_a^2 m_{DOS}^*}{\hbar^4 N_v}x(1-x)\sqrt{E(1+\alpha E)}(1+2\alpha E) \quad \textbf{(2-39)}$$

Intervalley scattering. Intervalley scattering, both between equivalent and non-equivalent valleys, occurs at a far slower rate than do the other scattering mechanisms, and as a result it is usually neglected. The relaxation time for equivalent valley scattering is given by:

$$E_f = E \pm \hbar\omega_0$$

$$N_i = \frac{1}{e^{\hbar\omega/kT}-1}\pm\frac{1}{2} \quad \textbf{(2-40)}$$

$$\frac{1}{\tau}=\sum_i \frac{(Z-1)m_{DOS}^{3/2}D_{ij}^2}{\sqrt{2}\pi\hbar^3\omega\rho}\sqrt{E_f(1+\alpha E_f)}(1+2\alpha E_f)N_i$$

where Z is the number of equivalent valleys, ħω corresponds to the intervalley phonon energy, and the plus or minus in E_f indicates the absorption or emission of a phonon, respectively.

Short range vacancy scattering [39]. Some materials have large amount of vacancies that also serve as doping mechanism. The vacancy scattering is given by

$$\tau_0 = \frac{\pi\hbar^4}{m_{DOS}(2m_{DOS}kT)^{1/2}U_{vc}^2 N_{vc}}$$

$$A = \frac{\beta x(1-K_{vc})}{1+2\beta x} \quad \textbf{(2-41)}$$

$$B = \frac{8\beta x(1+\beta x)K_{vc}}{3(1+2\beta x)^2}$$

$$\tau = \frac{\tau_0}{(x+\beta x^2)^{1/2}(1+2\beta x)\left((1-A)^2-B\right)}$$

2.4 Electron Transport over Nanoscale Grain Boundaries

The strong influence that the nanocomposite exerts on the electron and phonon properties is connected with the increased interfacial scattering at GBs as a result of the small grainsizes (~40nm). In addition to the common scattering mechanisms in bulk material, electrons in nanostructured material experience further scatterings from the induced crystal defects. Defects introduce potential barriers that can scatter electrons and affect the thermoelectric efficiency. These defects can include vacancies, dislocations, or the grain boundaries (GBs) space charge potentials. Unlike in conventional electronic materials where defects deteriorate electronic properties of the material and are not favored, in thermoelectric materials they can improve the

energy conversion efficiency by scattering lower energy carriers, and thus resulting in higher Seebeck coefficient, S.

Grain boundaries (GBs) are two dimensional networks or line charges in juxtaposition. The broken bounds at these interfaces attract free carriers and form a space charge. The high density of states at GBs (broken bonds) and a space charge on either side represents a double Schottky barrier at the boundary; thereby a high resistance to lateral current flow. Early works on modeling of GBs in polycrystalline materials used a double diode or two back-to-back diodes model [40]. There have been several models for the conductivity of the GBs since then. Most researchers now start with the simple Richardson thermionic emission expression for the current across the barrier that for the case of non-degenerate semiconductor is [41]:

$$I = A^{*}T^{2}\exp(-\Phi_{B}/k_{B}T)\exp(\frac{E_{F}-E_{C}}{k_{B}T})\times[\exp(eV_{e}/k_{B}T)-1] \quad \textbf{(2-42)}$$

where Φ_B is the barrier height, V_e is the external voltage, and A^* is the Richardson's constant. Nanocomposites compared to polycrystalline materials have smaller grains and possess completely random crystal orientations that require some additional considerations. Moreover, thermoelectric properties of the nanocomposites, is more interesting than only the carrier mobility. GBs can increase the Seebeck coefficient and thus the thermoelectric power factor. The potential barrier at GBs act as carrier energy filters as shown in Figure 2.1, eliminating lower energy carriers that results in an improvement of the efficiency of thermoelectric energy conversion (energy filtering method).

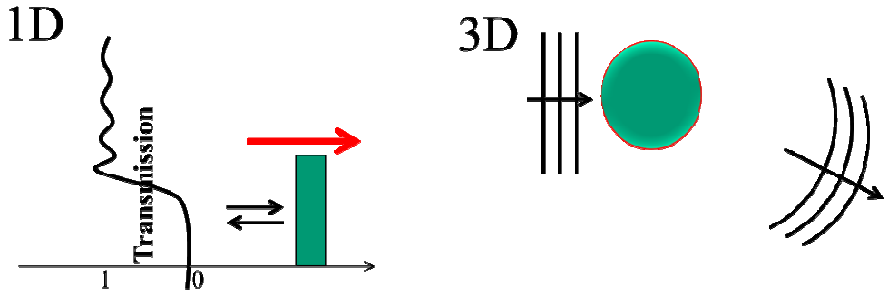

Figure 2.1: Sharp energy cutoff for the allowed electrons increases the power factor significantly. Only electrons with energy higher than barrier can pass it. For low energy electrons the transmission is almost zero.

There are several mechanisms for the existence of an interfacial potential. One is accumulation of charge at interface; another is due to different orientations of adjacent grains.

Space charge. The space charge extension can be approximated by solving the Poisson's equation in connection with the expression for the potential energy of a degenerate electron gas:

$$\frac{d^{2}\varphi}{dx^{2}} = -4\pi e p(x)/\varepsilon \quad \textbf{(2-43)}$$

$$e(\varphi_B - \varphi) = \frac{h^2}{2m^*}\left(\frac{3}{8\pi}\right)^{2/3} p(x)^{2/3} \qquad \textbf{(2-44)}$$

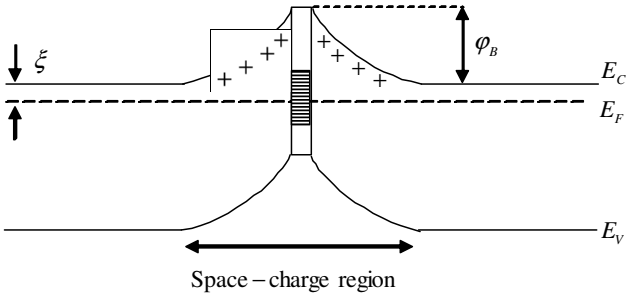

Figure 2.2: Space charge domain at a grain boundary.

Eliminating φ and integrating under appropriate boundary conditions lead to p(x) and hence the size of the depletion region. Figure 2.2 shows the space-charge region at a sample grain boundary.

In order to find φ_B, some arbitrary assumption has to be made about the form of the distribution and density of the trap states in the boundary. For instance, one may assume a mono-energetic distribution of states $N_t(E)$. Therefore, φ_B can be calculated from:

$$Q_{sc} = \left(\frac{8\varepsilon\varepsilon_0 N_G \varphi_B}{e^2}\right)^{1/2} = w\int_{E_v}^{E_C} N_t(E)dE \qquad \textbf{(2-45)}$$

where N_G is the doping level in the grains, and w is the width of the grain boundary region and Q_{sc} is the total number of trap states in the grain-boundary region. Such potential barriers form when the GB region has a lower chemical potential for majority carriers than the grains. The incident majority carriers into the barrier region create a space charge which repels further flow of majority carriers. Therefore, if the chemical potential of the GB region lies somewhere in the middle of the band gap, the barriers exist in both n and p type nanocomposite material. Otherwise, if it lies close to thevalance (or conduction) band, the GB boundary barrier only exists in the n (or p) type nanocomposite material.

Potential barrier due to crystallographic orientation difference. Apart from the space charge potential barrier, electrons may experience a potential barrier (or well) due to the rotation of the adjacent grains. For example, an electron moving in L valley in one grain has to enter the Σ valley in the next grain, which, in lead telluride as an example, presents a potential barrier of about 0.7 eV.

Intervalley Scattering at GBs. In a nanocomposite, the grains are randomly distributed with an arbitrary crystal orientation. Electrons with sufficiently large energies can pass over the barrier

and enter a different valley in the adjacent grain. Electrons with smaller energies may encounter an intervalley scattering and enter an equivalent valley in the adjacent grain. Figure 2.3 shows how an electron enters an equivalent valley after encountering an intervalley scattering. This can happen through electron scattering by phonons or the interface roughness potential. Such scatterings reduce the boundary resistance as they provide alternate means for electron transport between the grains. The electron conductivity due to the intervalley scattering at GBs can be estimated by:

$$\sigma_v = e^2 \ell^2 \frac{d}{d\varepsilon}\left(\frac{n}{\tau_v}\right) \qquad \textbf{(2-46)}$$

where ℓ is the electron mean free path.

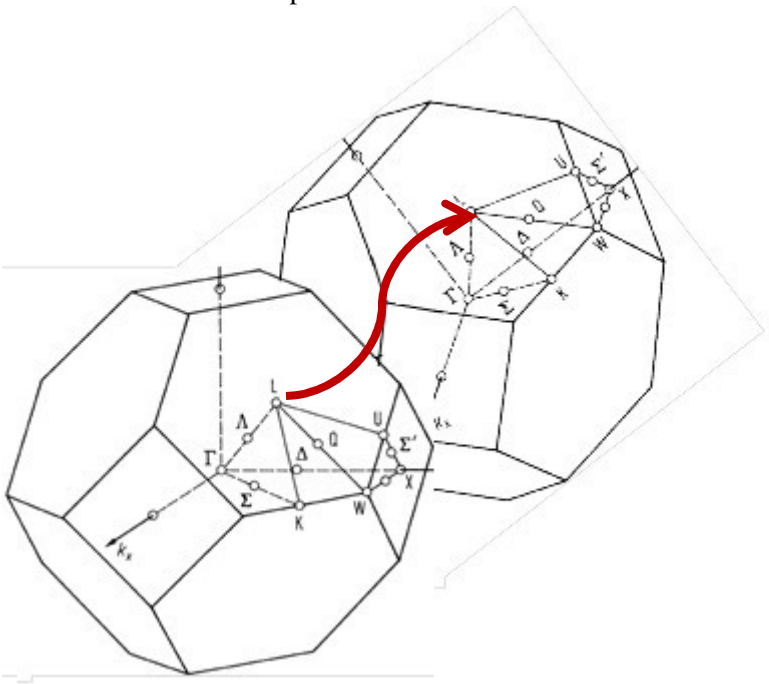

Figure 2.3: Equivalent intervalley scattering between adjacent grains.

Interface roughness. The above calculations represent the importance of each process at GB. Interface roughness scattering at the GBs decreases the electron mobility in the material. However, the roughness scattering can lead to a significant increase in the thermionic current. Interface scattering conserves energy but not for interfaces parallel to wave vector. Therefore, the scattering at the interfaces mixes the planar motion of the carriers with the longitudinal motion perpendicular to the GBs, and removes the requirement for the conservation of transverse momentum. In this case, the transmission probability depends on the total kinetic energy of the electrons rather than only the perpendicular component to the barrier. This will dramatically increase the number of electrons that are transmitted over the barrier, which significantly increase the electrical conductivity. Non-conservation of transverse momentum does not significantly

change the Seebeck coefficient; therefore, optimizing the material parameters (such as doping and barrier height) to gain an overall benefit from the interface roughness scattering is possible.
For an accurate treatment of the interface scattering, one needs to develop a more comprehensive model that includes all the important effects. Interface roughness scattering must be properly modeled as interface roughness scattering can have a significant effect on the electron mobility and the transmission probability at GBs. For this purpose, one may model the interface roughness potential by an effective height Δ and a lateral correlation length Λ of a Gaussian fluctuation. Therefore, the perturbation potential is a random potential that is assumed to have a Gaussian distribution with the following autocorrelation:

$$< U(r)U(r') >= U_0^2 \Delta^2 \delta(x - L/2)\delta(x' - L/2)\exp(-\frac{(r-r')^2}{\Lambda^2}) \quad \textbf{(2-47)}$$

where $< \cdots >$ is an ensemble average, U_0 is the barrier height, and L is the size of the grain. *r* and *r′* are in the plain of free motion, *x* and *x′* are normal to the GB (boundaries are at $x = \pm L/2$). This expression can be used to calculate the square of the matrix element for the roughness scattering:

$$\left|M_{kk'}\right|^2 = \left|< k' | U(r) | k >\right|^2 \quad \textbf{(2-48)}$$

where k and k′ correspond to the initial and final states.

Energy relaxation length. Carriers that are passed over the barrier have higher average energy than carriers far from the barrier. Carrier distribution function becomes that of the bulk material in a length equal to the energy relaxation length ℓ_E from the barrier. If the grain sizes do not exceed ℓ_E, the carrier distribution function does not return to that of the bulk between GBs. Also, if the momentum relaxation length is much shorter than the distance between the GBs, the behavior of the carriers with energies greater than that of the barrier may be similar to that of carriers in the bulk. In other words, for carriers with energies above those of barriers, the differentialconductivity $\sigma(\varepsilon)$ of a material with potential barriers can be approximated by that of the material without potential barriers if $\ell_m << \ell$. Therefore, under the condition of $\ell_m << \ell < \ell_E$,the energy relaxation time for the filtered electrons from the following expression can be calculated:

$$\frac{\langle \varepsilon \rangle_{Filtered} - \langle \varepsilon \rangle_{Bulk}}{\tau_\varepsilon} = \left\langle -\frac{d\varepsilon}{dt} \right\rangle_{Coll} \quad \textbf{(2-49)}$$

where:

$$\left\langle -\frac{d\varepsilon}{dt}\right\rangle_{Coll} \equiv \frac{\int_{\varepsilon B}^{\infty} d\varepsilon \varepsilon g(\varepsilon)\left(\frac{\partial f}{\partial t}\right)_{Coll}}{\int_{\varepsilon B}^{\infty} d\varepsilon g(\varepsilon) f^{0}(\varepsilon)} \tag{2-50}$$

$\left(\frac{\partial f}{\partial t}\right)_{Coll}$ is the collision term in the Boltzmann equation. Energy averages are given by:

$$\langle \varepsilon \rangle_{Bulk} \equiv \frac{\int_{0}^{\infty} d\varepsilon \varepsilon g(\varepsilon) f^{0}(\varepsilon)}{\int_{0}^{\infty} d\varepsilon g(\varepsilon) f^{0}(\varepsilon)} \quad \text{and} \quad \langle \varepsilon \rangle_{Filtered} \equiv \frac{\int_{\varepsilon B}^{\infty} d\varepsilon \varepsilon g(\varepsilon) f^{0}(\varepsilon)}{\int_{\varepsilon B}^{\infty} d\varepsilon g(\varepsilon) f^{0}(\varepsilon)} \tag{2-51}$$

Using the hot electron theory [42], the energy relaxation time can be calculated as:

$$\tau_{\varepsilon} = \frac{\pi \rho \hbar^{4}}{2^{3/2} m^{*5/2} E_{ac}^{2} \xi_{B}^{2} (k_{B}T)^{1/2}} \times \left[F_{3/2}(\xi_{B}, \eta) - F_{3/2}(0, \eta) \frac{F_{1/2}(\xi_{B}, \eta)}{F_{1/2}(0, \eta)} \right] \tag{2-52}$$

where ξ_B is the reduced barrier height $\varepsilon_B / k_B T$, and it is defined that:

$$F_{s}(a, \eta) \equiv \int_{a}^{\infty} d\varepsilon \frac{\varepsilon^{s}}{e^{\varepsilon - \eta} + 1} \tag{2-53}$$

Energy relaxation length can be approximated from the following expression:

$$\frac{\ell_e}{\ell_m} \approx \left\langle \frac{1}{\tau_m} \right\rangle \tau_{\varepsilon} = \frac{k_B T}{2 m^{*} v_s^{2} \xi_B^{2}} \left[\frac{F_{3/2}(\xi_B, \eta)}{F_{1/2}(\xi_B, \eta)} - \frac{F_{3/2}(0, \eta)}{F_{1/2}(0, \eta)} \right] \left[F_{1}(\xi_B, \eta) + r F_{-1}(\xi_B, \eta) \right] \tag{2-54}$$

where *r* is the ratio of the impurity scattering to acoustic phonon scattering.

Spherical potential model. At presence of such potential barriers, carriers that are passed over the barriers have higher average energy than carriers far from the barriers. Under the condition of $\ell_m << \ell < \ell_E$, energy filtering mechanism can increase the effective material Seebeck coefficient. It is also understood that since such defects can reduce the electron mobility,

the overall effect appears in the power factor $S^2\sigma$. For this reason, studying in detail the effect of defects in a nanocomposite is essential.

For small particles embedded inside a host, such particles can be a specific grain of any material or its alloy embedded in a larger domain crystalline material, or a cluster of impurity atoms, we can approximate the grain/particle as a spherical region with a constant potential height. A model for the charge scattering process at GBs that can be combined with the relaxation time approximation of the Boltzmann transport equation has been developed. This model enables us to study the energy filtering mechanism consistently with the size and distribution of the grains. In this mode, the scattering center is considered as a spherical potential of magnitude U_0. The bending of the bands at GBs will be neglected and it will be assumed that the electron scattering is elastic. The first step to estimate the quantum mechanical momentum relaxation time is to calculate the Hamiltonian matrix element $H_{kk'}$ from:

$$H_{kk'} = \langle \psi_k | U(r) | \psi_{k'} \rangle \qquad \textbf{(2-55)}$$

Here, $U = U_c \Theta(\mathrm{r} - r_c) e^{-\frac{z}{z_c}}$ is a potential barrier with cylindrical symmetry at the interface, where z_c models the width of the space charge region and r_c models the lateral extension of the scattering potential. U_c is the strength of the potential barrier. Θ is the Heaviside step function. An exponentially decaying potential was chosen to model the depletion region in the GB region. Figure 2.4 presents a crystallite interface scattering potential modeled with a disk-shaped potential.

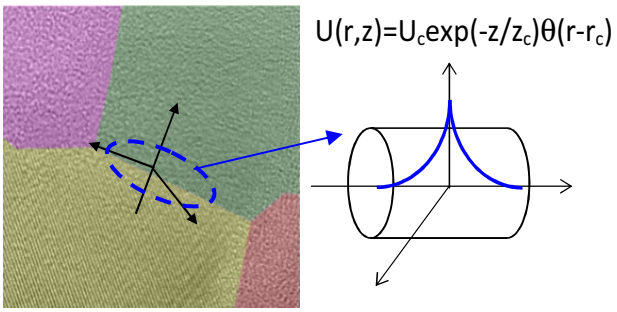

Figure 2.4: Schematic diagram of the crystallite interface scattering potentials modeled with disk-shaped potentials with exponential decay in direction normal to the interface.

In a rigorous calculation of the matrix element, we must use the matrix element of the full Hamiltonian of the crystal plus grain boundaries between the Bloch functions of the band. To simplify the calculations, a free electron gas wave-function is assumed which is often also used for treating common scattering mechanisms such as scatterings by ionized impurities or phonons. The total inverse momentum relaxation time is calculated from:

$$\frac{1}{\tau_m} = \frac{2\pi}{\hbar}\sum_{\vec{k}'}\left|\left\langle \psi_k \middle| U(r) \middle| \psi_{k'} \right\rangle\right|^2 \left(1-\cos(\theta)\right) \tag{2-56}$$

When the electron energy is less than the potential height, the electron is completely reflected off the boundary, and the scattering process does not couple the different components of the electron wave-vectorby assumption; therefore, the transverse momentum of the electron is conserved. The momentum relaxation time is thus numerically calculated as follows:

$$\frac{1}{\tau_m(E_k)} = \frac{\pi^3 U_0^2 g(E_k)}{2V\hbar k^6} \times \begin{cases} \frac{1}{2}\left[Sin(\xi) - \xi Cos(\xi)\right]^2 & for \quad E_k < U_0 \\ \xi Sin(2\xi) - Sin^2(\xi) + \xi^2\left[\ln(2\xi) + \gamma - Ci(2\xi) - 1\right] & for \quad E_k > U_0 \end{cases} \tag{2-57}$$

where V is the volume, k is the electron wave vector, $\xi = 2kR$, $g(E_k)$ is the electron density of states, γ is the Euler's constant, and Ci is the so called Cosine Integral [43]. This form of relaxation time allows including the effect of non-parabolicity of the band, for example, within the Kane's model. In the limit of small ξ, Equation

(2-57) shows that the energy dependent momentum relaxation time changes with $E^{-1/2}$ versus energy, which is similar to the energy dependency of the small point defects [44]. In the limit of large ξ when $E_k > U_0$, the relaxation time changes with $E^{3/2}$, which is similar to the characteristics of ionized impurity scattering [44]. In the latter limit when $E_k < U_0$, the scattering rate oscillates due to the wave nature of the reflection, and its envelope approaches to zero with a similar energy dependency as in $E_k > U_0$.

$$\frac{1}{\tau_m(E_k)} = \frac{\pi^3 U_0^2 g(E_k)}{2V\hbar k^6} \times \begin{cases} \frac{1}{2}\left[Sin(\xi) - \xi Cos(\xi)\right]^2 & for \quad E_k < U_0 \\ \xi Sin(2\xi) - Sin^2(\xi) + \xi^2\left[\ln(2\xi) + \gamma - Ci(2\xi) - 1\right] & for \quad E_k > U_0 \end{cases} \tag{2-58}$$

For grains with randomly different sizes with a normal distribution we have:

$$\frac{1}{\tau(E_k)} = \int_{-\infty}^{\infty} \frac{1}{\tau(E_k)} \left[\frac{1}{2\sqrt{\pi\sigma^2}} e^{-\frac{(\varepsilon - E_k)^2}{2\sigma^2}} \right] d\varepsilon$$

$$= \frac{\pi^3 U_0^2 g(E_k)}{2V\hbar k^6} F \qquad \textbf{(2-59)}$$

For $E_k < U_0$ this result in:

$$F = \frac{1}{2}\left(\frac{2\sqrt{2}\sigma}{\sqrt{\pi}} e^{-\frac{E_k^2}{2\sigma^2}} + E_k\left(1 + \operatorname{erf}\left(\frac{E_k}{\sqrt{2}\sigma}\right)\right)\right)\left(\frac{2\sqrt{2}\sigma}{\sqrt{\pi}} e^{-\frac{E_k^2}{2\sigma^2}} + E_k\left(1 + \operatorname{erf}\left(\frac{E_k}{\sqrt{2}\sigma}\right)\right)\right)$$
$$+ \frac{1}{2}\left(\frac{2\sqrt{2}\sigma}{\sqrt{\pi}} e^{-\frac{E_k^2}{2\sigma^2}} + E_k\left(1 + \operatorname{erf}\left(\frac{E_k}{\sqrt{2}\sigma}\right)\right)\right)\left(\frac{2\sqrt{2}\sigma}{\sqrt{\pi}} e^{-\frac{E_k^2}{2\sigma^2}} + E_k\left(1 + \operatorname{erf}\left(\frac{E_k}{\sqrt{2}\sigma}\right)\right)\right)$$
$$+ \frac{1}{2}\left(\frac{2\sqrt{2}\sigma}{\sqrt{\pi}} e^{-\frac{E_k^2}{2\sigma^2}} + E_k\left(1 + \operatorname{erf}\left(\frac{E_k}{\sqrt{2}\sigma}\right)\right)\right)\left(\frac{\sigma^2}{\sqrt{\pi}} e^{-\frac{E_k^2}{2\sigma^2}} + \frac{E_k}{2}\left(1 + \operatorname{erf}\left(\frac{E_k}{\sqrt{2}\sigma}\right)\right)\right)$$
$$+ \frac{1}{3}\left(\frac{\sigma^2}{\sqrt{\pi}} e^{-\frac{E_k^2}{2\sigma^2}} + \frac{E_k}{2}\left(1 + \operatorname{erf}\left(\frac{E_k}{\sqrt{2}\sigma}\right)\right)\right)\left(\frac{2\sqrt{2}\sigma}{\sqrt{\pi}} e^{-\frac{E_k^2}{2\sigma^2}} + E_k\left(1 + \operatorname{erf}\left(\frac{E_k}{\sqrt{2}\sigma}\right)\right)\right)$$
$$+ \frac{1}{8}\left(\frac{\sigma^2}{\sqrt{\pi}} e^{-\frac{E_k^2}{2\sigma^2}} + \frac{E_k}{2}\left(1 + \operatorname{erf}\left(\frac{E_k}{\sqrt{2}\sigma}\right)\right)\right)\left(1 + e^{-\frac{E_k^2}{2\sigma^2}}\right)$$
$$+ \frac{1}{4}\left(\frac{\sigma^2}{\sqrt{\pi}} e^{-\frac{E_k^2}{2\sigma^2}} + \frac{E_k}{2}\left(1 + \operatorname{erf}\left(\frac{E_k}{\sqrt{2}\sigma}\right)\right)\right)\left(\frac{\sigma^2}{\sqrt{\pi}} e^{-\frac{E_k^2}{2\sigma^2}} + \frac{E_k}{2}\left(1 + \operatorname{erf}\left(\frac{E_k}{\sqrt{2}\sigma}\right)\right)\right)$$
$$+ \frac{1}{4}\left(\frac{\sigma^2}{\sqrt{\pi}} e^{-\frac{E_k^2}{2\sigma^2}} + \frac{E_k}{2}\left(1 + \operatorname{erf}\left(\frac{E_k}{\sqrt{2}\sigma}\right)\right)\right)^2$$
$$+ \frac{1}{4}\left(\frac{\sigma^2}{\sqrt{\pi}} e^{-\frac{E_k^2}{2\sigma^2}} + \frac{E_k}{2}\left(1 + \operatorname{erf}\left(\frac{E_k}{\sqrt{2}\sigma}\right)\right)\right)\left(\frac{2\sqrt{2}\sigma}{\sqrt{\pi}} e^{-\frac{E_k^2}{2\sigma^2}} + E_k\left(1 + \operatorname{erf}\left(\frac{E_k}{\sqrt{2}\sigma}\right)\right)\right) + \frac{1}{2}\left(\frac{2\sqrt{2}\sigma}{\sqrt{\pi}} e^{-\frac{E_k^2}{2\sigma^2}} + E_k\left(1 + \operatorname{erf}\left(\frac{E_k}{\sqrt{2}\sigma}\right)\right)\right)\left(\frac{\sigma^2}{\sqrt{\pi}} e^{-\frac{E_k^2}{2\sigma^2}} + \frac{E_k}{2}\left(1 + \operatorname{erf}\left(\frac{E_k}{\sqrt{2}\sigma}\right)\right)\right)$$
$$+ \left(\frac{\sigma^2}{\sqrt{\pi}} e^{-\frac{E_k^2}{2\sigma^2}} + \frac{E_k}{2}\left(1 + \operatorname{erf}\left(\frac{E_k}{\sqrt{2}\sigma}\right)\right)\right)^2 \qquad \textbf{(2-60)}$$
$$+ \frac{1}{2}\left(\frac{\sigma^2}{\sqrt{\pi}} e^{-\frac{E_k^2}{2\sigma^2}} + \frac{E_k}{2}\left(1 + \operatorname{erf}\left(\frac{E_k}{\sqrt{2}\sigma}\right)\right)\right)\left(\frac{1}{2} + \frac{1}{2}\operatorname{erf}\left(\frac{E_k}{\sqrt{2}\sigma}\right)\right)$$

where *erfi* is the imaginary error function [43].

This form of relaxation time allows including the effect of non-parabolicity of the band, for example, within the Kane's model. The model predicts that in the limit of large electron wavelength compare to the radius of the sphere, the energy dependent momentum relaxation time changes with $E^{-1/2}$ versus energy, which is similar to the energy dependency of the small point defects [44]. In the limit of large wavelength when $E_k > U_0$, the relaxation time changes with $E^{3/2}$, which is similar to the characteristics of ionized impurity scattering [45]. In the latter limit when $E_k < U_0$, the scattering rate oscillates due to the wave nature of the reflection, and its envelope approaches to zero with a similar energy dependency as in $E_k > U_0$.

2.5 Treating Some Special Systems

The results developed in the last section are applicable to simulate most of bulk thermoelectric materials. Here the difficulties unique to modeling special systems are examined. Some problems possibly can arise:

- Several scattering mechanisms are usually acting at a given carrier density and temperature; therefore, dependence of the relaxation time $\tau(\varepsilon)$ cannot be represented by a power law. The reciprocal of the relaxation times due to the different scattering processes $\tau_i(\varepsilon)$ can be summed to estimate the total relaxation time as follows:

$$\tau(\varepsilon)^{-1} = \sum_i \tau_i(\varepsilon)^{-1} \qquad \textbf{(2-61)}$$

- The energy band is anisotropic with ellipsoidal constant-energy surface and two components of longitudinal $m_{\parallel}$ and transverse $m_{\perp}$ effective mass. Therefore, the dependence of the relaxation time on the direction of the electron crystal momentum relative to the ellipsoid axes is different for different scattering mechanisms. In particular, with the acoustical scattering that is the dominant scattering process over a wide range of temperature and doping concentration, the relaxation time depends weakly on the direction and is practically inversely proportional to the effective density-of-state mass:

$$m_d = (m_{\parallel}^* m_{\perp}^2)^{3/2} \qquad \textbf{(2-62)}$$

  This is in contrast with the case of ionized impurities where the scattering is anisotropic.

- The system has a non-parabolic band where the dependence of the carrier energy on the crystal momentum is non-quadratic at sufficiently high energies. This implies that the effective mass has the energy-dependence:

$$m^* = \left(\frac{1}{\hbar^2} \frac{1}{k} \frac{d\varepsilon}{dk} \right)^{-1} \quad \textbf{(2-63)}$$

The same mass gives the density of states $g(\varepsilon)$ and is used in the calculation of the relaxation times:

$$\tau \alpha \frac{1}{|M|^2 g(\varepsilon)} \quad \textbf{(2-64)}$$

where M is the average matrix element of the interaction of the electron with a scatterer. The influence of the non-parabolicity on the momentum dependence of the relaxation time enters only through the density of states as the matrix element is assumed to depend on the value of the crystal momentum in the same way as inthe case of parabolic band. For the specific case of acoustic scattering, the matrix element is independent of the crystal momentum and the quantity τg does not vary with the carrier energy.

- The bandgap is small (< 0.5 eV). Therefore, at relatively higher temperatures, or low carrier densities, contributions from both the conduction and valance bands become comparable and use of a two-band model is necessary. For the two-band model, the total electrical conductivity is $\sigma_n + \sigma_p$ and Seebeck coefficient is given by:

$$S = \frac{\sigma_n S_n + \sigma_p S_p}{\sigma_n + \sigma_p} \quad \textbf{(2-65)}$$

where subscripts n and p refer to contributions from electron and hole bands respectively.

- The effective mass is strongly temperature dependent, which contributes to the temperature dependency of the carrier mobility. The temperature dependency is particularly strong in the scattering by the acoustic phonons, when the mobility is proportional to $m^{*-5/2}$.

Transport coefficients are derived from Boltzmann equation in the framework of relaxation time approximation. Electrical conductivity depends on the carrier density and mobility which itself depends upon the mean free path lengths between successive collisions. In lead telluride material, the carriers are primarily scattered by the thermal vibrations of the crystal lattice and ionized impurities. The latter is only important at very large doping concentrations (>10^{20} cm^{-3}). Both the acoustic and the optical phonon modes must be considered in the temperature range of interest. The relaxation times for the electron scattering by acoustic and optical modes are given by [46]:

$$\frac{1}{\tau_{ac}(z)} = \frac{\pi k_B T_\rho(z) \Xi^2}{\hbar C_1 N}\left[1 - \frac{8\beta(z+\beta z^2)}{3(1+2\beta z)^2}\right] \quad \textbf{(2-66)}$$

$$\frac{1}{\tau_{op}(z)} = \frac{2^{1/2} k_B T e^2 m_d^{*1/2}(\varepsilon_\infty^{-1} - \varepsilon_0^{-1})}{\hbar^2 (z k_B T)^{1/2}} \frac{1+2\beta z}{(1+\beta z)^{1/2}} \left\{\left[1 - \delta \ln\left(1+\frac{1}{\delta}\right)\right] - \frac{2\beta(z+\beta z^2)}{(1+2\beta z)^2}\left[1 - 2\delta + 2\delta^2 \ln\left(1+\frac{1}{\delta}\right)\right]\right\}, \quad \textbf{(2-67)}$$

Here C_1 is the elastic constant, Ξ is the deformation potential constant, ε_∞ and ε_0 are the high frequency and static dielectric constants. z is the reduced energy $z = \varepsilon / k_B T$ and β is the dimensionless non-parabolicity factor $\beta = k_B T / \varepsilon_g$.

Also:

$$\delta(z) = (2 k r_{SC})^{-2}, \quad \textbf{(2-68)}$$

The electron wave vector including the nonparabolicity of the band is:

$$k^2 = \frac{2 m_d^*(z k_B T)(1+\beta z)}{\hbar^2}; \quad \textbf{(2-69)}$$

r_{sc} is the electron screening length given by:

$$r_{SC}^{-2} = \frac{2^{5/2} e^2 m_d^{*3/2} (k_B T)^{1/2}}{\pi \hbar^3 \varepsilon_\infty} {}^0L_1^{1/2} \quad \textbf{(2-70)}$$

where we have the following definition:

$${}^nL_k^m = \int_0^\infty (-\frac{\partial f}{\partial z}) z^n (z+\beta z^2)^m (1+2\beta z)^k dz \quad \textbf{(2-71)}$$

Ionized impurity scattering

Ionized impurity scattering is an important factor in determining the charge transport in highly doped regime. Ionized impurity scattering is often formulated with either the Born approximation or the more exact partial-wave method. The formalism given by Csavinsky [47]which uses a combination of the variational and perturbation technique in the partial-wave method has been followed in this dissertation. This method for the calculation of the resistivity of ionized impurity

scattering is valid over a large range of doping concentration that neither the uncorrelated Born approximation nor the simplest form of the partial-wave method can be applied.

Thermal Conductivity

At high doping concentration the electronic and hole contributions may become significant. In the intrinsic conduction the bipolar contribution may also be important. The electronic part of the thermal conductivity is given by:

$$\Gamma_0 = (\frac{k_B}{e})^2 \left\{ \frac{\int_0^\infty (-\frac{\partial f}{\partial z})\tau(z) z^2 \frac{(z+\beta z^2)^{3/2}}{1+2\beta z} dz}{\int_0^\infty (-\frac{\partial f}{\partial z})\tau(z) \frac{(z+\beta z^2)^{3/2}}{1+2\beta z} dz} - \left[\frac{\int_0^\infty (-\frac{\partial f}{\partial z})\tau(z) z \frac{(z+\beta z^2)^{3/2}}{1+2\beta z} dz}{\int_0^\infty (-\frac{\partial f}{\partial z})\tau(z) \frac{(z+\beta z^2)^{3/2}}{1+2\beta z} dz} \right]^2 \right\}, \quad \textbf{(2-72)}$$

Electrical conductivity and Seebeck coefficient

The expression for the electron mobility μ, electrical conductivity σ, and Seebeck coefficient S with the inclusion of nonparabolicity of the band are given by:

$$\mu = \frac{e}{m_\chi^*} \frac{\int_0^\infty (-\frac{\partial f}{\partial z})\tau(z) \frac{(z+\beta z^2)^{3/2}}{1+2\beta z} dz}{\int_0^\infty (-\frac{\partial f}{\partial z})(z+\beta z^2)^{3/2} dz} \quad \textbf{(2-73)}$$

$$\sigma = \frac{(2m_d^* k_B T)^{3/2} e^2}{3\pi^2 \hbar^3 m_\chi^*} \int_0^\infty (-\frac{\partial f}{\partial z})\tau(z) \frac{(z+\beta z^2)^{3/2}}{1+2\beta z} dz \quad \textbf{(2-74)}$$

$$S = \frac{k_B}{e} \frac{\int_0^\infty (-\frac{\partial f}{\partial z})\tau(z)(z-\xi) \frac{(z+\beta z^2)^{3/2}}{1+2\beta z} dz}{\int_0^\infty (-\frac{\partial f}{\partial z})\tau(z) \frac{(z+\beta z^2)^{3/2}}{1+2\beta z} dz} \quad \textbf{(2-75)}$$

Intervalley scattering. Intervalley scattering reduces the beneficial effect of the multivalley energy band structure of the lead telluride. However, as intervalley scattering will be discussed in the next section, it can reduce the boundary resistance. The relaxation time for the intervalley scattering is given by:

$$\frac{1}{\tau_v} = \frac{N_f m^{*3/2} \Xi_{ij}^2}{\sqrt{2}\pi\rho\omega_{ij}\hbar^3} E_f^{1/2} \begin{cases} N & absorption \\ N+1 & emission \end{cases} \quad \textbf{(2-76)}$$

Ξ_{ij} is the intervalley deformation potential, N_f is the number of equivalent final valleys, E_f is the final energy of the electron, ρ is the mass density, ω_{ij} is the frequency of the phonons responsible for the scattering.

CHAPTER III

SEMICLASSICAL THEORY OF PHONON TRANSPORT

For phonon thermal conductivity in nanocomposites, several techniques can be used to capture the thermal conductivity, including (1) solving Boltzmann equation for a unit cell of the composites, (2) Monte-Carlo simulation of transport in nanocomposites, (3) relaxation time treatment in combination with the standard integral expressions for thermal conductivity, and (4) modifying the effective medium theory. The CPA is extended for phonons to calculate the scattering time due to grain and interface boundary scattering mechanism. The grain boundary scattering time calculated by the CPA in combination with other scattering times can be used in Boltzmann transport equation for phonons. The results are in good agreement with available experimental data.

3.1 Phonons

The quantized vibrations of a lattice which are major energy and momentum carriers in crystalline solids are named phonons. Phonons are the main energy carriers for heat conduction [48]. Phonons like photons can be treated as waves or as particles. They obey the Bose-Einstein distribution statistically and therefore are bosons. The phonons are said to be transversely or longitudinally polarized when the lattice vibration direction is perpendicular to the energy propagation direction, or the vibrations are along the direction of energy propagation, respectively. The phonon wave-vector $\vec{k}$represents the momentum of a phonon and has the same direction as the wave propagation. The norm of the wave-vector is expressed as its wavenumber as,

$$k = \frac{2\pi}{\lambda} = \frac{2\pi v_g}{\omega} \quad \textbf{(3-1)}$$

in which v_g and ω are the phonon group velocity and phonon angular frequency in rad/s, respectively. The momentum of a phonon can be related to its wave-vector $\vec{k}$ by

$$\vec{p} = \hbar\vec{k} \quad \textbf{(3-2)}$$

where$\hbar$=1.05457148× 10^{-34} J-s is the reduced Planck's constant. The total energy of a phonon is quantized so [48]

$$E_n = (n + \tfrac{1}{2})\,\hbar\omega \quad \textbf{(3-3)}$$

wheren is an integer representing the number of phonons and $E_0 = \sim\hbar\omega/2$ is called thezero-point energy which means even in zero temperature the energy of particles cannot be zero as a result of uncertainty principle [48].
The probability that a phonon will have energy $E = \sim\hbar\omega$ at equilibrium temperature T is the so-called energy distribution function. For phonons, this probability is described by the Bose-Einstein statistics expressed as [48]

$$f_{BE}(T,\omega) = \frac{1}{e^{\hbar\omega/k_B T} - 1} \quad \textbf{(3-4)}$$

wherek_B is the Boltzmann constant equal to 1.380×10^{-23} J/K. In the limiting cases,$f_{BE}(T,\omega)$ goes to infinity as E tends to zero and vanishes for energy E much larger than$k_B T$.
The relationship between phonon frequency ω and wavevector $\vec{k}$is called the dispersion relation and may be different along different wave-vector directions. Bulk phonon dispersion spectra are interesting not only for their relevance to the properties of pure materials but also as ingredients of approximate calculations for complex systems such as semiconductor alloys, superlattices, and other quantum microstructures. In the research field of thermoelectrics much attention is presently being paid to the vibrational properties of such materials both because of their role in thermal conductivity.
Figure 3.1 shows a typical dispersion relation for crystalline silicon. It indicates that phonons can follow an acoustic and an optical branch. Each branch can support longitudinal as well as transverse polarizations. The acoustic branch represents the lattice vibration at relative low frequencies. It strongly influences heat conduction in a crystal solid. One the other hand, the optical branch corresponds to higher frequencies. Indeed, it is so named because it mainly affects optical properties of a crystal solid [4]. The first Brillouin zone, is such that $-\frac{\pi}{a} \leq k \leq \frac{\pi}{a}$ where a is the lattice constant. It corresponds to the k-space of a crystal lattice with an atomic spacing of$a$. The allowable wavevector in a crystal solid is confined to the first Brillouin zone [48].

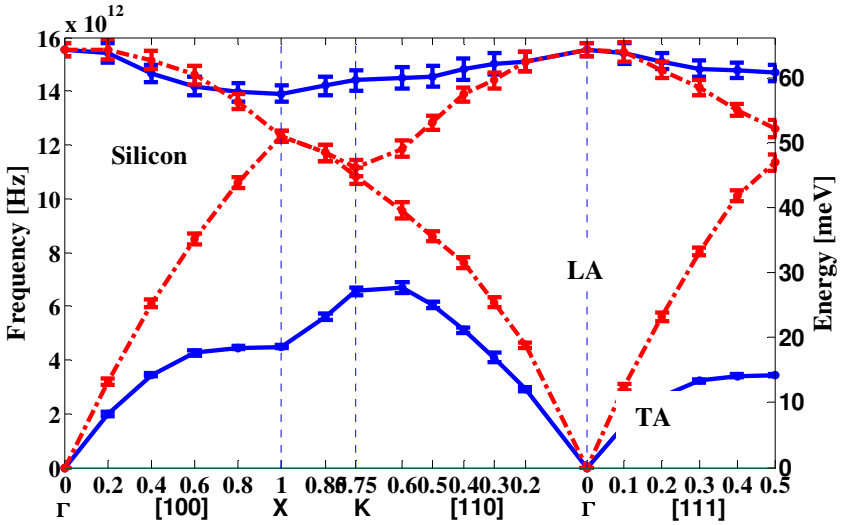

Figure 3.1: Dispersion relation for silicon crystal vibrations.

The speed of energy propagation by phonons is named group velocity. It is defined as $v_{g,i} = d\omega_i/dk$ which i indicated polarization. In the long wavelength limit as $k \to 0$, a linear $\omega - k$ relation forms in the acoustic branch, indicating that the group velocity does not depend on frequency. In fact, the phonon group velocity in optical branch is negligible compared with that of the acoustical branch. Therefore, optical phonons are typically assumed not to contribute to heat conduction [48].

The number of phonon modes per unit volume of material between wave-vector k and $k + dk$ is defined as phonon density of states. In the k-space, the volume of a sphere of radius k is equal to $4\pi k^3/3$. So, it can be shown that every phonon mode occupies a cube of volume $(2\pi/L)^3$ where the material volume is $L \times L \times L$[48]. Thus, the number of phonon modes in a sphere of radius k in the k-space and the phonon density of states are expressed as [48]

$$N = \frac{4\pi k^3/3}{(\frac{2\pi}{L})^3}$$

and

$$D_{ph}(k) = \frac{d(\frac{N}{V})}{d(k)} = \frac{k^2}{2\pi^2} \qquad \textbf{(3-5)}$$

respectively.

Acoustic phonons dominate thermal transport and travel at the speed of sound. The Debye model which is based on the following assumptions is used to describe acoustic phonons:

(1) The phonon frequency cannot be larger than the Debye cut-off frequency $\omega_{D,i}$ for polarization $i$defined as [48],

(2)

$$\omega_{D,i} = v_{g,i} k_{D,i} \quad \textbf{(3-6)}$$

in which $k_{D,i}$indicates the Debye cut-off wavenumber for polarization i. In the Debye model, phonon wave-vectors are not allowed to be larger than $k_{D,i}$. Physically, this corresponds to the fact that phonons cannot assume wavelength smaller than twice the atomic spacing.

(3) The group velocity $v_{g,i}$ of phonons with polarization i is constant so that $\omega_i = v_{g,i} k$. This approximation is valid at low energies where acoustic phonons populate but is not appropriate at high energy.

(4) The Debye density of states $D_{D,i}$ as a function of frequency ω_i for phonons with polarization $i$is given by

$$D_{D,i}(\omega_i) = \frac{k^2}{2\pi^2} = \frac{3\omega_i^2}{2\pi^2 v_{g,i}^3} \quad \textbf{(3-7)}$$

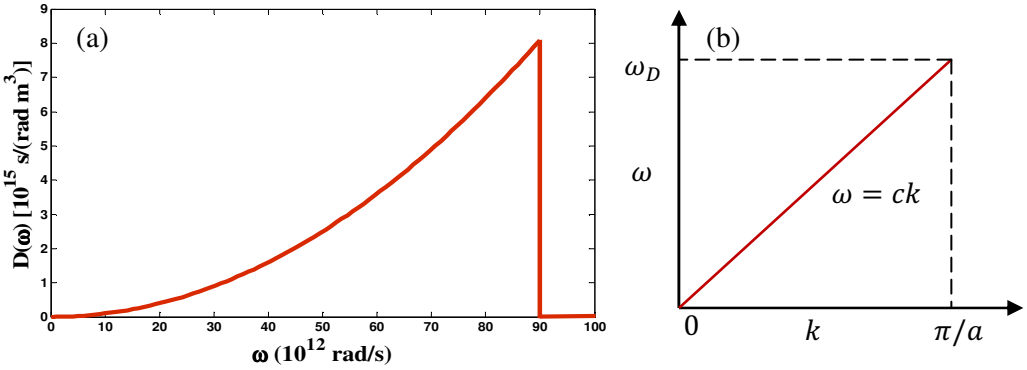

Figure 3.2: Typical (a) density of states and (b) phonon dispersion in Debye model.

A typical density of states and phonon dispersion based on Debye model has been presented in Figure 3.2. The phonon dispersion and density of states in nanocomposites can be different from bulk materials in general and it is assumed that the phonon concept still is valid in nanostructures. It should be noted that the change in phonon dispersion, group velocity and density of states in nanostructures is not the main cause for reduction in thermal conductivity.New experiments show that the nanostructure interfaces induce a diffuse scattering which reduces intensity of phonon mini-bands [49].Therefore, the phonon transport obeys the Boltzmann transport equation which is explained in next section.

3.2 General Formulation of Thermal Conductivity

Boltzmann Transport Equation for Phonons. In order to discuss the thermal conductivity of metals it isassumed that there exists a temperature gradient across the specimen. The transport of energy in the metals is due to conduction electrons and lattice waves. Here we shall consider the thermal conductivity only due to conduction electrons although lattice conduction may

become important under certain circumstances such as low temperature, high magnetic field, large impurity contents etc.

We will now consider the application of the Boltzmann equation to effects that involve heat transport. Let there be a thermal gradient *dT/dx* in a metal and a current density Q. In the measurement of thermal conductivity the specimen is electrically insulated from its surroundings; thus the current vanishes but not the electric fields. This is due to the fact that the temperature gradient produces a drift velocity of the electrons, and small electric fields. Counteraction the drift velocityis set up internally. Thus the Boltzmann transport equation beside the thermal gradient *dT/dx* includes a term containing an electric field ξ_x . In this case the Boltzmann equation can be written as

$$\frac{df}{dT} = 0 = -u_x \frac{\partial f}{\partial x} + \frac{e\xi_x}{m} \frac{\partial f}{\partial u_x} - \frac{(f - f_0)}{T}$$

or

$$u_x \left(\frac{\partial f}{\partial T} \right) \left(\frac{\partial T}{\partial x} \right) - e\xi_x \frac{\partial f}{\partial p_x} = -\frac{(f - f_o)}{T} \qquad \textbf{(3-8)}$$

When the electric field and $\partial T / \partial x$ are small, we can replace $\frac{\partial f}{\partial x}$ and $\frac{\partial f}{\partial p_x}$ by $\frac{\partial f_o}{\partial x}$ and $\frac{\partial f_o}{\partial p_x}$ respectively. Substituting in above equation we get

$$f = f_o = e\xi_{xT} \partial f_o / \partial p_x - \tau u_x \partial f_o \partial x.$$

Now in view of f_o being the Fermi-Dirac distribution function we write

$\therefore$

$$\frac{\partial f_o}{\partial x} = \frac{\partial f_o}{\partial T} \frac{\partial T}{\partial x} \frac{\partial}{\partial T} \left[\frac{1}{1 + \exp\{(E - E_f) K_B T\}} \right] \frac{\partial T}{\partial X}$$

$$= f_o + \tau \frac{\partial f_o}{\partial p_x} \cdot \frac{\partial f_o}{\partial E} \left[e\xi_x + \left\{ \frac{\partial E_f}{\partial T} + \frac{E - E_f}{T} \right\} \frac{\partial T}{\partial X} \right]. \qquad \textbf{(3-9)}$$

Now considering that E_f is independent of *T,* we get

$$f = f_o + \tau v_x \frac{\partial f_o}{\partial E} \left[e\xi_x + \left\{ \frac{E}{T} - \frac{E_F}{T} \right\} \right] \frac{\partial T}{\partial X} \qquad \textbf{(3-10)}$$

The electric current density I_c and thermal current density Q_x are defined as

$$I_x = -\left(\frac{2e}{h^3}\right)\iiint \upsilon_x (f - f_o) dp_x dp_y dp_z \qquad \textbf{(3-11)}$$

and

$$Q_x = -\left(\frac{2e}{h^3}\right)\iiint \upsilon_x (f - f_o) E dp_x dp_y dp_z \qquad \textbf{(3-12)}$$

where$E$ is the energy of an electron.

Substituting the value of $(f\text{-}f_0)$ from above equations, it is found that:

$$I_x = -\left(\frac{2e}{h^3}\right)\iiint \tau \upsilon_x{}^2 \frac{\partial f_o}{\partial E}\left[e\xi_x + \left\{\frac{E}{T} - \frac{E_F}{T}\right\}\right]\frac{\partial T}{\partial X} dp_x dp_y dp_z \qquad \textbf{(3-13)}$$

$$Q_x = -\left(\frac{2e}{h^3}\right)\iiint \tau \upsilon_x{}^2 + E\frac{\partial f_o}{\partial E}\left[e\xi_x + \left\{\frac{E}{T} - \frac{E_F}{T}\right\}\frac{\partial T}{\partial X}\right] dp_x dp_y dp_z \qquad \textbf{(3-14)}$$

Assuming that (3-13) and (3-14)depend on energy and not on the direction of motion, we see that the integrals in equation are functions of energy alone. The triple integrals may be transformed into single integrals by replacing $\upsilon_x{}^2$ by $\upsilon^2/3$ and $dp_x dp_y dp_z$ by $4\pi p^2 dp$ .Thus

$$I_x = -\frac{16\pi e(2m)^{1/2}}{3h^3}\int_0^\infty E^{3/2\tau}(E)\frac{\partial f_o}{\partial E}\left[e\xi_x + \left\{\frac{E}{T} - \frac{E_F}{T}\right\}\frac{\partial T}{\partial X}\right] dE$$

$$Q_x = -\frac{16\pi e(2m)^{1/2}}{3h^3}\int_0^\infty E^{5/2\tau}(E)\frac{\partial f_o}{\partial E}\left[e\xi_x + \left\{\frac{E}{T} - \frac{E_F}{T}\right\}\frac{\partial T}{\partial X}\right] dE \qquad \textbf{(3-15)}$$

Introducing a set of integral J_N

$$J_N = \frac{16\pi e(2m)^{1/2}}{3h^3}\int_0^\infty \tau(E)E^{N+1}\frac{\partial f_o}{\partial E} dE, \qquad N = 1,2,3.... \qquad \textbf{(3-16)}$$

$$I_x = -e\left(\frac{J_2}{T}\frac{E_F J_1}{T}\right)\frac{\partial T}{\partial X} - e^2 J_1 \xi_x$$

$$Q_x = \left(\frac{J_2}{T}\frac{E_F J_2}{T}\right)\frac{\partial T}{\partial X} - e^2 J_2 \xi_x. \qquad \textbf{(3-17)}$$

Now Q_x is calculated under the condition I_x = o, because the thermal conductivity of metals is defined as the rate of energy flow divided by thermal gradient when I_x=O.

$$K = -\left[\frac{Q_x}{(\partial T / \partial x)}\right] I_{x=O} \quad \textbf{(3-18)}$$

From equation when I_x=O., Now

$$Q_x = \left(\frac{J_2}{T} - \frac{J_2^2}{J_1 T}\right)\frac{\partial T}{\partial x} \quad \textbf{(3-19)}$$

Comparing the above equations we get

$$K = -\left[\frac{J_1 J_3 - J_2^2}{J_1 T}\right]. \quad \textbf{(3-20)}$$

The value of integral J_N is given by

$$J_N = -\frac{16\pi(2m)^{1/2}}{}\left[\tau E_F{}^{N+1} + \frac{\pi^2}{6} K_B T^2 \left\{\left(\frac{\partial^2\left(\tau E^{N+1/2}\right)}{\partial E^2}\right) E = E_F\right\}\right],\ N = 1,2,3 \quad \textbf{(3-21)}$$

Substituting (3-21) into (3-20)we get $K = \frac{\pi^2}{3}\frac{K_B{}^2 T N \tau_F}{m}$ where N is the density of electrons.

In most of the materials, τ_F varies approximately as 1/T, and hence K is nearly temperature independent. If the metal contains impurities, then electron-phonon scattering as well as electron impurity scattering takes place. If the two scatterings are considered to be independent to each other, then the total conductivity K can be represented by

$$\frac{1}{K} = \frac{1}{K_1} + \frac{1}{K_\tau} \quad \textbf{(3-22)}$$

whereK_l is the contribution arising from electron-lattice scattering and K_l is the contribution from electron impurity scattering. This expression shows that the impurities decrease the thermal conductivity.

Callaway method. As an alternative and simple approach Callaway developed an expression for thermal conductivity of solids, assuming isotropic Debye model, but including both normal and Umklapp scattering mechanisms. The final expression for thermal conductivity is given by [50]:

$$k_l = k_1 + k_2 \quad \textbf{(3-23)}$$

where k_1 and k_2 can be expressed as:

$$k_1 = CT^3 \int_0^{\theta/T} \tau_C(x) G(x) dx \quad \textbf{(3-24)}$$

$$k_2 = CT^3\beta I \tag{3-25}$$

with

$$\beta = \frac{\int_0^{\theta/T} \frac{\tau_c(x)}{\tau_N(x)} G(x)dx}{\int_0^{\theta/T} \frac{\tau_c(x)}{\tau_N(x)\tau_R(x)} G(x)dx} \text{ and } I = \int_0^{\theta/T} \frac{\tau_c(x)}{\tau_N(x)} G(x)dx \tag{3-26}$$

where

$$G(x) = \frac{x^4 e^x}{(e^x-1)^2} \quad , \quad \frac{1}{\tau_C(x)} = \frac{1}{\tau_N(x)} + \frac{1}{\tau_R(x)} \quad , \quad x = \frac{\hbar\omega}{k_B T} \quad , \quad m = \frac{\hbar}{k_B} \quad , \quad C = \frac{k_B m^3}{2\pi^2 v_g} \tag{3-27}$$

inwhich ħ and $k_B$arePlanck's and Boltzmann constants, respectively. The phonon angular frequency, the phonon group velocity (sound velocity), Debye temperature and absolute temperature are indicated by ω, v_g, θ , and T, respectively. τ_C , $\tau_N$andτ_U represent combined, N (resistive), and Umklapp relaxation times, respectively.

3.3 Relaxation Time

Phonons are dominant thermal energy carriers in semiconductors and dielectric materials. Resistance to heat transfer in a porous material is determined by phonon scattering with (1) three-phonon scattering, including normal (N) and Umklapp (U) processes, (2) electron-phonon scattering, (3) point defect (alloy) scattering, and (4) grain boundary phonon scattering.

Umklapp scattering. The Umklapp (U) three phonon scattering rate τ_U is given by:

$$\frac{1}{\tau_u} = \frac{20\pi}{3}\hbar N_A \left(\frac{6\pi^2}{4}\right)^{1/3} \times \frac{1+\frac{5}{9}\beta}{1+\beta}\frac{\gamma^2}{Ma^2}\left(\frac{T}{\theta}\right)^3 x^2 \tag{3-28}$$

where $\hbar = h/2\pi$, h is Planck's constant, θ is the Debye temperature, T is the absolute temperature, $x = \hbar\omega/k_B T$, ω is the phonon frequency, M is the total average mass for a specific material, γ is the Grüneisen constant (or the anharmonicity parameter), assumed to be 1 in most cases, a is the atomic size determined by the cubic root of the atomic volume, and β is the ratio of the normal three phonon-scattering rate to the Umklapp three-phonon-scattering rate, which is assumed to be temperature-independent.

Normal scattering. The normal three-phonon-scattering rate, τ_N , is given by:

$$\tau_N = \beta\tau_\beta \tag{3-29}$$

Electron-phonon scattering. An estimate of the electron-phonon relaxation time, τ_{e-ph}, is given by Ziman [45,51] as:

$$\frac{1}{\tau_e} = \frac{E_a^2 m_d^3 v_s}{4\pi\hbar^4 \rho(\frac{1}{2}m_d v_s^2/k_B T)} \times \ln\left(\frac{1+\exp(-(\frac{1}{2}m_d v_s^2/k_B T)+E_F/k_B T - x^2/16(\frac{1}{2}m_d v_s^2/k_B T)+x/2)}{1+\exp(-(\frac{1}{2}m_d v_s^2/k_B T)+E_F/k_B T - x^2/16(\frac{1}{2}m_d v_s^2/k_B T)-x/2)}\right) \tag{3-30}$$

where v_s is the sound velocity, m_d is the density-of-states effective mass, ρ is the mass density.

Point defects scattering. The relaxation time due to point defects, τ_{pd}, is given by:

$$\frac{1}{\tau_{PD}} = \left(\frac{a}{v_s}\right)^3 \left(\frac{k_B T}{\hbar}\right)^4 \sum_i \left[y_i \left(1-\frac{M_i}{M}\right)^2 + \varepsilon_s y_i \left(1-\frac{a_i}{a}\right)^2 \right] x^4 \tag{3-31}$$

Here, y_i ,M_i, and a_i are the fractional concentration, mass, and atomic size of each element in the alloy respectively, where $M = \sum_i f_i M_i$ and $a = \sum_i f_i a_i$. ε_s determines the contribution of strain disorder to point defect scattering of phonons. If the lattice constants of the elements in the compound do not differ largely, the effect of strain is small compared with the mass fluctuation.

Impurity atom/vacancy scattering. The phonon relaxation time due to scattering by impurity atoms on a single atomic site is given by:

$$\frac{1}{\tau_{i-ph}} = \left(\frac{a}{v_s}\right)^3 \left(\frac{k_B T}{\hbar}\right)^4 \sum_i f_i \left(1-\frac{M_i}{M}\right)^2 x^4 \tag{3-32}$$

where f_i is the fractional concentration of the impurity atom i, and M_i is its mass.

3.4 Grain Boundary Scattering

Relaxation time due to grain boundary scattering, τ_{GB} worthy special attention as it is a dominant mechanism for enhanced ZT in nanostructured materials. Modeling of the grain boundary scattering, however, is not accurate at this stage. Grain boundaries can scatter phonons via three different possibilities: (1) regular reflection and refraction, τ_{Ref} ,arising from the difference of

phonon group velocities when phonons, (2) diffusive scattering due to the corrugation ofthe GB, τ_{Diff} , caused by impurities or interface roughness, and (3) diffraction of waves when the wavelength is comparable to the particle size, τ_{Ray} .

Phonon reflection and refraction at a flat interface. Phonon reflection at a boundary leads to the Kapitza resistance, a phenomenon that has been known for a long time but has escaped quantitative description except at very low temperatures when the phonon wavelength is long such that wave reflection can be treated based on acoustic wave theory. At room temperature, the phonon reflectivity is difficult to calculate because mainly diffuse phonon reflection and also due to the phonon spectrum mismatch between two sides of the interface. We will approximate here the phonon relaxation time due to reflection inside a single grain as:[52]

$$\tau_{\text{Ref}} \sim \ell_{GB} v_s^{-1} (\Delta\nu)^{-2} \tag{3-33}$$

where ℓ_{GB} is the mean distance of the GBs, and $\Delta\nu$ is the difference of refraction indices of the elastic waves in different grains. In the above expression, ℓ_{GB} /v_s gives the average time phonon transverse a single grain and $\Delta\nu^{-2}$ is a measure of the strength of interface reflection, which can arise, for example, due to different orientations of the crystal in the adjacent grains. If the crystal orientation is slightly rotated by an angle δ , one can estimate:

$$\Delta\nu \approx \delta \tag{3-34}$$

Phonon scattering by a small grain. If the GB region is much smaller than the wave lengths of the excited phonons, the problem should be treated as a diffraction process. If the scattering is diffuse, the phonon relaxation time can be estimated from:

$$\tau_{\text{Diff}} \sim \ell_{GB} v_s^{-1} \left(\frac{k_B\theta}{\hbar\omega}\right)^2 \frac{1}{\eta} \tag{3-35}$$

where η is a parameter that characterizes the degree of corrugation of the GB (typically $1<\eta<10$).

When the grain boundary region is much smaller than the wavelength and surface corrugation is also much smaller than the wavelength, the scattering can be described by Rayleigh scattering for which the relaxation time can be calculated from:

$$\tau_{\text{Ray}} \sim \left(\frac{v_s}{\ell_{GB}}\right)^3 \left(\frac{\theta}{T\omega}\right)^4 \Xi \tag{3-36}$$

where Ξ is some constant. This approximation is valid for low frequency phonons.

Phonon relaxation time due to grain-boundary scattering. In real materials, where the above discussion of grain boundary scattering mechanism dominates, scattering depends on the grain-

boundary region size, interface roughness, and phonon wavelength. At this stage, there is noa rigorous way to combine all these mechanisms. All the mechanismsare includedwith the Mathiessen's rule [53]

$$\frac{1}{\tau_{GB}} = \frac{1}{\tau_{\text{Ref}}} + \frac{1}{\tau_{\text{Diff}}} + \frac{1}{\tau_{\text{Ray}}} \tag{3-37}$$

Total relaxation time of phonons. By combining all the scattering mechanisms, the total phonon relaxation time τ_c can be obtained from Matthiessen's rule as follows:

$$\frac{1}{\tau_c} = \frac{1}{\tau_U} + \frac{1}{\tau_N} + \frac{1}{\tau_{e-ph}} + \frac{1}{\tau_{pd}} + \frac{1}{\tau_{i-ph}} + \frac{1}{\tau_{\text{Ref}}} + \frac{1}{\tau_{Diff}} + \frac{1}{\tau_{Ray}} \tag{3-38}$$

CHAPTER IV

THEORY FOR THE ELECTRONIC DENSITY OF STATES BY GREEN'S FUNCTION

4.1 Green's Function for Schrodinger Equation

The following discussion is very general and is presented in order to familiarize the reader with the Green's function method. This method is a standard theoretical tool in a number of areas of physical sciences and many review papers and books exist which discuss it in more detail than what is donein this chapter. The discussion will be brief and in the nature of a quick review. Much of what follows is based on the discussions found in Refs. [10,54,55] and more details may be found in those resources. In quantum mechanics, a system is described by a wave function $|\psi>$ which is the solution of the Schrodinger equation

$$H|\psi>=E|\psi \quad \textbf{(4-1)}$$

or

$$(E-H)|\psi>=0, \quad \textbf{(4-2)}$$

where H is the total Hamiltonian operator of the system, and E is an energy eigenvalue of the Hamiltonian (multiplied by the identity operator). Instead of solving the Schrodinger equation directly, an operator called the Green's function operator which is defined as the following is introduced:

$$G(z)=(z-H)^{-1} \quad \textbf{(4-3)}$$

where z is a complex variable (again, multiplied by the identity operator). It can easily be seen that $G(z)$ is the solution of the following equation

$$(z-H)G(z)=1, \quad \textbf{(4-4)}$$

where 1 is the identity operator. In a nanocomposite (random alloy), the Hamiltonian H is an operator which is a random function of position within the nanocomposite. Its eigenvalues are thus random variables and its eigenfunctions depend upon the particular configuration of components that exists in a given sample. Let us now consider such a nanocomposite and set up a Hilbert space formed by the electronic eigenstates $|\alpha>$ of the nanocomposite. These eigenstates are assumed to have the following properties:

$$H|\alpha >= \varepsilon_\alpha|\alpha >, \quad \textbf{(4-5)}$$

$$< \alpha'|\alpha >= \delta_{\alpha\alpha'}, \quad \textbf{(4-6)}$$

and

$$\sum_\alpha < \alpha|\alpha > = 1. \quad \textbf{(4-7)}$$

These equations respectively define the random variable eigenvalues of the Hamiltonian, require that the eigenstates $|\alpha >$ be orthogonal to one another, and require that they be a complete set. Using combinations of Equation. (4-4) to (4-7) any arbitrary state $|\psi >$, the Hamiltonian H, and the Green's function operator $G(z)$ can all be expanded in terms of the eigenstates $|\alpha >$ and the eigenvalues ε_α. This results in the following formal equations:

$$|\psi >= \sum_\alpha |\alpha >< \alpha\,|\psi >, \quad \textbf{(4-8)}$$

$$\mathrm{H} = \sum_\alpha \varepsilon_\alpha|\alpha >< \alpha|, \quad \textbf{(4-9)}$$

and

$$G(z) = \sum_{\alpha\alpha'} |\alpha' >< \alpha'\,|(z - H)^{-1}|\alpha >< \alpha|$$

$$=\sum_{\alpha\alpha'} |\alpha' > \frac{<\alpha'|\alpha>}{z-\varepsilon_\alpha} < \alpha|$$

$$=\sum_{\alpha\alpha'} |\alpha' > \frac{\delta_{\alpha\alpha'}}{z-\varepsilon_\alpha} < \alpha|$$

$$= \sum_\alpha \frac{|\alpha><\alpha|}{z-\varepsilon_\alpha}. \quad \textbf{(4-10)}$$

From Equation (4-10), it can be seen that the positions of the poles of $G(z)$ give the eigenvalues of Hamiltonian, and that the residues at those poles provide information about the corresponding eigenfunctions. It can be easily shown that $G(z)$ is an analytic function everywhere in the complex z-plane except at the points $z=\varepsilon_\alpha$. Because the ε_α are the eigenvalues of the Hermitian operator H, they must be real. So the possible singularities of $G(z)$ can only occur at those points or portions of the real z-axis which correspond to the eigenvalues. The operator $G(z)$ thus exhibits simple poles at the ε_α . If a particular ε_α belongs to the continuous spectrum of the Hamiltonian H, $G(z)$ will not be well defined.

4.2 Calculation of Density of States by Using Green's Function

The definition of $G(z)$can be generalized by a limiting procedure as following

$$G^{\pm}(\varepsilon) = \lim_{\lambda\to 0^+} G(\varepsilon \pm i\lambda), \quad \textbf{(4-10)}$$

where $G^{\pm}(\varepsilon)$ is often known as the retarded (advanced for -) Green's function operator. From Equation (2-9), one can see that

$$G^{*}(z) = G(z^{*}). \quad \textbf{(4-11)}$$

If z is real, z=εand $\neq \{\varepsilon_{\alpha}\}$, it follows from Eq.(4-10) that $G(\varepsilon)$ is Hermitean. In particular, $G(\varepsilon)$ is real. On the other hand, if ε belongs to the continuous spectrum, we have from Equations (4-10) and (4-11) that

$$G^{-}(z) = [G^{+}(z)]^{*}, \quad \textbf{(4-12)}$$

which shows that

$$\mathrm{Re}\{G^{-}(\varepsilon)\} = \mathrm{Re}\{G^{+}(\varepsilon)\}, \quad \textbf{(4-13)}$$

and

$$\mathrm{Im}\{G^{-}(\varepsilon)\} = -\mathrm{Im}\{G^{+}(\varepsilon)\}. \quad \textbf{(4-14)}$$

Applying the formal identity (which is really only valid under an integration operation)

$$\lim_{y\to 0} \frac{1}{x \pm iy} = P\left(\frac{1}{x}\right) \mp i\pi\delta(x) \quad \textbf{(4-15)}$$

where P denotes the principal part and $\delta(x)$ is the Dirac delta function, one can express the function $G^{\pm}(\varepsilon)$by the following relation:

$$\begin{aligned} G^{\pm}(\varepsilon) &= lim_{\lambda\to 0^{+}}\, G(\varepsilon \pm i\lambda) \\ &= lim_{\lambda\to 0^{+}} \sum_{\alpha} \frac{|\alpha><\alpha|}{\varepsilon-\varepsilon_{\alpha}\pm i\lambda} \\ &= \sum_{\alpha} lim_{\lambda\to 0^{+}} \frac{|\alpha><\alpha|}{\varepsilon-\varepsilon_{\alpha}\pm i\lambda} \\ &= \sum_{\alpha} |\alpha><\alpha| \left[P\left(\frac{1}{\varepsilon-\varepsilon_{\alpha}}\right) \mp i\pi\delta(\varepsilon-\varepsilon_{\alpha}) \right]. \end{aligned} \quad \textbf{(4-16)}$$

By definition, the density of states for electrons per unit cell is given by

$$D(\varepsilon) = \sum_{\alpha} \delta(\varepsilon - \varepsilon_{\alpha}), \quad \textbf{(4-17)}$$

This relation can be related to the imaginary part of the Green's function by combining Equations (4-16) and (4-17). This results in the following formula

$$D(\varepsilon) = \mp \frac{1}{N\pi} Im[TrG^{\pm}(\varepsilon)], \quad \textbf{(4-18)}$$

in whichN is the total number of unit cells in the alloy and the trace runs over all cells. It simply expresses that the density of states is directly proportional to imaginary part of the Green's function so, once we have the Green's function operator we can calculate the density of states.
The matrix elements of Green's function for some simple configurations have been presented in section Appendices.

CHAPTER V

COHERENT POTENTIAL APPROXIMATION

The Coherent Potential Approximation (CPA) theory for obtaining the electronic properties of random alloys and nanocomposites is about seventeen years old, having been first discussed by Taylor [12] and Soven [13] in 1967. The following discussion is in the form of a brief review and is included to presenta general review of the theory. The formal theory as presented here is valid for the electronic properties of any random alloy or nanocomposite. It has been shown that the CPA can be derived in various ways [8,56,57,58,59]. In much of what follows, the discussion is based on the reviewes found in Refs. [54,55]. First the Green's function formalism of the coherent potential approximation is introduced and then it is shown how to model the CPA with the boundary value formalism of the CPA.

5.1 Green's Function Formalism of the CPA

As discussed in chapter IV, a random substitutional alloy system is characterized by a random distribution of different substances over the lattice sites. In case of a nanocomposite lattice sites are exist just locally and are randomly oriented. The lack of periodicity in the underlying lattice structure and randomly distributed grains cause theoretical difficulties in the development of a model of the electronic properties of such a system, because the usual condensed matter theory methods, such as Bloch's Theorem, are only valid for perfectly periodic crystals. The CPA method has been shown to be among the most effective approximation methods for dealing with this kind of system.

For the alloy system one can write the total random Hamiltonian as

$$H = H_0 + V = H_0 + \sum_n v_n, \qquad \textbf{(5-1)}$$

where H_0 is a suitably chosen periodic Hamiltonian, and V is the total random potential written in terms of the sum of atomic potentials v_n at each site. At this point, let us introduce a periodic, effective (coherent) potential (at this point unknown but which will be determined later) and add and subtract it from Equation (5-1). Then, the Hamiltonian can be rewritten as

$$\begin{aligned} H &= (H_0 + \Sigma) + (V - \Sigma) \\ &= H'_0 + U \\ &= H'_0 + \textstyle\sum_n U_n, \end{aligned} \qquad \textbf{(5-2)}$$

wherea new (effective) periodic Hamiltonian has been defined as following

$H'_0 = H_0 + \Sigma$, **(5-3)**

and a new random potential as

$$U = \sum_n U_n = V - \Sigma = \sum_n (v_n - \sigma_n). \quad \textbf{(5-4)}$$

As mentioned already, the effective Hamiltonian H'_0 is still periodic, and it will be shown later that the self-energy will replace V when one does the configuration average. The corresponding alloy Green's function operator can then beexpressed as

$$G(z) = (z - H_0 - V)^{-1} = (z - H'_0 - U)^{-1} \quad \textbf{(5-5)}$$

in which the z is a complex number in general. Of course the total Hamiltonian H can be constructed in detail for a piece of a particular alloy sample and the eigenvalue problem and the density of states can then be solved numerically. Ideally, the alloy sample in such a case should be sufficiently large that the calculated physical properties do not depend upon the boundary conditions. It should also be large enough that the particular configuration of constituents in the piece of alloy under consideration is largely irrelevant and assumptions of total randomness are valid. This is the idea of the Negative Eigenvalue Theorem Method (NETM) [60]. Such a method of approach, while relatively straightforward to implement for simple model alloy systems, becomes impractically difficult if applied to real alloy and nanocomposite systems. For realistic models of three-dimensional alloys or nanocomposites, the Negative Eigenvalue Theorem Method becomes almost hopelessly numerically complex and cumbersome.

By contrast, rather than attempt to exactly solve for the detailed properties of a large piece of a particular disordered alloy or nanocomposite, effective medium theories in general and the CPA in particular regard the idea of configuration averaging as fundamental. A macroscopic property of the system, such as, for example, the density of states, is then described in terms of an average over all configurations of components which are consistent with the known structure of the alloy.

The basic idea of what follows is to develop a method to choose the self-energy in such a manner that the resulting periodic effective medium (that described by the effective Hamiltonian H'_0) has as many of the properties of the random alloy as possible. First, a perfect crystal Green's function operator corresponding to the periodic Hamiltonian $H'_0$is defined as

$$P(z) = (z - H_0)^{-1}, \quad \textbf{(5-6)}$$

and define the effective medium Green's function operator corresponding to the effective Hamiltonian H'_0 as

$$g(z) = (z - H'_0)^{-1}. \quad \textbf{(5-7)}$$

Using Equations (5-2) and (5-6), Equation (5-7) can be rewritten as

$$\begin{aligned} g(z) &= (z - H_0 + \Sigma)^{-1} \\ &= (P^{-1} + \Sigma)^{-1} \\ &= P(1 + \Sigma P)^{-1}. \end{aligned} \quad \textbf{(5-8)}$$

One of the basic ideas of the CPA is to choose the self-energy Σ in such a way that the effective medium Green's function is, in fact, identical to the configuration average of the alloy Green's function. From Equation (5-5), one can formally express the alloy Green's function operator G in terms of the effective medium Green's function operator g as

$$\begin{aligned} G &= (z - H'_0 - U)^{-1} \\ &= (g^{-1} - U)^{-1} \\ &= g(1 - Ug)^{-1} \\ &= (1 - gU)^{-1} g \\ &= g + gUG. \end{aligned} \tag{5-9}$$

In this form, this equation is known as the Dyson equation. Further formal manipulation can easily be shown to lead to

$$\begin{aligned} G &= g + gUg + gUgUg + \cdots \\ &= g + gTg, \end{aligned} \tag{5-10}$$

wherethe scattering matrix Tis defined as

$$\begin{aligned} T &= U(1 - gU)^{-1} \\ &= (1 - Ug)^{-1} U. \end{aligned} \tag{5-11}$$

Formally, this scattering matrix specifies the deviations of the random alloy from the periodic effective medium. Microscopically, this is manifested by electrons scattering off of the random atomic potentialsu_n. Another form for the scattering matrix is

$$\begin{aligned} T &= U + UgT \\ &= u_n + \sum_n u_n g \sum_n u_n + \sum_n u_n g \end{aligned} \tag{5-12}$$

Physically, T is the total scattering operator due to electrons scattering from the disorder in the alloy or nanocomposite system. Now the configuration-average (denoted by the symbol <>) of the Green's function operator is taken as:

$$\begin{aligned} < G > &= < g + gTg > \\ &= g + g < T > g. \end{aligned} \tag{5-13}$$

The second step in Equation (5-13) can be taken because the effective medium Green's function is periodic and is thus configuration independent. It can be seen from Equation (5-13) that if $< T >= 0$, the averaged Green's function G equals the effective medium Green's function g. The main approximation of all CPA theories is to require that this be so and thus that g $=< G >$. This requirement, in turn, will determine the self-energy of the periodic effective medium and thus all properties of that medium itself. At this point, however, the "single-site" (or "single- cell")

approximation in which the total scattering matrix T can be written as the sum of the scattering matrix contributed from each site is made:

$$T = \sum_n t_n \tag{5-14}$$

where

$$\begin{aligned} t_n &= u_n + u_n g u_n + u_n g u_n g u_n + \cdots \\ &= u_n (1 - g u_n)^{-1} \\ &= u_n + u_n g t_n. \end{aligned} \tag{5-15}$$

Comparing Equations (5-12) and (5-15), one can see that this approximation neglects terms such as

$$\sum_n u_n g \sum_{m \neq n} u_m + \sum_n u_n g \sum_{m \neq n} u_m \, g \sum_p u_p + \sum_n u_n \, g \sum_m u_m \, g \sum_{p \neq n} u_p + \ldots \tag{5-16}$$

which correspond to scattering off of pairs and higher order clusters. Many generalizations of this theory, where scattering off of such clusters is accounted for can be found in the literature [9,61,62]. As is mentioned above, the CPA requires that

$$< T >= 0. \tag{5-17}$$

A consequence of this condition is, from Equation (5-13),

$$< G >= g. \tag{5-18}$$

In this averaging process, the random potential V of the alloy is thus replaced by an effective or coherent potential, $= \sum_n \sigma_n$, which simulates the electronic properties of the actual alloy, and yet is periodic. In the single site approximation,Equation (5-17) becomes

$$< t_n >= 0 \tag{5-19}$$

for all n. Because of the periodicity of the averaged quantities, it is sufficient to consider only a single site.

For convenience, let us choosen $= 0$. It should be emphasized that the averaging done in the CPA is not a simple arithmetic average. The effective, averaged, self-energy is self-consistently chosen to replace and fit the configuration-dependent, real alloy potential. Equation (5-19) is the self-consistency condition that determines the self-energy. Since t_n is related to the self-energy via Equations (5-15) and (5-4), the self-energy Σ is to be regarded as an unknown in that equation. To find the self-energy, one thus solves Equation (5-19) for that quantity. Once this is done all other quantities such as the effective medium Green's function and configuration averaged density of states are then determined. The configuration-averaged density of states is thus the density of states corresponding to the effective medium Green's function g. That is

$$< D(E) >= -\frac{1}{N\pi} Im[Tr(g)]. \tag{5-20}$$

The framework of the general CPA single-site formalism may be finally summarized as follows:

(1) Choose a perfect crystal as a reference and calculate the corresponding perfect-crystal Green's function P. (It should be noted that the choice of reference crystal, while important for actual computational purposes, is arbitrary from the general theoretical viewpoint. Since the CPA is a self-consistent theory, the solution for the self-energy l is independent of this choice.)
(2) From Equations (5-8) and (5-19), solve for the self-energy Σ, as a function of energy.
(3) Use Equation (5-8) to obtain the configuration averaged or effective medium Green's function which can then be used to calculate the configuration averaged density of states via Equation (5-20).

5.2 Boundary Value Formalism to Calculate the Scattering Amplitude

The properties of the effective medium are affected by its microstructure. The volume fractions of the components, the shapes and geometric arrangement of the inhomogeneties specify the microstructure of an effective medium. The microstructure represents the statistical correlation in a disordered alloy or composite. Therefore, to determine an effective medium both the material properties of the components and their microstructure should be specified. Therefore, the CPA is based on three main concepts:

(1) Introduction of a periodic effective medium with a complex propagation constant by a self-consistency requirement. The CPA condition sets the average value of scattering amplitude equal to zero and vanishes its local fluctuations.
(2) Calculating the average of a desired property of a disordered material.
(3) Choosing a structural unit to represent the microstructural information of a disordered medium.

Structural unit is a concept which helps us to capture the microstructural information of a disordered medium. There are two frequently encountered microstructures [4]:

(1) Symmetric structural unit and
(2) Dispersion structural unit.

Symmetric microstructure. First a symmetric microstructure as our structural unit is considered. It is symmetric in the statistical sense; i.e., an interchange of the components results in the same type of medium with interchanged volume fraction. In this case, there are two components and two structural units, each approximated by a sphere of one material component. Therefore, the volume fractions are *x* and 1-x (P and 1-P in the Figure 5.1). The main CPA idea is visualized in Figure 5.1 which corresponds to a symmetric case [4].

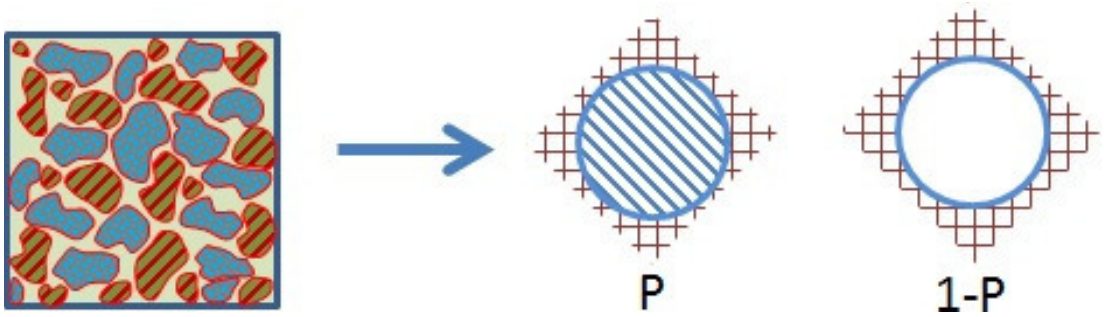

Figure 5.1: The CPA concept for symmetric structural units.

To calculate the forward scattering amplitudes, each structural unit, characterized by $k^2_m$and radius a_m (m = 1, 2), is embedded in an effective medium with $k_e$separately. The computational scheme introduced by Sheng [4] is followed to calculate the scattering amplitude. In brief, the scattering amplitude $f(k'_0, k_0)$ is defined by:

$$\psi(\omega,r)_{|r|\to\infty} \to e^{ik_0 r} + f(k'_0,k_0)\frac{e^{ik_0 r}}{r} \qquad \textbf{(5-21)}$$

in which the $\psi(\omega,r)$ is the solution to the scalar wave equation $(\nabla^2 + k^2)\,\psi$=0. The boundary condition is the continuity of ψ and its normal derivative $\partial\psi/\partial r$ across the interface of sphere and effective medium. The angular frequency ω inside and outside of sphere is the same but wave speeds are v and v_e respectively. The index e refers to effective medium. Inside the sphere the solution is an expansion in terms of spherical Bessel functions and Legendre polynomials. Outside the sphere, the solution is a sum of two expressions as incident plane wave and scattered wave respectively. The scattered wave can be expressed as spherical Hankel function and Legendre polynomials. In brief we have:

$$\begin{cases} \psi^{<}(r) = \sum_{l=0}^{\infty} A_l\, j_l(kr) P_l(\cos\theta) & for \quad r \le a \\ \psi^{>}(r) = e^{ik_e\cdot r} + \sum_{l=0}^{\infty} D_l h_l^{(1)}(k_e r) P_l(\cos\theta) i^l (2l+1) & for \quad r > a \end{cases} \qquad \textbf{(5-22)}$$

where j_n and $h_n^{(1)}$ are the spherical Bessel functions and spherical Hankel functions of the first kind respectively. We should apply two boundary conditions for above solutions and then utilize the expansion of plane waves in terms of spherical Bessel functions and Legendre polynomials and the orthogonality of these special functions for different angular momentum indices l to derive the coefficients D_n as below:

$$\begin{cases} A_l j_l(ka) P_l(cos\theta) = i^l(2l+1)P_l(cos\theta)\left[j_l(k_e a) + D_l h_l^{(1)}(k_e a)\right] \\ \dfrac{k}{k_e} A_l j_0'(ka) P_l(cos\theta) = i^l(2l+1)P_l(cos\theta)[j_l'(k_e a) + D_l h_n^{(1)'}(k_e a)] \end{cases} \qquad \textbf{(5-23)}$$

and

$$e^{ik_e \cdot r} = \sum_{l=0}^{\infty} i^l \, (2l+1) P_l(cos\theta) j_l(k_e a) \tag{5-24}$$

After dividing the second row of Equation (5-23) by the first row to remove coefficients A_l from both sides one can get:

$$D_l^{(m)} = \frac{k_e j_l(k_m a) j_l'(k_e a) - k_m j_l'(k_m a) j_l(k_e a)}{k_m j_l' \ (k_m a) h_l(k_e a) - k_e h_l'(k_e a) j_l(k_m a)} \tag{5-25}$$

where*m* refers to different components and the prime means derivative with respect to the argument of the function. Moreover, a comparison of Equations (5-21) and (5-24) gives us the scattering amplitude in terms of Legendre polynomials and coefficients $D_l^{(m)}$ as:

$$f(k_e', k_e) = \frac{-i}{k_e} \sum_{l=0}^{\infty} D_l^{(m)} P_l(cos\theta)(2l+1) \tag{5-26}$$

The θcan be set to zero (forward scattering) using optical theorem.

Dispersion microstructure. Secondly, the mathematical formula to calculate the scattering amplitude due to a dispersion microstructure is presented. For dispersion microstructure, a component is always the dispersed phase in the other component as host or matrix. In the dispersion microstructure, as can be seen in the Figure 5.2 (left side) the medium includes similar structural units, each consisting of a dispersed component particle surrounded by a layer of the host component. These similar structural units can be approximated by a coated sphere. The thickness of coating layer R-R_0can be calculated from the local volume fraction of the dispersed components as following:

$$t = R - R_0 = \left(P'^{-1/d} - 1\right) R_0 \tag{5-27}$$

in which R is the radius for the whole unit, R_0 is the radius for the dispersed particle and

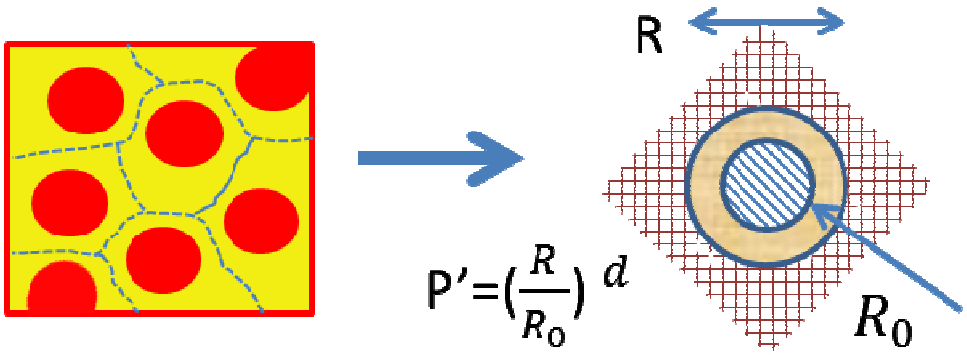

Figure 5.2: The CPA concept for dispersion structural units.

P′ is its local volume fraction which is varying from one location to the next [4]. For the dispersion microstructure the structural unit in 3D,2D and 1D is a sphere, a circle and two neighboring components respectively. To obtain the CPA equations it is assumed that the structural unit is embedded in a homogenous effective medium as shown in the Figure 5.3. Figure 5.3 shows a dispersion microstructure in 2D. In this case we have two interfaces which divide our unit cell into three regions. The solutions of scalar wave equation for each region in 3D can be written as the following [4]:

$$\begin{cases} \psi^{(1)} = \sum_{l=0}^{\infty} A_l\, j_l(k_1 r) P_l(cos\theta) & for \quad r \le R_0 \\ \psi^{(2)} = \sum_{l=0}^{\infty} [B_l\, j_l(k_2 r) + C_l n_l(k_2 r)] P_l(cos\theta) & for\ R_0 < r \le R \\ \psi^{(3)} = e^{ik_e \cdot r} + \sum_{l=0}^{\infty} i^l\,(2l+1) D_l h_l^{(1)}(k_e r) P_l(cos\theta) \\ = \sum_{l=0}^{\infty} i^l\,(2l+1) P_l(cos\theta)\left[j_l(k_e r) + D_l h_l^{(1)}(k_e r)\right] & for\ r > R \end{cases}$$

(5-28)

Above mentioned wave functions should satisfy two boundary conditions. The wave functions and their normal derivatives are continuous across the two interfaces so, two equations at the two interfaces $r=R$and $r=R_0$ are attained:

$$\frac{k_1 j_l'(k_1 R_0)}{k_2 j_l'(k_1 R_0)} = \frac{B_l j_l'(k_2 R_0) + C_l n_l'(k_2 R_0)}{B_l j_l(k_2 R_0) + C_l n_l(k_2 R_0)} \quad \textbf{(5-29)}$$

and

$$\frac{k_e j_l'(k_e R) + D_l h_l'(k_e R)}{k_2 j_l(k_e R) + D_l h_l(k_e R)} = \frac{B_l j_l'(k_2 R) + C_l n_l'(k_2 R)}{B_l j_l(k_2 R) + C_l n_l(k_2 R)} \quad \textbf{(5-30)}$$

The subscript (1) from the spherical Hankel function has been removed. Now, it is assumed that

$$\frac{k_1 j_l'(k_1 R_0)}{k_2 j_l'(k_1 R_0)} = \chi_l \quad \textbf{(5-31)}$$

and

$$\frac{-\chi_l n_l(k_2 R_0) + n_l'(k_2 R_0)}{\chi_l j_l(k_2 R_0) - j_l'(k_2 R_0)} = \mathcal{I}_l \quad \textbf{(5-32)}$$

thenB_l can be expressed in terms of C_l as

$$B_l = \mathcal{I}_l C_l \quad \textbf{(5-33)}$$

$D_l^{(m)}$is solved by inserting (5-33) into (5-30) as following:

$$D_l^{(m)} = \frac{-\frac{k_e j_l'(k_e R)}{k_2} + \mathcal{H}_l j_l(k_e R)}{k_e h_l'(k_e R)/k_2 - \mathcal{H}_l h_l(k_e R)} \quad \textbf{(5-34)}$$

in which we have

$$\mathcal{H}_l = \frac{\mathcal{J}_l j_l'(k_e R) + n_l'(k_2 R)}{\mathcal{J}_l j_l(k_e R) + n_l(k_2 R)} \quad \textbf{(5-35)}$$

and scattering amplitude can be calculated as in symmetric case:

$$f(k_e', k_e) = \frac{-i}{k_e} \sum_{l=0}^{\infty} D_l^{(m)}(2l+1) \quad \textbf{(5-36)}$$

wherethe optical theorem that states for forward scattering $\theta = 0$ has been used .

5.3 Numerical Procedure

Numerical solution of 1D time-independent Schrodinger equation. To calculate the t-matrix of each configuration which in turn gives us the average scattering matrix $< T >_c = < \sum_i n_i < t >_i$ where n_i is the concentration of each configuration, we need to solve the Schrodinger equation. The 1D time-independent form of Schrodinger equation which is given by $\frac{\partial^2}{\partial x^2} + k^2 = 0, k^2 = \frac{2m}{\hbar^2}(E - V)$can be integrated by stable and accurate Numerov algorithm:

$$\psi_{n+1} = \frac{2(1 - 5/12 l^2 k_n^2)_n - (1 + 1/12 l^2 k_{n-1}^2)_{n-1}}{1 + 1/12 l^2 k_{n+1}^2} \quad \textbf{(5-37)}$$

where*l* is the spatial step size. For specific values of energy the boundary conditions are satisfied and there will be a solution. To find the solution we integrate from both sides to the matching point for a given energy knowing the boundary conditions $(\mathrm{x_{left}}) = (\mathrm{x_{right}}) = 0$.

The matching point is chosen to be in the middle of the well. If the trial energy is not an Eigenvalue the slope will be discontinuousat the matching point. The code will search for the eigenvalue by minimizing the difference in the slopes of thetwo wave functions (ψ_{left} and ψ_{right}) at the matching point. The procedure is started with a trial energyE below the eigenstate.Then the$\psi_{\mathrm{left}}(\mathrm{x})$ and $\psi_{\mathrm{right}}(\mathrm{x})$ and thedifference in slopes at the matching point, $\psi'_{\mathrm{left}}(\mathrm{x_{match}}) - \psi'_{\mathrm{right}}(\mathrm{x_{match}})$,forE + ΔE, where ΔE is a suitably chosen energy increment are computed. If the difference changed sign, then it is put $\Delta E = -\Delta E/2$ and it is iterated until the desired accuracy is reached.

Scattering time. As mentioned in previous section, the basic idea of CPA is the replacement of the disordered medium by an effective medium with a complex propagation constant k_e. By demanding that the scattering amplitude resulting from the local substitution of the effective

medium by the real medium should vanish on the average, we can calculate $k_e$self consistently [4,10]. For a multicomponent composite the CPA condition can be written as:

$$Re(\sum_{i=1}^{n} x_i f_i(k_e, k_e) = 0 \quad \textbf{(5-38)}$$

whichx_i is the volume fraction of each component. $f_i$is the forward scattering amplitude for an incident plane wave scattered by a structural unit of type *i*embedded in the effective medium with probability x_i. It simply states that the real part of the average forward scattering amplitude in the effective medium is zero. The solutions of the CPA equation for different energies give us the effective band structure. The Mean Free Path (MFP) can be calculated in the long wavelength regime where the CPA is correct. In an effective medium there is no scattering to the first order but the higher order terms in expansion of scattering amplitude in terms of k_eR contain the information of MFP [4]. The MFP is exactly the leading order imaginary part of scattering amplitude or self-energy, given by

$$l = \frac{-2\pi}{Im \sum_m c_m f_m(k_e, k_e)} \quad \textbf{(5-39)}$$

Moreover, the total scattering cross section can be obtained from the optical theorem as following:

$$\sigma = \frac{4\pi}{k_e} Im \sum_m c_m f_m(k_e, k_e) \quad \textbf{(5-40)}$$

*m*refers to different species in effective medium and c_m are the local volume fractions for each configuration. It is known that the relaxation time τ is inversely proportional to the total cross section. Additionally, calculation of the scattering in terms of MFP is possible as following:

$$\tau = \frac{l}{v_g} \quad \textbf{(5-41)}$$

in which the $v_g = \frac{\hbar k}{m_{eff}}$ is the group velocity and $\hbar$, k and$m_{eff}$are reduced Planck's constant, effective medium wave vector and effective mass respectively. As all the above procedure is repeated for each amount of energy to get the effective wave vector the effective medium band structure is obtained. Therefore, one may calculate Boltzmann integrals to get the thermoelectric properties of composites by knowing the effective band structure and scattering rate [63].
It should be noted here that, by using the CPA scattering time we are incorporating the insights of an atomic-level approach into the BTE approach as a high-level approach so, a significant higher fidelity in our simulations is expected.

Root finder engine. The core of the above numerical procedure is finding the effective wave number for each value of energy k_e as a solution of the CPA condition. Therefore, a root finder engine to calculate the k_e values which satisfy the CPA condition is needed. In general, the k_e values are complex numbers [10] and complex solutions of the CPA condition should be look for.

There are many complex root finders for linear and non-linear equations which may be real-valued or complex-valued. In this dissertation two methods which are easier to understand areintroduced. In practice, the second one is followed. The first method is an extended version of secant method for real roots. It uses an iterative formula and needs two initial values but, does not need to calculate the derivative of functions and is considerably stable. To extend the regular secant method the variable *x* shouldbe replaced by the complex variable *z* to get the complex secant method formula. It is separable into two formulas, a real and an imaginary one. The initial value of the complex secant formula should be a complex number. Therefore, the method canbe expressed as the following:

$$z_{n+1} = z_n - f(z_n)\frac{z_n - z_{n-1}}{f(z_n) - f(z_{n-1})}. \quad \textbf{(5-42)}$$

By putting the $z=x+iy$in the above formula and rearranging the real and imaginary terms and equating them in both sides of the formula we get:

$$\begin{cases} x_{n+1} = x_n - f(x_n)\dfrac{x_n - x_{n-1}}{f(x_n) - f(x_{n-1})} \\ y_{n+1} = y_n - f(y_n)\dfrac{y_n - y_{n-1}}{f(y_n) - f(y_{n-1})} \end{cases} \quad \textbf{(5-43)}$$

where$n$=1,2,3,….is the iteration number. Based on above formulas the input values are two complex numbers like z_0 and $z_1$and a tolerance that determines the precision of calculations. In each step the above formulas are evaluated by two input values z_0 andz_1.

If the difference between the value of calculated root and the second input is less than the value of tolerance then the true root has been found. Otherwise, the above procedure should be repeated to get the true root within the desired precision.

Another approach that is adopted to find the solutions of the CPA condition is relatively easy. By assumption$f(z)$ is a complex valued function of the complex variable z. The procedure of finding the complex root is started from an initial value z_0. First, two successive points z_1 and $z_1 + \Delta z$ are used to define a hyperspace and then by doing a mapping in that hyperspace, the third value which is the true complex root of the hyperspace is found. This way, convergence to the true root of the main function is achieved. This procedure may be stopped in two cases: the difference between successive values is very small and the maximum number of iteration is reached. This numerical scheme should be repeated for different initial values to find all possible roots of the original function. In practice, the original function in our calculations which is the scattering amplitude has multiple roots that make the interpretation of results difficult. In fact, we need to make decision which roots be selected as a reasonable physical result. A key concept which is very useful is that in the low frequency limit, the solution for the CPA is indeed unique. When

the frequency (energy) increases, we encounter multiple roots. That is a signal that the k-dependence of the self-energy can no longer be ignored. For such situations, we can always use the so-called continuation method, i.e., we can use the solution to the CPA equation at a lower frequency (where it is unique) as an initial guess, and then use iteration or Newton's method to find the solution at a slightly higher frequency. Then,this process should be repeated to obtain solutions at higher frequencies.However, such approach breaks down eventually when the frequency is too high, and this can occur when we encounter the situation when the solution suddenly jumps to a wildly different value from the one at a lower frequency. At that point we have to quit using the CPA, and use the spectral approach as detailed in Ref. [4].

Extension to a random distribution of grain and nanoparticle sizes.Incorporation of grain sizes or nanoparticle radiuses in the CPA numerical scheme provides an additional degree of freedom for optimizing the thermoelectric properties of materials. Some parameters are related to the grain size or nanoparticle radius distribution function. Assuming a unique grain size or nanoparticle radius is not physical, but it helps to improve both the charge carrier mobility and Seebeck coefficient. Applying a distribution function for grain size or nanoparticle radius actually introduces a type of randomness or disorder to the material which in turn increases the rate of scattering [64]. In the absence of a distribution function the randomness is decreased and charge carriers have more freedom to move which means the carrier mobility will be higher. Moreover, the absence of a distribution function leads to sharp profiles in the differential conductivity versus energy. Therefore, introducing a distribution function causes less smearing. This sharpness results in a larger Seebeck coefficient and power factor.

Figure 5.3 presents the concept of assigning a size distribution function to each component grain. In the model nanocomposite as a symmetric medium there are many grains of each component as shown in the figure 5.3. Each component in nanocomposite is depicted by a different orientation of parallel lines. In this picture,the nanocomposite has been shown as an assembly of grains of three components and the model is extendible to more components. By assumption, for each component the grains are represented by a sphere which is filled with that component. The filled sphere is placed inside the effective medium. For grains of each component a discrete size distribution is assigned. The assumed distribution functions have their own average and variance.

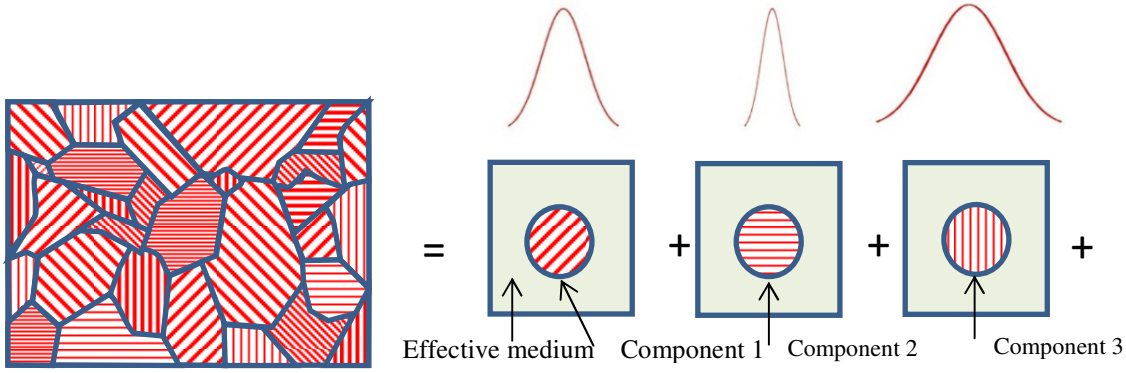

Figure 5.3: Grain size distribution function for different materials in a symmetric medium.

As it can be seen in Figure 5.4, the model material as a dispersion medium which has different embedded nanoparticles (3 components here) can be considered as an assembly of three different nanoparticles inside a host material. Each type of nanoparticle is assumed to be like a sphere inside a bigger sphere as host material. Both spheres are placed inside an effective medium. For each type of nanoparticles a discrete radius distribution is assumed. The assigned distribution functions to each nanoparticle have their own average and variance as indicated in the figure 5.4.

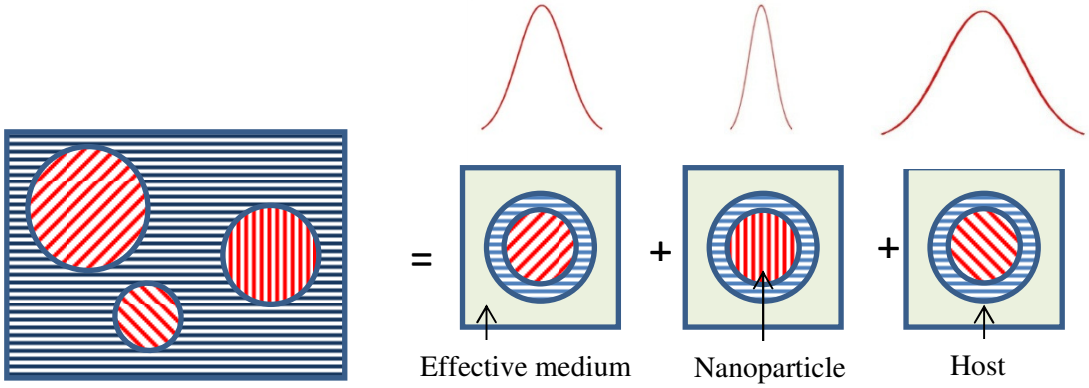

Figure 5.4: Nanoparticle radius distribution function for different materials in a dispersion medium.

For both symmetric and dispersion mediums a Gaussian distribution is assumed to investigate the size distribution effect on thermoelectric properties of materials. The average and variance of distribution can be changed. The scattering amplitude of each size is calculated by solving the scalar wave equation inside and outside the spheres. The wave functions should satisfy the boundary conditions at interfaces. The roots of the CPA equation at each energy k_e (E) define the effective band structure. Therefore, at the end of calculations we will have the effective band structure and the scattering rates. Solving the Boltzmann transport equation by given scattering times and calculated effective band structure leads to thermoelectric properties.

Extension to randomly orientated grains and nanoparticles. The orientation of grains is another property of materials which adds a new degree of freedom for optimizing the thermoelectric properties. Where crystallites or grains join together, the crystal lattice cannot be perfect and therefore a grain boundary exists. At the atomistic scale, each boundary in the atomic packing is a discontinuity. The grain boundaries are unavoidable due to geometrical reasons. In most of crystals the thickness of grain boundary is approximately few atoms. It is expected that the randomness due to new freedom decreases the electrical and thermal conductivities as a result of increase in scattering rates. It is assumed that grains follow a Gaussian distribution function to be orientated in different directions. The average and variance of Gaussian function for each component can vary. Figure 5.5 shows randomly orientated grains inside a nanocomposite versus preferred orientation grains.

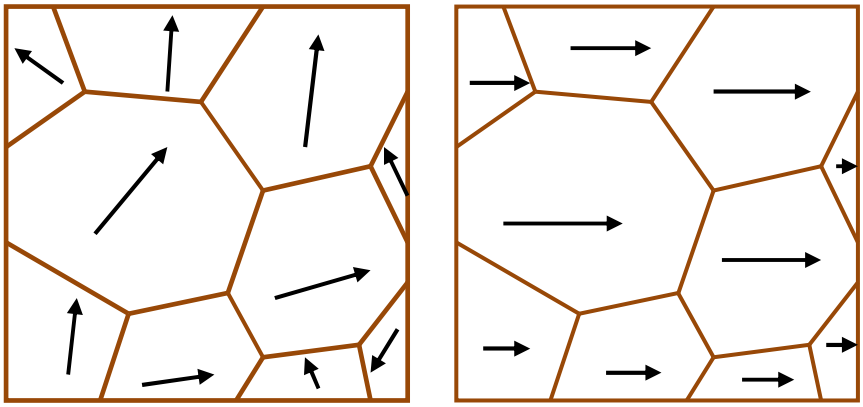

Figure 5.5: Randomly orientated grains versus preferred orientation grains.

A possibility to assign an orientation to grains is through the angular dependency of effective mass in the CPA formalism. In anisotropic materials, the effective mass varies with the direction of particle movement respect to main axes of crystals because the group velocity and crystal momentum do not point to the same direction. Therefore, the effective mass depends on the angle between group velocity and momentum. The cyclotron resonance is the most common experimental method to measure the effective mass of semiconductor materials.

For each energy step and within the parabolic band assumption, the carrier energy is a function of effective mass as the following:

$$E = \frac{\hbar^2 k_x^2}{2m_{x,eff}} + \frac{\hbar^2 k_y^2}{2m_{y,eff}} + \frac{\hbar^2 k_z^2}{2m_{z,eff}} \quad \textbf{(5-44)}$$

where k_x ,k_y, k_z are the components of wave vector along main axes of crystal. After scattering of carriers by grain boundary or interfaces, their energy does not change but their momentum (which is a vector quantity) may change. By equating the energies before and after scattering the effective mass of carriers can be expressed as a scalar function of individual effective masses along main axes of a crystal as below:

$$\begin{aligned} E &= \frac{\hbar^2 k_x^2}{2m_{x,eff}} + \frac{\hbar^2 k_y^2}{2m_{y,eff}} + \frac{\hbar^2 k_z^2}{2m_{z,eff}} \\ &= \frac{\hbar^2 k'^2_x}{2m_{x,eff}} + \frac{\hbar^2 k'^2_y}{2m_{y,eff}} + \frac{\hbar^2 k'^2_z}{2m_{z,eff}} \end{aligned} \quad \textbf{(5-45)}$$

where k'_x, k'_y and k'_z are the components of scattered wave vector and are given by $k'_x = k\sin\theta\cos\varphi$, $k'_y = k\sin\theta\sin\varphi$ and $k'_z = k\cos\theta$. By inserting the primed components of wave vector in above expression for energy results in the following equation:

$$\frac{1}{m^*} = \frac{\sin^2\theta cos^2\varphi}{m_x} + \frac{\sin^2\theta sin^2\varphi}{m_y} + \frac{cos^2\theta}{m_z} \quad \textbf{(5-46)}$$

Now, the scalar effective mass is not a function of energy and varies with angles $\theta$and φ. Therefore, the carrier energy can be expressed as $E = E(\theta, \varphi)$.

Extension of the CPA formalism for phonons. The phonon waves can be treated like electron waves in the CPA formalism as well. For the phonon case, we should take into account two key concepts. Firstly, the phonon energy is given by:

$$E = \hbar\omega = \hbar v_g k, \quad k_{x,y,z} = \frac{l,m,n}{\sqrt{l^2+m^2+n^2}} \quad \textbf{(5-47)}$$

wherev_g is the phonon group velocity or sound speed, ω is the angular frequency and l, m, n are the Miller indices. The Miller indices are the coordinates of the normal in a system defined by the reciprocal lattice, rather than the direct lattice. The Miller indices are directions in the reciprocal lattice. Therefore, for the charge carrier each new material in nanocomposite is introduced by its different effective mass, while for phonon each new material or component in the nanocomposite is introduced by its specific phonon group velocity. So, a possibility to incorporate the orientation of grains in the CPA formalism for phonons is assigning a particular direction to phonon energy through the wave vector. In reality, the group velocity of phonons depends on the direction and magnitude of the phonon wave vector and is specific to the phonon polarization. The second point is that we should take into account the Bose-Einstein distribution function (look at Equation (3-4)) instead of Fermi-Dirac distribution in calculation of average values of scattering times over different grain sizes and different directions:
The goal is to find the phonon group velocity in a desired direction in terms of θ and φ given the elastic constants of the grain or crystallite. For this purpose, solving the elastic wave equations in a crystal are needed [48]:

$$\rho\frac{\partial^2 u}{\partial t^2} = C_{11}\frac{\partial^2 u}{\partial x^2} + C_{44}\left(\frac{\partial^2 u}{\partial y^2} + \frac{\partial^2 u}{\partial z^2}\right) + (C_{12}+C_{14})\left(\frac{\partial^2 v}{\partial x\partial y} + \frac{\partial^2 w}{\partial x\partial z}\right)$$

$$\rho\frac{\partial^2 v}{\partial t^2} = C_{11}\frac{\partial^2 v}{\partial y^2} + C_{44}\left(\frac{\partial^2 v}{\partial x^2} + \frac{\partial^2 v}{\partial z^2}\right) + (C_{12}+C_{14})\left(\frac{\partial^2 u}{\partial x\partial y} + \frac{\partial^2 w}{\partial y\partial z}\right)$$

$$\rho\frac{\partial^2 w}{\partial t^2} = C_{11}\frac{\partial^2 w}{\partial x^2} + C_{44}\left(\frac{\partial^2 w}{\partial x^2} + \frac{\partial^2 w}{\partial y^2}\right) + (C_{12}+C_{14})\left(\frac{\partial^2 u}{\partial x\partial y} + \frac{\partial^2 v}{\partial y\partial z}\right) \quad \textbf{(5-48)}$$

in which ρ is density of atoms, *u* ,*v, w* are the displacements of atomic planes in *x, y* and *z* directions respectively and C_{ij} are the elastic stiffness constants. It should be noted that the above equations are valid only for cubic crystals. Similar equations are available for hexagonal crystals. In this dissertation a random distribution of phonon group velocity for non-cubic crystals is assumed. For each desired direction the relevant general solution is inserted into the above three equations and all the terms are rearranged to put the terms which include *u, v* and *w* together. Finally, an eigenvalue equation is obtained. The eigenvalues give us the phonon group velocity as a function of components of wave vector$k_{x,y,z}$. As stated in Equation (5-47) these components are related to Miller indices that in turn indicate a particular direction in terms of θ and φ. In this way, we can express the phonon group velocity as a function θ and φ i.e. v_g=$v_g(\theta,\varphi)$. Therefore, the phonon energy can be expressedas a function of angleas $E = E(\theta,\varphi)$.

For more clarification, the above mentioned procedure is applied for direction [111] in the following:

thedisplacements for waves in the [111] direction are set as:

$$u(r,t) = u_0 e^{i(\frac{k}{\sqrt{3}}(x+y+z)-\omega t))}, \qquad v(r,t) = v_0 e^{i(\frac{k}{\sqrt{3}}(x+y+z)-\omega t))} \qquad and$$

$$w(r,t) = w_0 e^{i(\frac{k}{\sqrt{3}}(x+y+z)-\omega t))} \qquad \textbf{(5-49)}$$

After substitution of above solutions in equation (5-48) and rearranging them an eigenvalue equation is obtained:

$$C_{11}k_x^2u_0 + C_{44}(k_y^2+k_z^2)u_0 + (C_{12}+C_{44})k_xk_yv_0 + (C_{12}+C_{44})k_xk_zw_0 = \rho\omega^2u_0$$

$$C_{11}k_y^2v_0 + C_{44}(k_x^2+k_z^2)v_0 + (C_{12}+C_{44})k_xk_yu_0 + (C_{12}+C_{44})k_yk_zw_0 = \rho\omega^2v_0$$

$$C_{11}k_z^2w_0 + C_{44}(k_x^2+k_y^2)w_0 + (C_{12}+C_{44})k_xk_zu_0 + (C_{12}+C_{44})k_yk_zv_0 = \rho\omega^2w_0 \qquad \textbf{(5-50)}$$

Setting the determinant of coefficients of u_0, v_0 and w_0 in the left hand side of (5-49) equal to zero:

$$\begin{vmatrix} C_{11}k_x^2 + C_{44}(k_y^2+k_z^2) & (C_{12}+C_{44})k_xk_y & (C_{12}+C_{44})k_xk_z \\ (C_{12}+C_{44})k_xk_y & C_{11}k_y^2 + C_{44}(k_x^2+k_z^2) & (C_{12}+C_{44})k_yk_z \\ (C_{12}+C_{44})k_xk_z & (C_{12}+C_{44})k_yk_z & C_{11}k_z^2 + C_{44}(k_x^2+k_y^2) \end{vmatrix} = 0 \qquad \textbf{(5-51)}$$

leads to a characteristic equation which has 3 roots. One root is the velocity of longitudinal wave:

$$v_l = \frac{k^2}{3}(C_{11}+2C_{12}+4C_{44}) \qquad \textbf{(5-52)}$$

and the other two roots are the velocities of transversal waves:

$$v_t = \frac{k^2}{3}(C_{11} - C_{12} + 1C_{44}) \quad \textbf{(5-53)}$$

which are equal meaning that the two transverse branches are degenerate. A single-branch polarization average velocity v along a particular direction can be calculated as the following [50, 65]:

$$v = \frac{1}{\frac{1}{3}(\frac{1}{v_l} + \frac{1}{v_t} + \frac{1}{v_t})} \quad \textbf{(5-54)}$$

This angle dependent average velocity, which is used to calculate the phonon energy, introduces angular dependency to numerical scheme for solving the phonon CPA formalism.

CHAPTER VI

RESULTS AND DISCUSSION

The present Chapter explores the use of Coherent Potential Approximationas introduced by Sheng [4] for investigating the charge and thermal transfer properties.The focus of the dissertation is on the SiGe and Bi_2Te_3-Sb_2Te_3nanocomposites without loss of generality.The developed MATLAB code is applicable for other nanocomposites as well. Only the symmetric microstructure unit in which the grains are exchangeable is considered for both SiGe and Bi_2Te_3-Sb_2Te_3nanocompositesin this research. Figure 6-1 depicts the schematics of the investigated systems.The nanocomposites include the separate single alloy grains. The grains are randomly orientated and have different sizes. Their orientation has been represented by the parallel lines. The main important result of the code for each material system is the grain boundary scattering time for both charge carriers and phonons. The calculated scattering times can be used directly in the Boltzmann transport equation. The band structure of charge carriers and also phonon dispersion in nanocomposite which give us the effective mass and the speed of sound in the calculated effective medium respectively are other outcomes of the code. Moreover, the variation of effective mass and speed of sound versus grain size are obtained. Some other quantities like scattering total cross section, non-parabolicityand band-gap change can be calculated. The code is able to consider the angular orientation of grains as well as grain size as the main independent variable but only grain size is used as the independent variable. The angular orientations are used

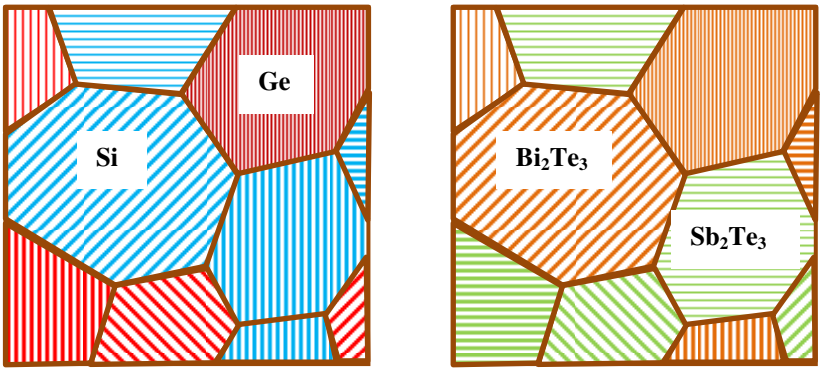

Figure 6.1: Schematics of nanocomposites investigated in this dissertation.

to show the effect of random orientation on the level of intensity of grain boundary scattering time for both charge carriers and phonons.

6.1 Basic Parameters

It has been mentioned already in Section 5.3 that for the charge carrier each new material in nanocomposite is introduced by its different effective mass, while for phonon each new material or component in the nanocomposite is introduced by its specific phonon group velocity (sound velocity) in CPA formalism.Other than effective mass and phonon group velocity we need to know the Debye temperature and the density of each material in nanocomposite. The operation and Debye temperatures are used for calculation of average scattering times over different configurations. The experimental data used in this dissertation are presented in the Table 6.1. In this dissertation the focus is on the nanocomposite structure and not specific materials. Therefore, the materials used for calculation are examples of the CPA application. The n-type Si-Ge system and p-type Bi_2Te_3 - Sb_2Te_3has been used for calculations unless stated.

Table 1: The basic parameters used in the CPA calculations.

Property	Reference	Bi_2Te_3	Sb_2Te_3	Si	Ge
Effective mass m_1*,kg	Ioffe [66] ,Landolt-Bornstein [67]	$0.69m_e$	$0.97m_e$	$0.98m_e$	$1.59m_e$
Effective mass m_2*,kg	Ioffe ,Landolt-Bornstein	$0.69m_e$	$0.97m_e$	$0.19m_e$	$0.0815m_e$
Effective mass m_3*,kg	Ioffe ,Landolt-Bornstein	$0.69m_e$	$0.97m_e$	$0.19m_e$	$0.0815m_e$
Phonon group velocity$v_s, m/s$	Landolt-Bornstein	3058	2888	8433	5400
Debye temperatureT_D, K	Landolt-Bornstein	165	160	645	374
Densityρ,g/cm^3	Ioffe,Landolt-Bornstein	7.86	6.50	2.329	5.3234

*In case of Bi_2Te_3 and Sb_2Te_3 the values of effective mass are calculated through fitting the charge carrier mobility resulted from Boltzmann transport equation to experimental data.

The standard deviation of grain size and angular orientation distributions used in calculations has been set to 0.1.

6.2 Fitting Procedure

To have smooth curves and avoid accumulated numerical errors the calculated curves are fitted to proper polynomials. The effect of induced numerical error resulted from applying fitted curves instead of original curves can be neglected due to averaging process which is performed for scattering time over different configurations. To have better understanding of the effect of fitting procedure on calculated quantities, the calculated scattering time and total cross section curves along with their relevant fitted curves for both charge carrier and phonon in case of Bi_2Te_3-Sb_2Te_3 nanocomposite are presented in Figures 6.2 and 6.3 respectively.

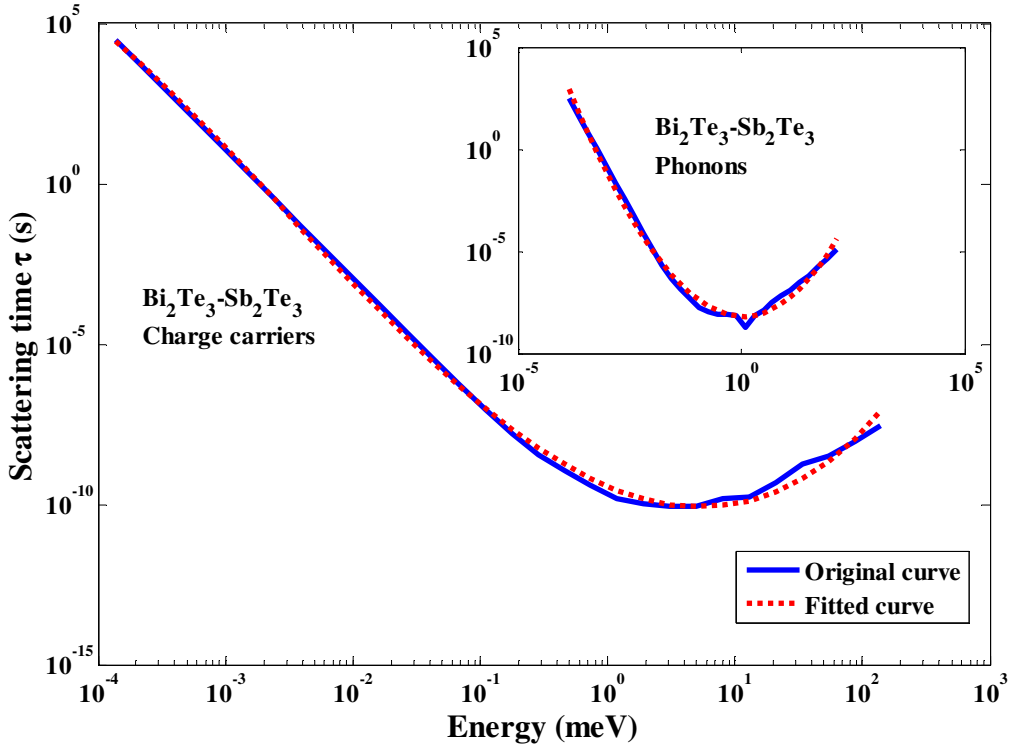

Figure 6.2: Original calculated scattering time curve along with the fitted curve for both of charge carriers and phonons in Bi_2Te_3-Sb_2Te_3 nanocomposite.

As it can be seen from Figure 6.2, the difference between original curve and fitted curve is negligible. The main Figure depicts the scattering time of charge carriers and the inset indicates the scattering time of phonons for Bi_2Te_3 - Sb_2Te_3.Additionally, Figure 6.3 clearly shows the difference between original curve and fitted one is negligible for both charge carriers and phonons. Moreover, from a statistical point of view the average discrepancy almost vanishes after the process of average calculation in which many different configurations are used.

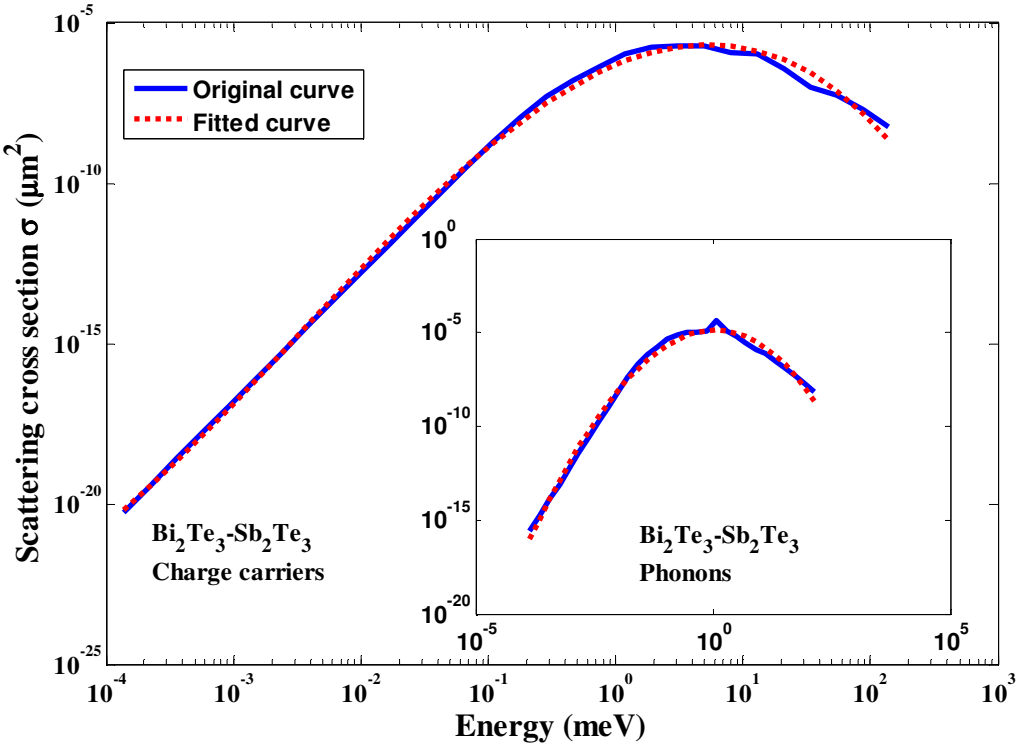

Figure 6.3:Original calculated total cross section curve along with the fitted curve for both of charge carriers and phonons in Bi_2Te_3-Sb_2Te_3 nanocomposite.

6.4 Band Structure, Phonon Dispersion, Effective Mass and Sound Velocity

The important factor for the effective mass is the curvature of the dispersion curve at the minimum of conduction band or maximum of the valence band because it is relevant to the second derivative of energy respect to wave number. Large second derivative or small radius of curvature gives small effective mass and small second derivative or large radius of curvature leads large effective mass.

The effective mass of charge carriers in effective medium can be calculated using the resulted band structure or E-k curve in the effective medium. For each energy level the CPA takes the wave numbers of components in nanocomposite and calculates the effective medium wave number for same energy level. The charge carrier energy is changed gradually and for each energy a corresponding wave number is calculated for effective medium.

The band structure diagram for Bi_2Te_3-Sb_2Te_3 as a two components nanocomposite has been presented in Figure 6.5. It shows a typical band structure diagram which is calculated by the CPA.

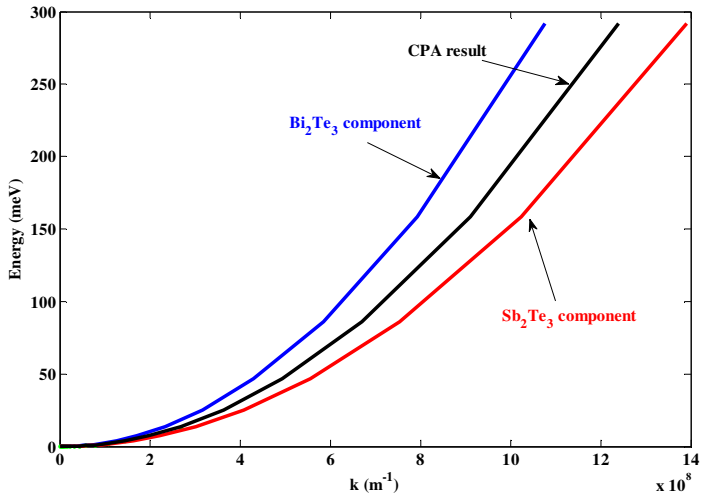

Figure 6.4: The energy band diagram for components of Bi_2Te_3-Sb_2Te_3 and the relevant effective medium.

It should be mentioned that the volume fraction for each component is 0.5 and the angular orientation which has been assigned to grains in this calculation was very small and negligible (0.001^o). The CPA wave number seems as an average of the wave numbers of components.

A phonon unlike a photon in a box cannot have infinite energy. Its frequency is determined by the medium of its propagation. So, in the effective medium which is specified with its effective wave number there will be a new speed for propagation of sound.

Acoustic phonons are main carriers of thermal energy in most of semiconductors and their spectrum in low energies is linear. Therefore, in low energy limit the Debye model can be used to describe the phonon dispersion relations. It is clear from Figure 6.5 that the slope of line resulted by the CPA calculation as the speed of sound in effective medium is like the average of speeds of sound in components of nanocomposite Bi_2Te_3-Sb_2Te_3. Again, the volume fraction for each component is 0.5 and the angular dependency of phonon group velocity is very small (0.001^o).

The presented band structure and phonon spectrum for Bi_2Te_3-Sb_2Te_3 nanocomposite are typical and without loss of generality the similar results are obtained for Si-Ge system.

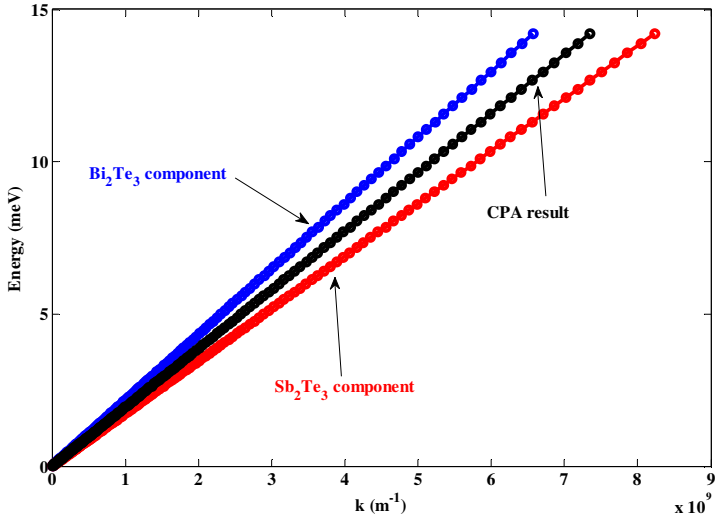

Figure 6.5:The phonon dispersion diagram for components of Bi_2Te_3-Sb_2Te_3 and the relevant effective medium.

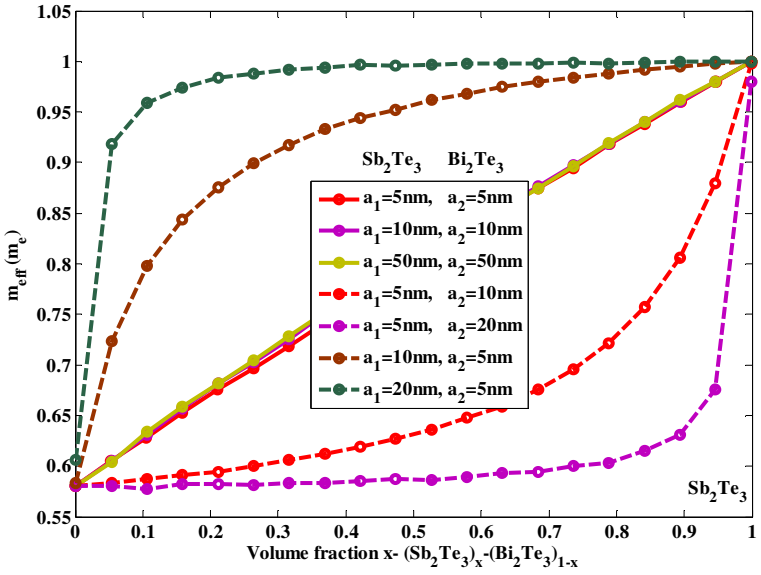

Figure 6.6:Variation of effective mass versus grain size in the calculated effective medium for Bi_2Te_3-Sb_2Te_3 nanocomposite.

The calculated values of effective mass for Bi_2Te_3-Sb_2Te_3 nanocomposite has been given in the Figure 6.6. It shows that if the grain sizes of both components in the nanocomposite are equal then the resulted effective mass is the average of effective masses. The resulted effective mass

has a linear dependency on volume fraction. Moreover, if the grain sizes are not equal then two cases are raised:

1- $a_1<a_2$
   In this case as the difference between a_1 and a_2 increases the contribution of component with smaller effective mass (a_1) in the effective mass of the effective medium increases.
2- $a_1>a_2$
   In this case as the difference between a_1 and a_2 increases the contribution of component with greater effective mass (a_2) in the effective mass of effective medium increases.

In summary, the value of effective mass of the effective medium depends on the ratio of grain sizes and the effective mass values of the components of the nanocomposite. In fact, the effective mass of effective medium follows the larger grain size.The Figure 6.7 shows a similar result for the phonon group velocity of the effective medium. The value of the phonon group velocity of the effective medium is a function of the ratio of the grain sizes of the components and the phonon group velocities of the components. Similar statements can be expressed for the effective phonon group velocity of effective medium. If the grain sizes of both

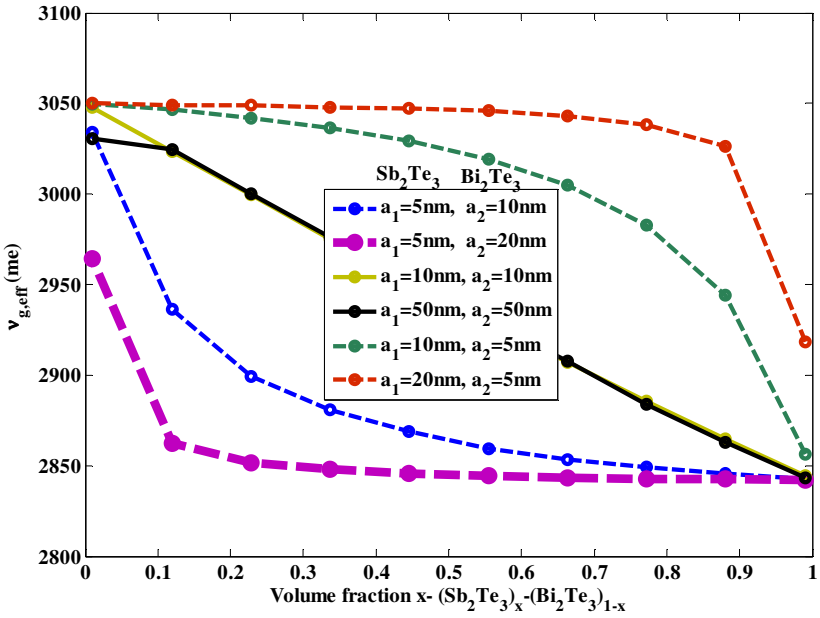

Figure 6.7:Variation of effective phonon group velocity versus grain size in the calculated effective medium for Bi_2Te_3-Sb_2Te_3 nanocomposite.

components in the nanocomposite are equal then the resulted effective speed of sound is the average of speeds of sounds in the component and has a linear dependency on volume fraction. Furthermore, if the grain sizes are not equal then two cases are raised:

3- $a_1<a_2$
In this case as the difference between a_1 and a_2 increases the contribution of component with smaller speed of sound (a_1) in the speed of sound of the effective medium increases.

4- $a_1>a_2$
In this case as the difference between a_1 and a_2 increases the contribution of component with greater speed of sound (a_2) in the speed of sound of the effective medium increases.

In brief, the effective phonon group velocity follows the larger grain size.

6.4 The Optimized Grain Size

One of the most useful results of the CPA is the optimum value for grain size in the nanocomposite. The minimum in the scattering time curve of charge carriers indicates the maximum number of scattering events which reduces the electrical conductivity. Therefore, staying away from the minimum of scattering time for charge carriers is desired and the range of grain sizes which the minimum scattering time occurs for them should be avoided. The minimum in the scattering time curve of phonons represents the maximum number of scattering events which reduces the thermal conductivity. The reduction of thermal conductivity in the context of thermoelectrics is favorable so, the range of grain sizes that the minimum scattering time occurs for them is desirable. If the minimums of charge carrier and phonon scattering times coincide then there is no chance to reduce the thermal conductivity without deteriorating the electrical conductivity

.

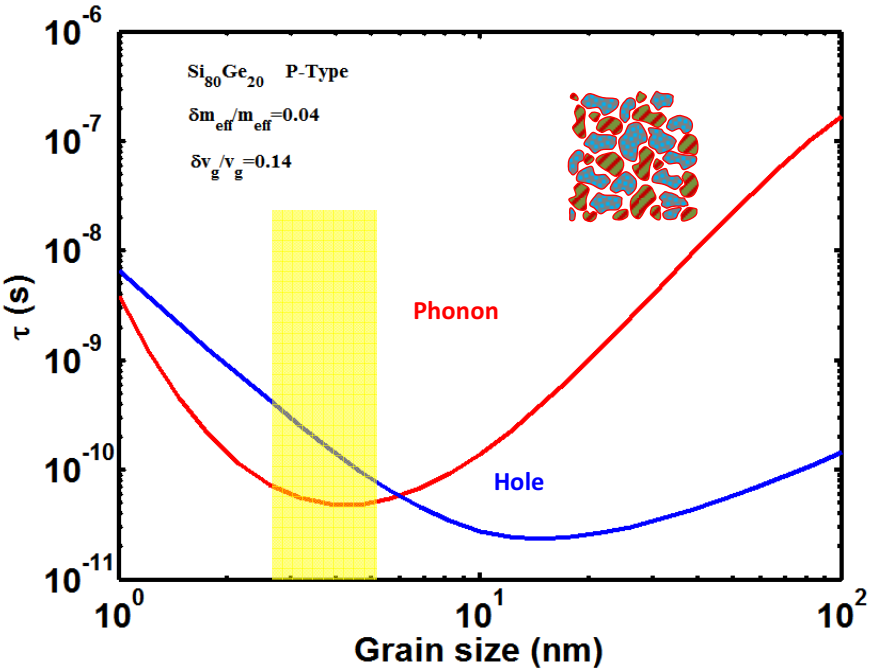

Figure 6.8: Hole and phonon GB scattering relaxation times versus grain size for nanostructured $Si_{0.8}Ge_{0.2}$.

Figure 6.8 shows the result of calculation of GB scattering times for holes and phonons via CPA formalism in a nanostrcutured $Si_{0.8}Ge_{0.2}$ material. First of all, the existence of minimum in the scattering time for both charge carriers and phonons is notable and helps us to find the optimum grain size. Secondly, the phonon relaxation time has a minimum at ~4nm and electron relaxation time has a minimum at ~10nm. This result presents a criterion for the grain size to be in the range of 4 nm for reducing the thermal conductivity without significantly affecting the charge carrier mobility. Such a result is the core of the CPA outcomes for designing optimized thermoelectric materials.

In Figure 6.9 the calculated GB scattering times for both charge carriers and phonons are depicted for a range of volume fractions. There exist minimums in scattering time for both charge carriers and phonons. Additionally, the phonon scattering time has a minimum at 1.5 nm and electron scattering time has a minimum at ~ 7 to 10 nm. These numbers indicate a criterion for the grain size to be in the range of 1-2 nm to reduce the thermal conductivity without affecting the electron mobility considerably.

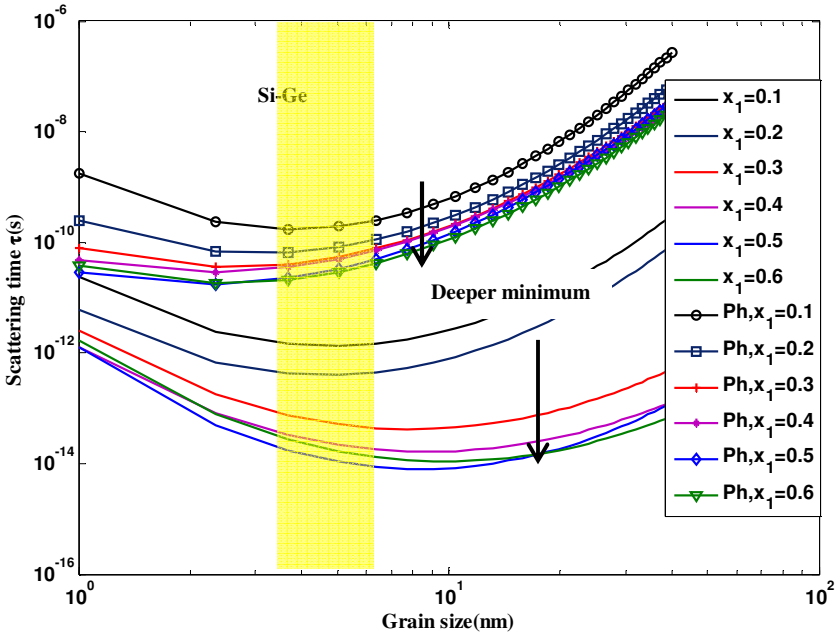

Figure 6.9:Charge carrier and phonon grain boundary scattering times versus grain size for nanocomposite Si-Ge. The grain size of Si is 10 nm and the grain size of Ge varies from 1nm to 100nm.

6.5 The Effect of Random Orientation

As mentioned in the Section 5.3 the orientation of grains is a property of materials which increases the degree of freedom for optimizing the thermoelectric properties. Where crystallites

or grains join together, the crystal lattice cannot be perfect and therefore a grain boundary exists. The grain boundaries are unavoidable due to geometrical reasons. The grains have randomly orientated crystal directions which can be expressed by a Gaussian distribution function for each component separately. The randomness due to new freedom decreases both electrical and thermal conductivities as a result of increase in number of scattering events. The effect of randomized orientation on phonon GB scattering time has been investigated for both Bi_2Te_3-Sb_2Te_3 and Si-Ge systems and the results have been presented in Figures 5.5 and 6.6 respectively. The average values of Gaussian distribution functions are increased gradually from 0.001^o to 180^o and 360^o for angles θ and φ respectively while the standard deviation is 0.1. The volume fractions of components for both nanocomposites are equal. The grain size of the second component a_2 varies from 1nm to 100 nm while the grain size of the first component a_1 was kept equal to 10 nm. It is clear from Figures 6.10 and 6.11 that as randomness of angles is increased the value of scattering time increases and the curve minimums go down. The similar result was obtained for phonon grain boundary scattering time in case of Si-Genanocomposite. These observations are in agreement to the physical intuition that more randomness leads to larger scattering rates.

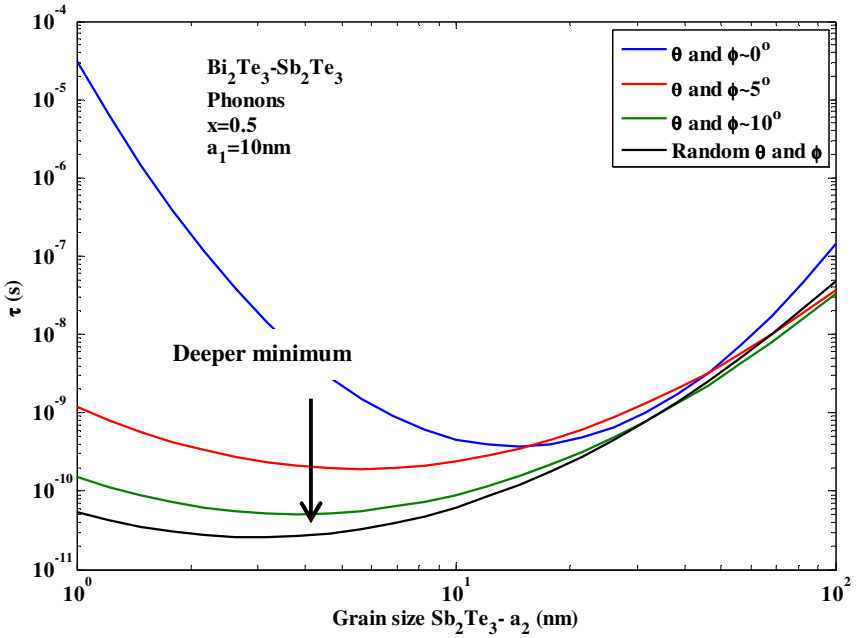

Figure 6.10: Variation of the phonon GB scattering time versus grain size of Sb_2Te_3 while the grain size of Bi_2Te_3 is kept constant and the volume fractions are equal.

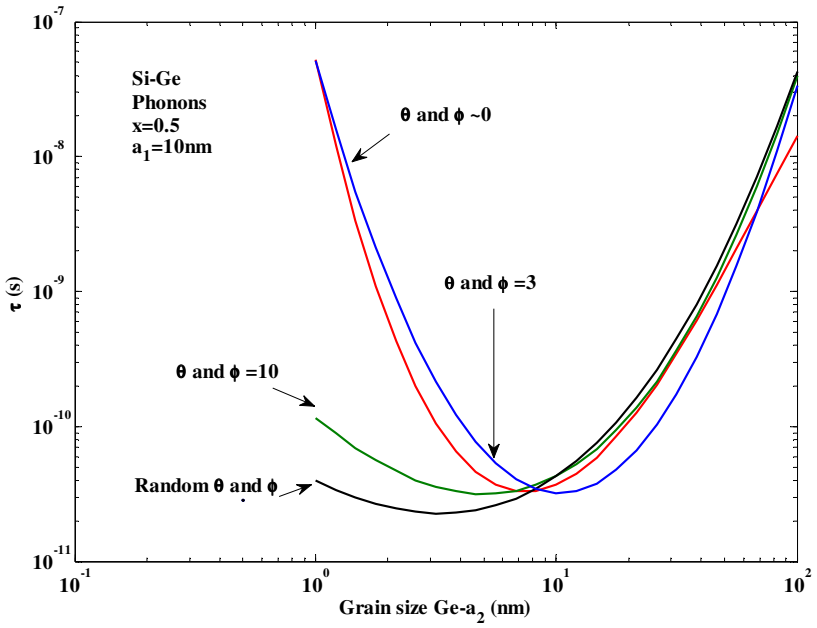

Figure 6.11:Variation of the phonon GB scattering time versus grain size of Ge while the grain size of Si is kept constant and the volume fractions are equal.

6.6 Validation of the Code

Validating the calculated grain boundary scattering time by comparison to experimental data is difficult. The experimental data are rare subject to specific conditions. Therefore, a direct comparison of theoretical and experimental data seems impractical. In practice, the estimated data of interfacial or grain boundary scattering time is combined with other types of scattering times like impurity, intervalley and alloy scattering based on Matthienssen's rule. Each scattering time has some unknown parameters which are obtained through fitting the calculated quantities like charge carrier mobility to available measured data of charge carrier mobility. By this method the fitting parameters are tuned.

Validation of the code can be achieved through checking the calculated results in physical limits. If the code meets some known physical requirements then it gains credit. The code predicts correctly the amount of scattering time while the effective masses for both components in a nanocomposite are equal. The charge carriers are scattered from grain boundaries whenever they see a new effective mass so, if the effective masses are equal then there will be no scattering and the written code satisfies this condition very well. Moreover, it is expected to have more scattering as the degree of freedom for scattering increases. For example, incorporation of angles

into scattering mechanism provides more freedom for scattering events and so, smaller scattering times are expected. As it has been shown in the Section 6.5 the angle increment leads to more scattering event, smaller scattering time and deeper minimum in the scattering time curve. Furthermore, for the both limits of volume fraction x=0 and x=1 there will be only one type of component meaning that there is no change in the effective medium and therefore, the scattering should vanish. The code shows that for very small or very large volume fractions like x=0.001 and x=0.999 the scattering time tends to go to infinity. This trend is another evident that the code is trustable. In summary, the code is able to correctly predict the scattering time in physical limits for effective mass, angles of orientation and volume fraction.

Additionally, it is known that the order of magnitude for charge carrier and phonon scattering times varies from 10^{-10} to 10^{-14} and from 10^{-8} to 10^{-12} second respectively. All the figures presented in Sections 6.4 and 6.5 show the expected order of magnitude for grain boundary scattering times.

6.7 Conclusionand Future Studies

The Boltzmann transport equation (BTE) is dominant in the field of semi-classical transport for devices. The sizes of semiconductor devices is decreasing into nanometer scale so, the Boltzmann transport equation which considers the charge carriers and phonons as particles gets more inaccurate. The size effects include a wide range of problems like interfaces, surfaces and metal boundaries and the influence of these boundaries onimportant semiconductor parameters.The BTE is named semi-classical because it includes both Newtonian mechanics and quantum scattering mechanisms. Therefore it is valid only in a specific regime in which the quantum effects are negligible. One solution is to use the Monte Carlo approach to solve the BTE.This approach is not suitable due to its heavy computational effort. The Landauer-Buttiker approach can be used for ballistic regime. In this regime scattering events don't affect the carriers. However, to incorporate the quantum effects in the nanoscale regime the Schrodinger equation is needed. Moreover, the non-equilibrium Green's function (NEGF) approach is suitable to handle open systems for both of ballistic and scattering dominated regime depending on the mean free path (MFP) of carriers. The system is in the ballistic regime if the MFP is longer than the device size and it is in the scattering dominated regime if the MFP is smaller than the device size. Another quantum approach which is used for both ballistic and scattering dominated regimes is the Wigner equation which is not positive definite but its results converge to BTE results in the classical limit. There are many other quantum approaches which are not common.
The proposed approach in this dissertation is based on the substituting the input scattering times resulted from a particle based formalism for the scattering times which are obtained from a wave based formalism in the BTE. The developed CPA in this dissertation can replace the particle based model grain boundary scattering time by a wave based model grain boundary scattering time.

A potentially promising work in future would be replacing all types of scattering times resulted from particle based models by scattering times resulted from wave based models.

Although the developed CPA in this dissertation is applies only for two nanocompositesBi_2Te_3-Sb_2Te_3 and Si-Ge but it is good to emphasize that it is applicable for all thermoelectric

nanocomposites. Nanocomposites have introduced a new paradigm in thermoelectric field and this field seems promising. Therefore, it is expected that the CPA has many applications in the field of thermoelectric nanocomposites.

REFERENCES

[1] G. Slack, in CRC Handbook of Thermoelectrics (Ed: D.M. Rowe), CRC Press (1995).

[2] A.F. Ioffe, Semiconductor Thermoelements and Thermoelectric Cooling, Infosearch Ltd.(1957).

[3] A. Fasolino and E. Molinari, Surf. Sci. 228, 112 (1990).

[4] P. Sheng, Introduction to Wave Scattering, Localization and Mesoscopic Phenomena, Academic, New York (1995).

[5] D. J. Bergman and L. J. Fel, J. Appl. Phys. 85, 8205, (1999).

[6] L.Nordheim, Ann. Phys. (Leips) 9, 607 (1931).

[7] R. J. Elliott and D. W. Taylor, Proc. R. Soc. Lond. A 296, 161 (1967).

[8] Yonezawa and Morigaki, Prog. Theor.Phys. Suppl. 53, 1 (1973).

[9] C. W. Myles and J. D. Dow, Phys. Rev. B 19, 4939 (1979).

[10] E. N. Economou, Green's Function in Quantum Physics, New York: Springer-Verlag, (1979).

[11] M. Lax, Rev. Mod. Phys. 23, 287 (1951).

[12] D. W. Taylor, Phys. Rev. 156, 1017 (1967).

[13] P. Soven, Phys. Rev. 156, 809 (1967).

[14] P.N.Sen and W.M.Hartmann, Phys. Rev. B9, 367 (1974).

[15] L. Schwartz, H. Krakauer and H. Fukuyama, Phys. Rev. Lett.30, 746 (1973).

[16] B.G.Nickel and J.A.Krumhansl, Phys. Rev. B4, 4354 (1971).

[17] T.M. Tritt, Ed., Semiconductor and Semimetals 71 (2001).

[81] L.D. Hicks and M.S. Dresselhaus, Phys. Rev. B 47, 16631 (1993).

[19] G. Chen, Phys. Rev. B 57, 14958 (1998).

[20] B. Yang, and G. Chen, Thermal Conductivity: Theory, Properties and Applications (Ed: T.M. Tritt), Kluwar Press (2005).

[21] C.R. Tellier and A.J. Tosser, Size Effects in Thin Films, Elsevier (1982).

[22] G. Chen, J. of Heat Trans, 119, p. 220, (1997).

[23] S. Tamura, Y. Tanaka, and H. J. Maris, Phy. Rev. B 60, p. 2627 (1999).

[24] B. Yang and G. Chen, Phys. Rev. B 67, 195311 (1-4), (2003).

[25] G. Chen, D. Borca-Tasciuc, and R.G. Yang, "Nanoscale Heat Transfer" in"Encyclopedia of Nanoscience and Nanotechnology", eds. H.S. Nalwa, AmericanScientific Publishers Vol. 7 (2004).

[26] R Landauer, IBM J. Res. Dev., Vol.1, p.223, 1957; Vol.32, p.306, (1988).

[27] M Buttiker, Phys. Rev. Lett., Vol.57, p.1761, (1986).

[28] G. Chen, Semiconductors and Semimetals 71, 2003 (2001).

[29] R.G. Yang and G. Chen, Phys. Rev. B 69, 195316 (2004).

[30] T.C. Harman, P.J. Taylor, M.P. Walsh, and B. E. LaForge, Science 297, 2229 (2002).

[31] R. Venkatasubramanian, E. Silvona, T. Colpitts, and B. O'Quinn, Nature 413, 597 (2001).

[32] P.L. Kapitza, J. Phys. 4, 181 (1941); E.T. Swartz and R.O. Pohl, Rev. Mod. Phys. 61, 605 (1989).

[33] Y. Benvensite and T. Miloh, J. Appl. Phys. 69, 1337 (1991).

[34] Z. Zamanipour and D. Vashaee , Comparison of Thermoelectric Properties of p-type NanostrcuturedBulk Si0.8Ge0.2 Alloy with Si0.8Ge0.2 Composites Embedded with CrSi2 Nano-inclusisons, in press at J. of Applied Physics, (2012).

[35] R. Kubo, Statistical-Mechanical Theory of Irreversible Processes. I. General Theory and Simple Applications to Magnetic and Conduction Problems, J. Phys. Soc. Jpn. 12 (1957).

[36] R. Landolt-Bornstein, Zahlenwerte und FunktionenausNaturwissenschaft und techni, N. S. VolIII 17a, Springer (1982) and references quoted therein.

[37] P Girault, C Blanchard, P Grosbras and J. F Barbot, J. Materials Science, Vol 32, Number 14 (1997).

[38] B. L. Gelmont, M Shur, et al, J. Appl. Phys. 77 (2), 657 (1995).

[39] D. M. Zayachuk, Semiconductors 31 (2), February (1997).

[40] W. E. Taylor, N. H. Odell, and H. Y. Fan, Phys. Rev. 93, 666-667 (1954).

[41] C. H. Seeger and T. G. Castner, J. Appl. Phys. 49, 3879-3889 (1978).

[42] K. Seeger, Semiconductor Physics (Springer-Verlag, New York, 1989) 4th ed.

[43] M. Abramowitz and I. Stegun, "Handbook of Mathematical Functions." Dover Publications Inc., New York, (1965).

[44] B. M. Askerov, "Electron Transport Phenomena in Semiconductors", World Scientific Pub Co Inc; Reissue edition (1994).

[45] R. J. M. Ziman, Philos. Mag. 1, 191 (1956).

[46] Yu. I. Ravich, B. A. Efimova, V. I. Tamarchenko, phys. stat. sol. (b) 43, 11 (1971)

[47] P. Csavinsky, Physical Review, 131, 5, (1963).

[48] C. Kittel, Introduction to Solid State Physics, John Wiley & Sons, INC, New York, 5th edition, (1976).

[49] G. Chen, Nanoscale Energy Transport and Conversion, Oxford, New York, (2005).

[50] J. Callaway, "Model for Lattice Thermal Conductivity at Low Temperatures", Phys. Rev.113, 1046 (1959).

[51] J. M. Ziman, Philos. Mag. 2,292 (1957).

[52] Pomeranchuk, J. of Physics, VI, 6, 237, (1942).

[53] P. G. Klemens, Proceedings of the Royal Society of London. Series A, Mathematical and Physical Sciences, Vol. 208, No. 1092.(Aug. 7, 1951), pp. 108-133.

[54] R.J.Elliott, J.A.Krumhansl and P.L.Leath, Rev. Mod.Phys. 46, 465 (1974).

[55] H.Ehrenreih and L.Schwartz, Solid State Phys. 31,(1976).

[56] Y.Onodera and Y.Toyazawa, J. Phys. Soc. Japan 24, 341 (1968).

[57] P. L. Leath, Phys. Rev. 171, 725 (1968).

[58] T. Matsubara, Prog. Theor.Phys. Suppl. 46, 326 (1970).

[59] P. L. Leath, Phys. Rev. 32, 3078 (1970).

[60] L. C. Pavis, Phys. Rev. B28, 6961, (1983).

[61] R. N. Aiyer, R.J.Elliott, J.A.Krumhansl and P.L.Leath, Phys.Rev.181, 1006 (1969).

[62] B. G. Nickel and J.A.Krumhansl, Phys. Rev. B4, 4354 (1971).

[63] M. P. Marder, Condensed Matter Physics, John Wiley and Sons, New York, (2000).

[64] M.Zebarjadi, K. Esfarjani, Z. Bian, A. Shakouri, Nano Lett. , 11 (1), 225−230 (2010).

[65] F. Seitz, D. Turnbull, Solid state physics, Vol. 7. Academic, New York, (1958).

[66]http://www.ioffe.ru/SVA/NSM/Semicond/

[67] http://www.springermaterials.com/navigation/

APPENDICES

A1.THE GREEN'S FUNCTIONS

The CPA method is mainly based on the nearest-neighbor, tight-binding Hamiltonian

$$H = \sum_{i} |i > \varepsilon_i < i| + \sum_{n.n.} |i > t_{ij} < j| \,, \qquad \textbf{(A1-1)}$$

where the symbol "n.n." denotes that the summation goes over the nearest-neighbor pairs , and |i> and |j> are atomic-like tight-binding wave-functions. If the eigenfunctions and eigenvalues of the Hamiltonian in k-space are denoted by$|k >$ and $E(k)$ respectively, then the corresponding Green's function can be expressed as

$$G(z) = \sum_{k} \frac{|k >< k|}{z - E(k)}. \qquad \textbf{(A1-2)}$$

In the tight-binding basis, the matrix elements of the Green's function between states $|l >$ and |m> can be written as

$$G_{lm}(z) =< l|G(z)|m >$$

$$= \sum_{k} \frac{< l|k >< k|m >}{z - E(k)}. \qquad \textbf{(A1-3)}$$

The summation over the first Brillioun zone in k-space can be transformed into an integral over the same Brilliounzone.

A2.Monoatomic Chain Green' s Function

The Hamiltonian for the perfect monoatomic chain is

$$H = \sum_{i} |i > \varepsilon_0 < i| + \sum_{n.n.} |i > t < j| , \quad \textbf{(A2-1)}$$

The eigenfunctions and eigenvalues are easily found to be

$$|k >= \frac{1}{\sqrt{N}} \sum_{n} e^{ikna} |n >, \quad \textbf{(A2-2)}$$

$$E(k) = \varepsilon_0 + 2t\cos(ka), \quad \textbf{(A2-3)}$$

wherea is the lattice spacing, and n denotes an atomic site. The Green's function matrix elements can be evaluated in closed form by using Equation (A2-3), (we denote the Green's function here by the symbol P, for perfect crystal),

$$P_{lm}(z) = \frac{1}{N} \sum_{k} \frac{e^{ik(l-m)a}}{z - E(k)}$$

$$= \frac{Na}{N(2\pi)} \int_{\frac{-\pi}{a}}^{\frac{\pi}{a}} dk \, \frac{e^{ik(l-m)a}}{z-2t\cos(ka)}$$

$$= \frac{1}{2\pi} \int_{-\pi}^{\pi} d\varphi \, \frac{e^{i\varphi(l-m)}}{z-2t\cos(ka)} \quad \textbf{(A2-4)}$$

$$= -\frac{1}{2\pi i t} \oint d\omega_{|\omega|=1} \frac{\omega^{|l-m|}}{\omega^2-2x\omega+1}$$

$$= -\frac{1}{2\pi i t} \oint d\omega_{|\omega|=1} \frac{\omega^{|l-m|}}{(\omega-\rho_1)(\omega-\rho_2)},$$

where $x = (z - \varepsilon_0)/2t'$, and ρ_1 and ρ_2 are the two roots of equation $\omega^2 - 2\omega x + 1=0$:

$$\rho_1 = x - \sqrt{x^2 - 1}, \quad \textbf{(A2-5)}$$

$$\rho_2 = x + \sqrt{x^2 - 1}. \quad \textbf{(A2-6)}$$

It follows that

$$\rho_1 \rho_2 = 1. \quad \textbf{(A2-7)}$$

1. If $|\rho_1| > 1$, then $|\rho_2| = \frac{1}{|\rho_1|} < 1$; and vice versa. This means that one root is inside of the unit circle and the other root is outside of the unit circle. For this case, the Green's function can be found, using residue theory, as,

$$P_{lm}(z) = -\frac{1}{t}\frac{\rho_1^{|l-m|}}{\rho_1-\rho_2} = \frac{1}{\sqrt{(z-\varepsilon_0)^2-4t^2}}\rho_1^{|l-m|}. \quad \textbf{(A2-8)}$$

2. Similarly, if |P2|>1, then l^ i| =1/| P^ | < 1, the Green's function can be found as,

$$P_{lm}(z) = -\frac{1}{t}\frac{\rho_2^{|l-m|}}{\rho_2-\rho_1} = \frac{1}{\sqrt{(z-\varepsilon_0)^2-4t^2}}\rho_2^{|l-m|}. \quad \textbf{(A2-9)}$$

3. If $|\rho_1| = |\rho_2| = 1$ implying that x is real and $-1 \le x \le 1$, the two roots lye on the unit circle. This condition gives the continuous spectrum of H which lies in the real E-axis. In this case, we must follow a limiting procedure as in Equation (4-10). The corresponding Green's function is found as

$$P_{lm}^{\pm}(E) = \frac{\mp i}{\sqrt{4t^2-(E-\varepsilon_0)^2}}(x \mp i\sqrt{1-x^2})^{|l-m|}. \quad \textbf{(A2-10)}$$

A3.Perfect Diatomic Chain Green's

For the diatomic chain with Hamiltonian (4-1), eigenfunctions (4-4) and eigenvalues (4-6), the matrix element of Green's function can be written as

$$P_{lm\alpha\beta}(E) = \frac{1}{N}\sum_{jk} \frac{c_\alpha^{j*}(k)c_\beta^{j}(k)}{E - E_j(k)} e^{ik(l-m)a}. \qquad \textbf{(A3-1)}$$

Some manipulation leads to

$$\begin{aligned} P_{lm}(E) &= \frac{1}{N}\sum_{k} \frac{E - \varepsilon_D}{[E - E_1(k)][E - E_2(k)]} e^{ik(l-m)a} \\ &= \frac{1}{N}\sum_{k} \frac{E - \varepsilon_D}{E^2 - E(\varepsilon_B + \varepsilon_D) + \varepsilon_B\varepsilon_D - 2t^2 - 2t^2\cos(ka)} e^{ik(l-m)a} \\ &= \frac{Na}{2\pi N}\int_{-\pi/a}^{\pi/a} dk \, \frac{E-\varepsilon_D}{E^2-E(\varepsilon_B+\varepsilon_D)+\varepsilon_B\varepsilon_D-2t^2-2t^2\cos(\varphi)} e^{ik(l-m)a} \\ &= \frac{E-\varepsilon_D}{2\pi}\int_{-\pi}^{\pi} d\varphi \, \frac{e^{i(l-m)\varphi}}{E^2-E(\varepsilon_B+\varepsilon_D)+\varepsilon_B\varepsilon_D-2t^2-2t^2\cos(ka)} \\ &= -\frac{E-\varepsilon_D}{2\pi i}\oint d\omega_{|\omega|=1} \frac{\omega^{|l-m|}}{t^2\omega^2-[E^2-E(\varepsilon_B+\varepsilon_D)+\varepsilon_B\varepsilon_D-2t^2]\omega+t^2} \\ &= -\frac{E-\varepsilon}{2\pi i t^2}\oint d\omega_{|\omega|=1} \frac{\omega^{|l-m|}}{(\omega-\rho_1)(\omega-\rho_2)}, \end{aligned} \qquad \textbf{(A3-2)}$$

where , we have

$\rho_1\rho_2 = 1.$

Comparing Equations (A-13) and (A-7), we obtain

$$P_{lm11}(E) = \frac{E - \varepsilon_D}{-t^2(\rho_1 - \rho_2)}\rho_1^{|l-m|} \qquad \textbf{(A3-3)}$$

Similarly, we get

$$P_{lm22}(E) = \frac{E - \varepsilon_B}{-t^2(\rho_1 - \rho_2)}\rho_1^{|l-m|}. \qquad \textbf{(A3-4)}$$

$$P_{lm12}(E) = P^{*}_{lm21}(E) = \frac{1}{N}\sum_{k}\frac{t(1+e^{-ika})}{[E-E_1(k)][E-E_2(k)]}. \qquad \textbf{(A3-5)}$$

VITA

PayamNorouzzadeh

Candidate for the Degree of

Doctor of Philosophy

Thesis: CHARGE CARRIER AND PHONON TRANSPORT IN NANOSTRUCTURED THERMOELECTRICS

Major Field: Electrical Engineering

Biographical:

Education:

Completed the requirements for the Doctor of Philosophy in electrical engineering at Oklahoma State University, Tulsa, Oklahoma in December, 2012.

Completed the requirements for the Master of Science in applied physics at Iran University of Science and Technology, Tehran, Iran in 1999.

Completed the requirements for the Bachelor of Science in applied physics at Sharif University of Technology, Tehran, Iran in 1996.

Experience: First Principles Materials Design, Transport Properties of Semiconductors, Statistical Physics, Econophysics

Professional Memberships: American Physical Society